NUREG/CR–6187
ANL–94/8
TMIV(93)AL02

Results of Mechanical Tests and Supplementary Microstructural Examinations of the TMI-2 Lower Head Samples

Prepared by D. R. Diercks, L. A. Neimark

Argonne National Laboratory

Prepared for
U.S. Nuclear Regulatory Commission

NUREG/CR-6187
ANL-94/8
TMIV(93)AL02

Results of Mechanical Tests and Supplementary Microstructural Examinations of the TMI-2 Lower Head Samples

Manuscript Completed: March 1994
Date Published: April 1994

Prepared by D. R. Diercks, L. A. Neimark

Argonne National Laboratory
9700 South Cass Avenue
Argonne, IL 60439

Prepared for
Division of Systems Research
Office of Nuclear Regulatory Research
U.S. Nuclear Regulatory Commission
Washington, DC 20555-0001
NRC FIN L1005

Abstract

Metallographic examinations and mechanical tests have been completed on specimens from 15 prism-shaped samples cut from the lower head of the TMI-2 pressure vessel as a part of the TMI–2 Vessel Investigation Project (VIP). The results of these examinations and tests are summarized here.

The metallographic results were in general agreement with earlier INEL observations. Four samples were found to have attained temperatures as high as 1100°C during the accident, with an estimated cooling rate of 10-100°C/min from the maximum temperature. Portions of two adjacent samples also exceeded 727°C, and one laboratory found that a region near the surface of another sample apparently also exceeded 727°C, even though this sample was not near the hot spot. The remaining samples apparently did not exceed 727°C, but four samples probably approached this temperature.

Tensile tests were conducted on the lower head material at room temperature and at temperatures of 600-1200°C. A strong dependence of yield and tensile strengths on temperature was observed, and the data generally matched well with literature data on A533, Grade B steel. However, the observed strengths of material from the hot spot in the as-received condition lay well above the remaining data, reflecting the heat treatment received during the accident.

Creep tests were conducted on the lower head material over the temperature range of 600-1200°C at stress levels resulting in failure times of 1-100 h. The data from the lower head material compared well with similar data obtained earlier on archive material from the Midland reactor 600°C. However, at higher temperatures, the TMI-2 lower head data fell increasingly above data from the Midland material. The TMI-2 data were fit using both Larson-Miller and Manson-Haferd time-temperature parameters.

Charpy V-notch impact tests were conducted on four groups of test specimens. Specimens from the hot spot showed significantly lower upper-shelf energies and higher transition temperatures than specimens from regions that did not exceed 727°C during the accident.

Cracks were found in the stainless steel cladding of boat samples from the hot spot. The cracks appeared to be the result of hot-tearing, probably assisted by intergranular penetration of liquid Ag-Cd. Crack propagation into the A533 vessel steel was a maximum of ≈6 mm. Materials in the cracks suggest the presence of control-assembly debris on the lower head before the massive fuel flow arrived.

Contents

List of Figures

List of Tables

Executive Summary

Metallographic examinations and mechanical tests have been completed on specimens from 15 prism-shaped samples cut from the lower head of the TMI-2 pressure vessel. These tests were conducted as a part of the TMI–2 Vessel Investigation Project (VIP), an international program conducted jointly by the U.S. Nuclear Regulatory Commission (NRC) and the Organisation for Economic Co–operation and Development/Nuclear Energy Agency (OECD/NEA). The results of these examinations and tests, which were conducted jointly by Argonne National Laboratory (ANL) and the European partner laboratories, are summarized and compared with the metallographic results reported earlier by the Idaho National Engineering Laboratory (INEL).

The metallographic results were in general agreement with INEL observations. Specimens from Samples E-6, E-8, F-10, and G-8, which comprised a so-called "hot spot" near the bottom of the lower head, were found to have attained temperatures as high as 1100°C during the accident. The cooling rate from the maximum temperature was generally estimated to have been 10-100°C/min. The end of Sample H-8 adjacent to the hot spot was also found to have attained temperatures in excess of 727°C, as did portions of nearby Sample F-5. One laboratory additionally found that a region near the surface of Sample M-11 apparently also exceeded 727°C, even though this sample was not near the hot spot. The remaining samples apparently did not exceed 727°C, but tempering of the bainite, which was observed by one laboratory in Samples H-4, H-5, M-8, and L-9, suggested that these remainng samples probably approached this temperature.

Tensile tests were conducted on the lower head material at room temperature and at temperatures of 600-1200°C. A strong dependence of yield and tensile strengths on temperature was observed; the room-temperature values were reduced by more than a factor of 2 at 600°C and by a factor of more than 10 at 900°C. The data generally matched well with data earlier obtained by the Japanese National Research Institute for Metals (NRIM) for five other heats of A533, Grade B steel. However, the observed strengths of material from Samples E-6 and E-8 in the as-received condition lay well above the remaining data, reflecting the austenitizing heat treatment and relatively rapid cooling to which this material was exposed during the accident.

Creep tests were conducted on the lower head material over the temperature range of 600-1200°C at stress levels resulting in failure times of 1-100 h. No significant effect of prior thermal history on stress-rupture life was observed, although no samples for which the maximum temperature had significantly exceeded 727°C were tested. The data from the lower head material compared well with similar data obtained earlier on archive material from the Midland reactor at 600°C. However, at higher temperatures, the TMI-2 lower head data fell increasingly above data from the Midland material. The TMI-2 data were fit using both Larson-Miller and Manson-Haferd time-temperature parameters. Of the two correlations, the Manson-Haferd analysis produced the better fit.

Charpy V-notch impact tests were conducted on four groups of test specimens. Specimens from Samples D-10, H-4, and E-11, for which the maximum temperature

did not exceed 727°C, showed similar behavior, with an upper-shelf energy of ≈170 J and a transition temperature on the order of 20°C. However, specimens from Sample F-10, for which the maximum temperature was as high as ≈1050°C, had an upper-shelf energy of ≈120 J and a transition temperature of ≈70°C.

Cracks were found in the stainless steel cladding of boat samples from the so-called "hot spot" (E-6, G-8, and F-10). The cracks appeared to be the result of hot-tearing, probably assisted by intergranular penetration of liquid Ag-Cd. Crack propagation into the A533 vessel steel was a maximum of ≈6 mm. Materials in the cracks suggest the presence of control-assembly debris on the lower head before the massive fuel flow arrived.

Foreword

The contents of this report were developed as part of the Three Mile Island Unit 2 Vessel Investigation Project. This project is jointly sponsored by eleven countries under the auspices of the Nuclear Energy Agency of the Organisation for Economic Cooperation and Development. The sponsoring organisations are:

* The Centre d'Etudes d'Energie Nucléaires of Belgium,
* The Säteilyturvakeskus of Finland,
* The commissariat à l'Energie Atomique of France,
* The Gesellschaft für Reaktorsicherheit mbH of Germany,
* The Comitato Nazionale per La Ricerca e per Lo Sviluppo Dell'Energia Nucleare e Delle Energie Alternative of Italy,
* The Japan Atomic Energy Research Institute,
* The Consejo de Seguridad Nuclear of Spain,
* The Statens Kärnkraftinspektion of Sweden,
* The Office Fédéral de l'Energie of Switzerland,
* AEA Technology of the United Kingdom,
* The United States Nuclear Regulatory Commission, and
* The Electric Power Research Institute.

The primary objectives of the Nuclear Energy Agency (NEA) are to promote cooperation between its member governments on the safety and regulatory aspects of nuclear development, and on assessing the future role of nuclear energy as a contributor to economic progress.

This is achieved by:

- encouraging harmonisation of governments' regulatory policies and practices in the nuclear field, with particular reference to the safety of nuclear installations, protection of man against ionising radiation and preservation of the environment, radioactive waste management, and nuclear third-party liability and insurance;

- keeping under review the technical and economic characteristics of nuclear power growth and of the nuclear fuel cycle, and assessing demand and supply for the different phases of the nuclear fuel cycle and the potential future contribution of nuclear power to overall energy demand;

- developing exchanges of scientific and technical information on nuclear energy, particularly through participation in common services;

- setting up international research and development programmes and undertakings jointly organised and operated by OECD countries.

In these and related tasks, NEA works in close collaboration with the International Atomic Energy Agency in Vienna, with which it has concluded a Cooperation Agreement, as well with other international organisations in the nuclear field.

Acknowledgment

The authors gratefully acknowledge the support and direction provided for this work by C. Z. Serpan, E. Hackett, A. Rubin, and M. Mayfield of the NRC. The financial support and significant technical contributions made by the OECD partner laboratories participating in the TMI-2 Vessel Investigation Project Metallurgical Program are also gratefully acknowledged. The following persons at ANL contributed to the completion of this work: T. L. Shearer, D. O. Pushis, F. M. Basso, and S. L. Phillips (sample inspection, decontamination and preparation); J. A. Zic, W. Kettman, and F. Pausche (metallography); J. E. Sanecki and A. G. Hins (SEM examinations); and W. F. Burke and W. A. Moll (mechanical testing).

1 Introduction

The TMI-2 Vessel Investigation Project (VIP) is an international program being conducted jointly by the U.S. Nuclear Regulatory Commission (NRC) and the Organisation for Economic Co-operation and Development/Nuclear Energy Agency (OECD/NEA). Participants in the international project include the U.S., Japan, Belgium, the Federal Republic of Germany (FRG), Finland, France, Italy, Spain, Sweden, Switzerland, and the United Kingdom (U.K.).

During the first phase of the project, 15 samples were recovered from the lower head by MPR Associates, Inc. The samples are prism-shaped, each ≈152-178 mm (6-7 in.) long, 64-89 mm (2.5 -3.5 in.) wide, and 64-76 mm (2-1/2-3 in.) deep, as shown in Fig. 1. The samples were cut from the inner surface of the lower head and typically extend through approximately half the lower head thickness. The specimens were taken from (1) near the area of impact by the primary stream of molten material on the lower head; (2) toward the radial center of the lower head underneath the maximum thickness of debris; (3) in the quadrant of the lower head where a "wall" of consolidated debris similar to a lava front had developed; (4) in a location of the lower head not contacted by the molten material (to act as a control sample); and (5) locations with one or more instrument penetrations, particularly where surface cracks had been observed visually. The locations from which the lower head samples were taken are shown in Fig. 2.

Cladding cracks were observed in three of the lower head samples, namely E-6, G-8, and F-10, during initial examinations conducted at Argonne National Laboratory (ANL). Cladding cracks were also detected at location G-6 in the TMI lower head, but no sample was removed at this location. Metallographic and scanning electron microscopy (SEM) examinations were conducted on Samples E-6 and G-8 in some detail, to characterize the nature and extent of the cracking. The results of these examinations are reported below.

Following the initial examinations, metallographic specimens were cut from the lower head samples, decontaminated, and sent to the Idaho National Engineering Laboratory (INEL). These specimens were subjected to detailed characterization by optical metallography and hardness measurements to determine the maximum temperature attained at various lower head locations during the accident.[1] Supplemental examinations, the results of which are summarized in this report, have been conducted by ANL and participating OECD partner laboratories. Based in part upon the results of the ANL examinations, a mechanical-testing matrix was developed to determine the tensile and creep properties of the lower head material under conditions relevant to the accident scenario. The tests were conducted by ANL and participating OECD partner laboratories, and the results are summarized here. These results have been used by analysts at INEL to assess the integrity of the lower head and its margin-to-failure during the accident.

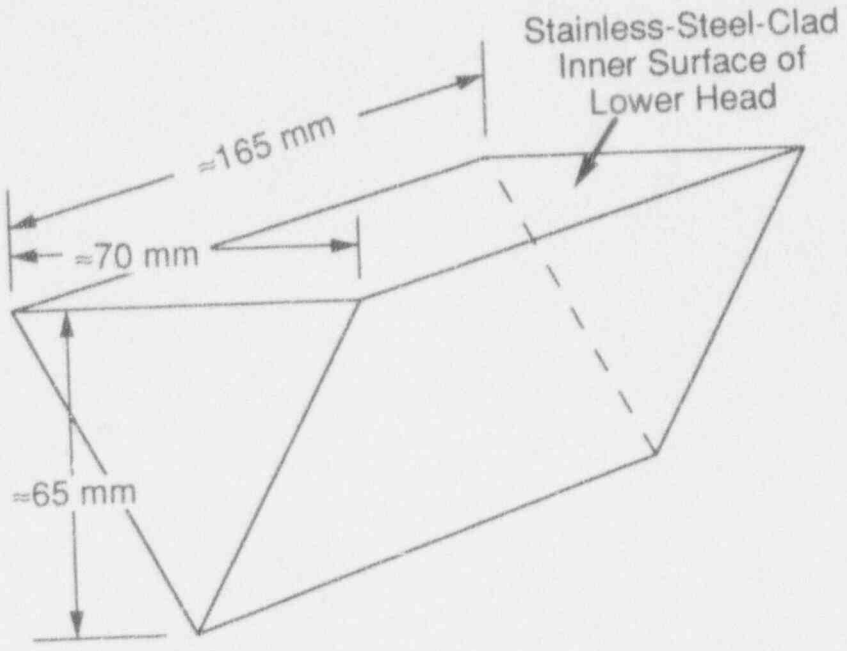

Fig. 1. Configuration and approximate dimensions of a typical sample from TMI-2 pressure vessel lower head.

2 Preparation of Mechanical-Test Specimens

The tensile and stress-rupture tests that are described below were conducted on specimens of rectangular-cross-section, as shown in Fig. 3. This design was chosen to satisfy ASTM Standards E8 and E139 and applicable standards of the Deutsches Institut für Normung (DIN). Specimens of both flat and circular cross section were used in earlier round-robin creep tests on archive material obtained from the lower head of the Midland reactor,[2] and no significant differences were observed in the results obtained from the two specimen designs. The flat design was used exclusively in the case of the TMI-2 lower head samples to conserve material. The specimen design used for the impact tests was the conventional Charpy V-notch test specimen (ASTM E23) shown in Fig. 4.

The mechanical-testing matrix developed by ANL and the participating OECD laboratories for specimens from the lower head material is summarized in Table 1. Input was obtained from the analysts at INEL responsible for assessing the lower head integrity to ensure that this test matrix included all of the properties and test conditions needed for these analyses. Tensile tests were conducted at room temperature for purpose of comparison with data in the literature. All other tensile and creep tests were conducted at a minimum test temperature of 600°C. It was judged that little or no damage would have occurred to those portions of the lower head for which the maximum temperature did not exceed this value and that failure was unlikely at these locations. The maximum temperature of 1200°C for these tests lies slightly above the maximum lower head temperature believed to have been attained during the accident.

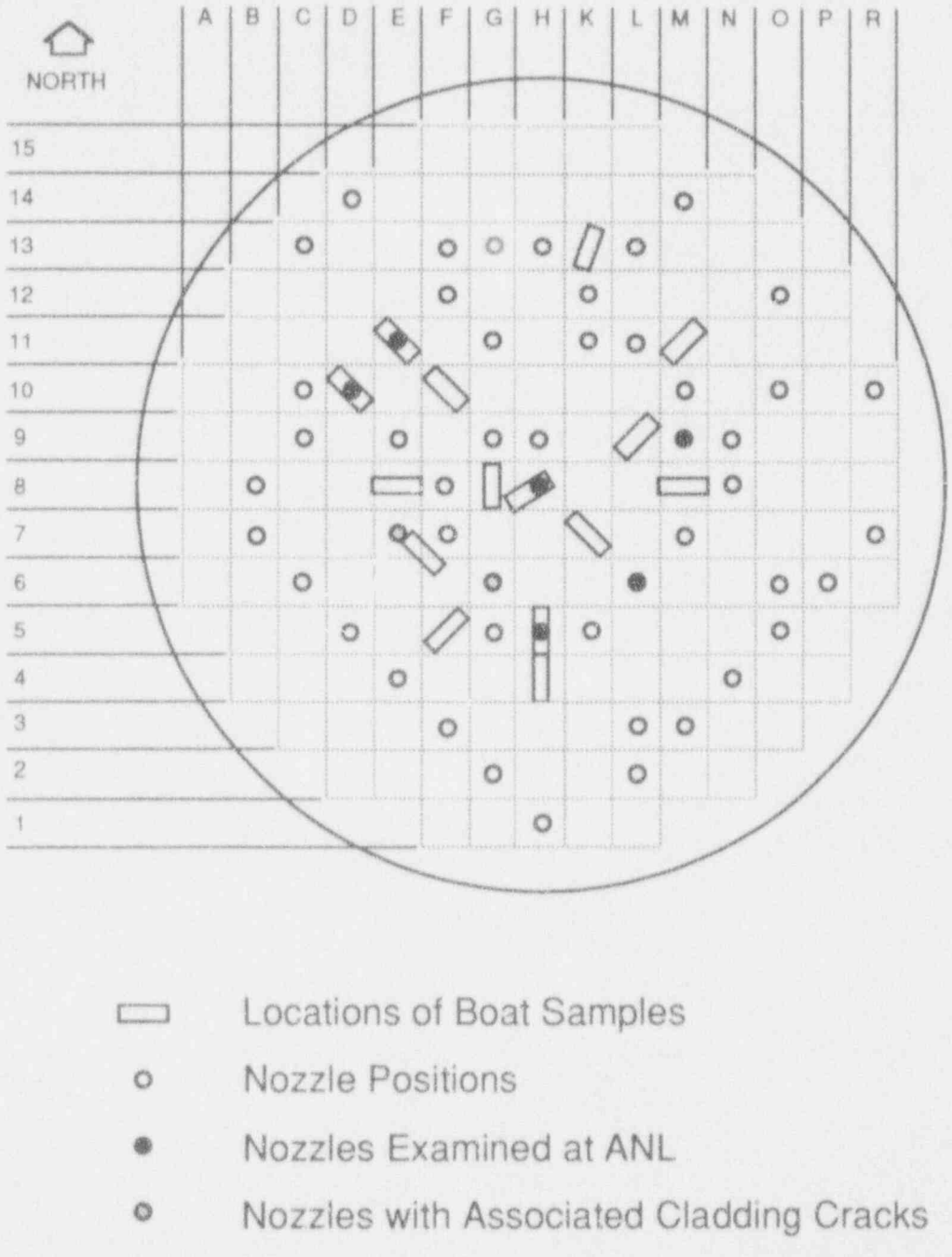

Fig. 2. Map of the the lower head of the TMI-2 pressure vessel showing locations from which samples were taken.

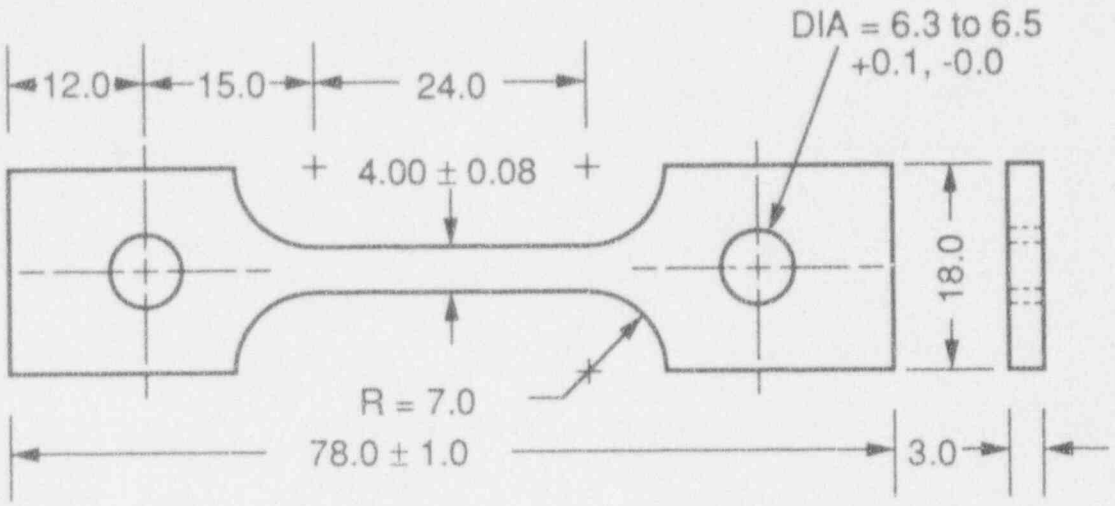

Fig. 3. Test specimen used for tensile and creep tests of TMI-2 lower head material. All dimensions are in mm.

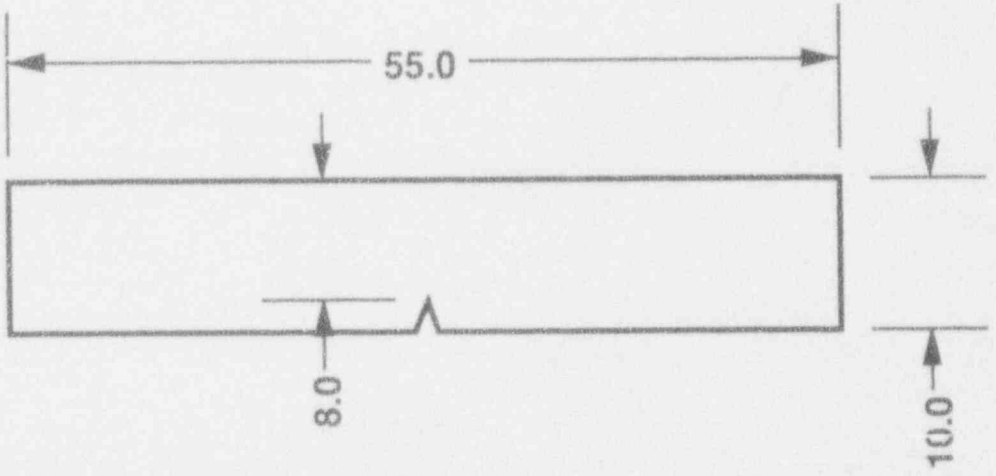

Thickness = 10.0 mm;
V-notch angle = 45° with 0.25 mm radius at tip.

Fig. 4. Charpy V-notch test specimen used for impact testing of TMI-2 lower head material. All dimensions are in mm.

Table 1. Summary of mechanical testing matrix for TMI-2 lower head material.

Temperature (°C)	Damage Level	Tensile Tests	Creep Tests[a]	Impact Tests
R. T.[b]	Low	Belgium France U. S.[c]	-	Italy
	Moderate	Spain U. S. Belgium[c]	-	Italy
	Severe	Belgium Spain	-	Italy
600	Low	Belgium France	Belgium	-
	Moderate	Spain U.S.	Spain	-
700	Low	Belgium France	France	-
	Moderate	Spain U.S.	U.S.	-
800	Severe	France U.S.	Belgium	-
900	Severe	Belgium Spain	U.S.	-
1000	Severe	France U.S.	Spain	-
1100	Severe	Belgium Spain Belgium[c]	France	-
1200	Severe	France U.S.	U.S.	-

[a]Each series of creep tests consists of four tests with stress-rupture lives of ≈1, 5, 20, and 100 h.
[b]R.T. = room temperature.
[c]Test on specimen from cladding.

The damage levels listed in Table 1 refer to the level of damage believed to have been sustained by the lower head samples during the accident, based upon preliminary metallographic and hardness information available at the time the test matrix was prepared. Low damage refers to that sustained at a maximum temperature of <727°C during the accident, moderate damage to that sustained at a maximum temperature of ≈727-900°C, and severe damage to that sustained at a maximum temperature >900°C. Subsequent examinations revealed that estimates of initial damage were not accurate for some lower head samples, but specimens with various damage levels were nonetheless tested.

Table 2. Number of metallographic and mechanical test specimens obtained from TMI-2 lower head samples.

Sample Number	Tensile and Creep Specimens		Impact Specimens	Metallography Specimens
	Base Metal	Cladding[a]		
D-10	0	0	6	5
E-6	1	0	0	4
E-8	8	2	0	9
E-11	0	0	5	5
F-5	15	3	0	8
F-10	0	0	10	4
G-8	11	0	0	3
H-4	0	0	12	6
H-5	14	2	0	5
H-8	17	3	0	4
K-7	14	3	0	8
K-13	18	3	0	7
L-9	17	3	0	8
M-8	14	3	0	5
M-11	17	3	0	8
Totals	146	25	33	89

[a]Some cladding specimens were not completely decontaminated and were therefore not tested.

Because the number specimens with severe-damage-levels was limited, it was necessary, in some cases, to heat treat low-damage specimens before testing to produce the microstructure associated with a severe level of damage. This heat treatment consisted of heating the specimen to 1000°C, holding it at this temperature for 2 h, and then cooling it to room temperature at ≈10-50°C per min. For specimens to be tested at 1000°C or above, this prior heat treatment was omitted, because its effects would be negated by the thermal treatment imposed during testing.

Detailed diagrams that show how the lower head samples were sectioned to provide the test specimens for the matrix of Table 1 are presented in Appendix A. The number of specimens of each type obtained from each of the lower head samples is summarized in Table 2. These specimens were distributed to the laboratories participating in the mechanical-testing program as indicated in Tables 3 and 4.

Table 3. Distribution of TMI-2 lower head mechanical test specimens to OECD partner laboratories.[a]

TMI-2 Lower Head Sample Number	OECD Partner Laboratory	Number of Test Specimens	Type of Specimen	Test Specimen Identification Numbers
D-10	Italy	6	Impact	k1-k6
E-8	Belgium	1	Tensile	t8
	Spain	1	Tensile	t7
E-11	Italy	3	Impact	k1-k3
F-5	Belgium	9	Tensile	t1, t2[b] t7-t13
	Spain	5	Tensile	t14-t18
F-10	Italy	9	Impact	k1-k3, k5, k7, k8, k10-k12
H-4	Italy	9	Impact	k1, k2, k4, k5-k8, k10, k12
K-7	Spain	8	Tensile	t7-t14
K-13	Belgium	8	Tensile	t7-t14
L-9	France	8	Tensile	t7-t14
	Spain	2	Tensile	t15, t16
M-11	France	8	Tensile	t7-t14

[a]The "tensile" specimens are used for both tensile and creep tests. All specimens are from the lower head base metal except as noted.

[b]Specimens t1 and t2 from Sample F-5 are cladding specimens.

Table 4. Distribution of TMI-2 lower head base metal metallographic specimens to OECD partner laboratories.

TMI-2 Lower Head Sample Number	OECD Partner Laboratory	Number of Specimens	Specimen Identification Numbers
D-10	Italy	1	m1
E-8	Belgium	1	m5
	Finland	2	m4 and m10
	France	1	m7
	FRG	1	m9
	Spain	1	m6
F-5	Belgium	1	m5
	FRG	1	m6
	U.K.	1	m4
F-10	Italy	1	m5
	U.K.	1	m4
H-4	FRG	1	m5
	Italy	1	m4
	U.K.	1	m6
H-5	FRG	1	m5
	U.K.	1	m1
K-7	FRG	1	m6
	Spain	1	m5
	U.K.	1	m4
K-13	Belgium	1	m4
	FRG	1	m5
	U.K.	1	m9
L-9	France	1	m10
	FRG	1	m9
	U.K.	1	m7
M-8	FRG	1	m4
	U.K.	1	m1
M-11	France	1	m7
	FRG	1	m5
	Spain	1	m6
	U.K.	1	m4

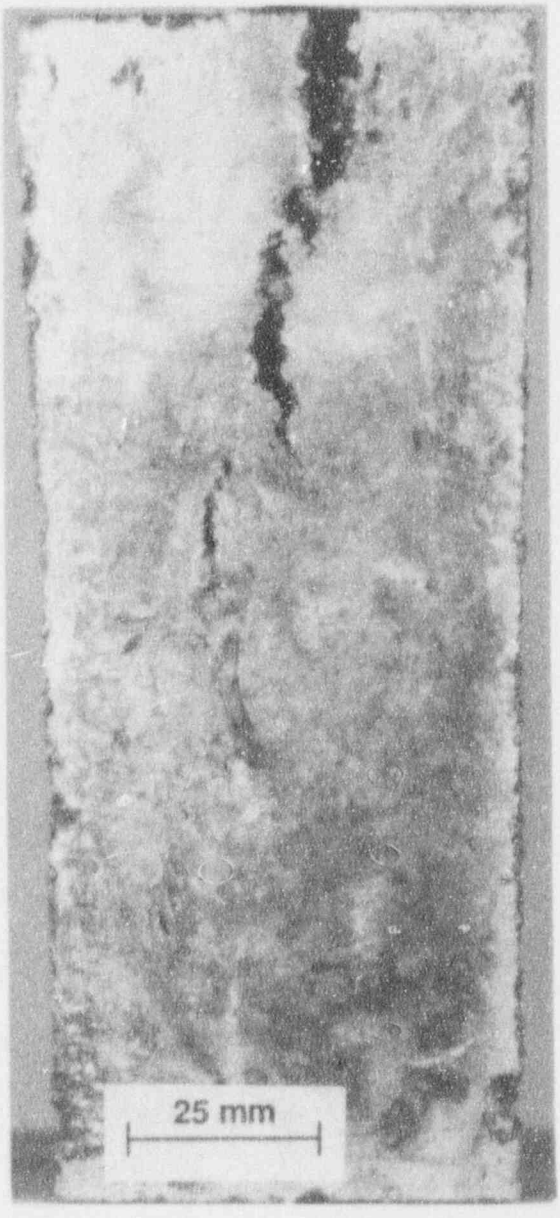

Fig. 5. Surface of Sample E–6 showing end of one leg of crack around Nozzle E–7.
MCT 276674

3 Examination of Lower Head Cladding

3.1 Physical Condition

After removal of the hard layer of core debris, the lower head was visually examined by video camera. It was found that a significant U-shaped crack in the surface encircled the E–7 nozzle. The E–6 boat sample that was taken encompassed one leg of this crack, as shown in Fig. 5. A cursory visual inspection of Sample E–6 by personnel at TMI–2 immediately after removal suggested that the crack penetrated

essentially through the entire depth of the sample, i.e., significantly more than 6 cm into the lower head. However, a closer examination at ANL revealed that what was thought to be the penetrating crack on the end of the sample was actually the intersection of the two cutting planes made by the metal disintegration machining process (MDM). Metallographic cross sections through the crack, Fig. 6, confirmed that the crack penetrated the A533 vessel steel only superficially, ≈3 mm.

The appearance of the crack in Fig. 6 strongly suggests that the Type 308L cladding failed along interdendritic boundaries by a hot-tearing process that apparently was the result of thermal stress when this location was cooled rapidly at the rate of 10–100°C per min.

Inspection of two other boat samples at ANL, G–8 and F–10, indicated that they, too, had cracks in the cladding. The cracks in the surface of G–8 are shown in Fig. 7. Whereas the activity of the E–6 metallographic sample was sufficiently low not to require preparation in a hot-cell, the G–8 sample was atypically very radioactive, indicating the presence of fuel/fission products in the cracks. Cross sections through both the large and small cracks, Figs. 8, 9, and 10, indeed, showed fuel particles trapped in an iron (oxide) binder. Both cracks show the same evidence of hot tearing as Sample E–6, with graphic evidence of the elevated-temperature ductility of the Type 308L weldment. Penetration of the A533 vessel steel was somewhat greater than at E-6, i.e., ≈6 mm.

After surface debris had been removed by chemical means, the surface of Sample F–10 was determined to be cracked. A portion of the etched cladding surface is shown in Fig. 11. Light cracking can be seen in the longitudinal interdendritic boundaries in the weld passes. This cracking could have occurred either during fabrication or at the same time as the formation of the cracks at E-6 and G-8; the F-10 sample was on the periphery of the oval-shaped hot spot in the vessel wall. The cracking at the G-8, E-6, and F-10 locations provides additional evidence for this hot spot.

3.2 Scanning Electron Microscopy Examinations

The debris contained in the cracks of the E–6 and G–8 samples and surface scrapings from other boat samples were analyzed by scanning electron microscopy and energy-dispersive X-ray analysis (SEM–EDX) in an attempt to better understand the conditions on the lower head when the cracks were formed. The crack surfaces in the E–6 sample were coated with adherent and conforming layers of non-metallic debris, apparently oxides of debris constituents, that appear to have been molten and present at the time of, or shortly after, crack formation. The principal constituents of these layers, some of which are shown in Fig. 12, were Fe, Cr, and Ni with Sn, In, Ag, and Cd in combinations as second phases or discrete particles. The structure within these layers indicates that the constituents were once in a molten state and not formed simply as oxidation products of the base material. In particular, there were trapped, rounded nodules of Ag–Cd and needles of In–Sn in a matrix of principally Fe–oxide. The material surrounding the stainless steel cladding fragment at the base of the crack in Fig. 6 indicates that the fragment, like the surfaces of the crack, was being dissolved by a liquid phase that contained Fe, Ni, and Cr as the major constituents, with Mn, In, and Sn as minor constituents.

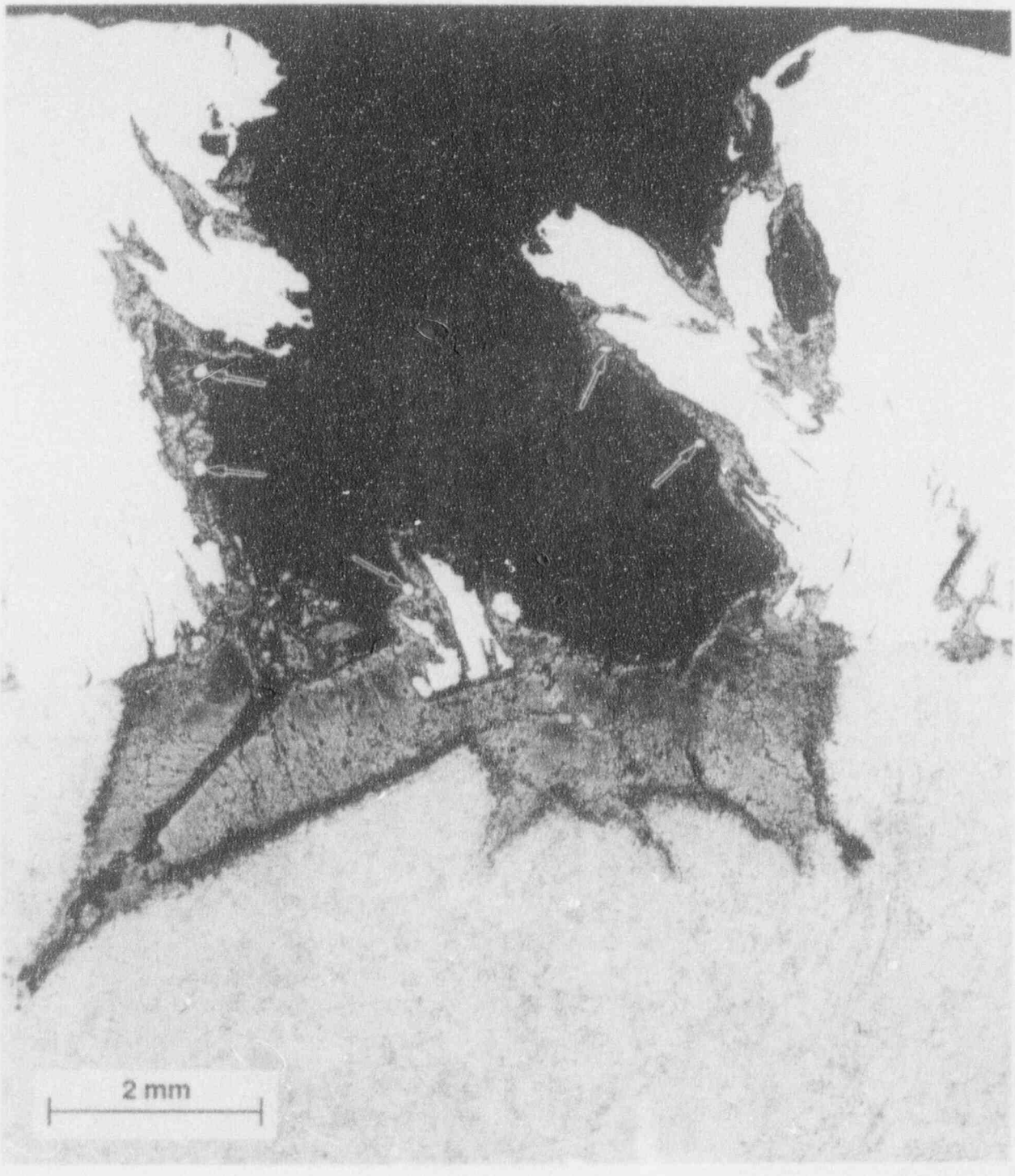

Fig. 6. Cross section through principal crack in Sample E–6. Arrows identify larger Ag–Cd nodules. Etched. MCT 276818

Fig. 7. Surface of Sample G–8 showing two cracks in cladding.
MCT 277888

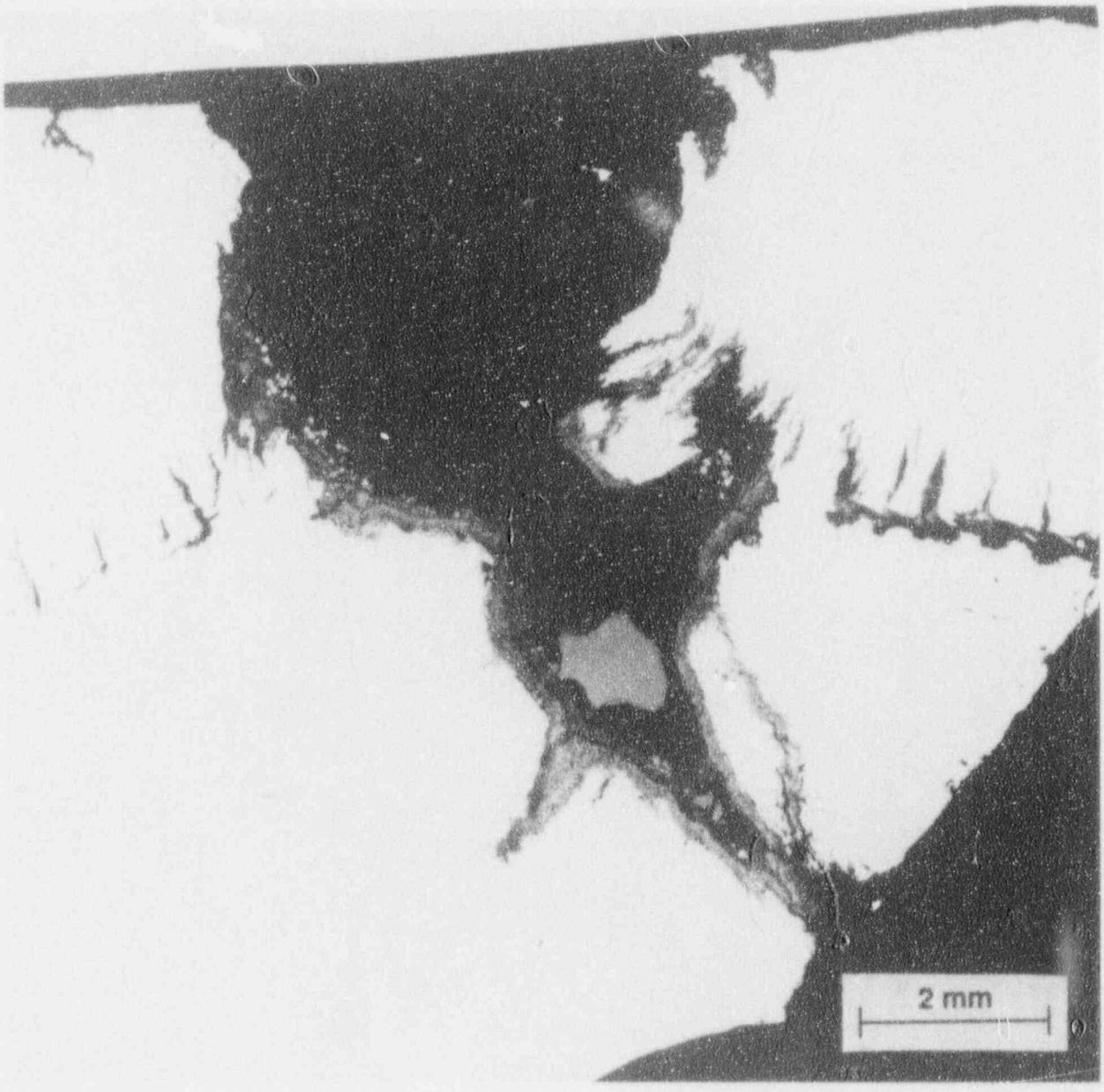

Fig. 8. Cross section of larger crack in Sample G-8. Multi-layered coating is on all crack surfaces. Gray mass at base is U-Zr "fuel." MCT 278760

Fuel fragments, such as those shown in Fig. 12, were generally present only atop the adherent surface layers as, apparently, adventitious material trapped somewhat in an Fe-oxide, not as material that had solidified in situ. Some solidified fuel flecks were found in a matrix of other in-situ solidified material in the base of the crack. Some fuel, therefore, was part of the molten material that was on top of the lower head when the cracks were formed. The grain boundaries of the wedge-shaped Fe-oxide in the crack extension into the vessel contained an In-Sn phase, indicating that a liquid was present when this high-temperature columnar-grained oxide was formed. The surface

Fig. 9. "Bottom" end of large crack shown in Fig. 8, showing fuel debris in an Fe-oxide matrix.
MCT 278756

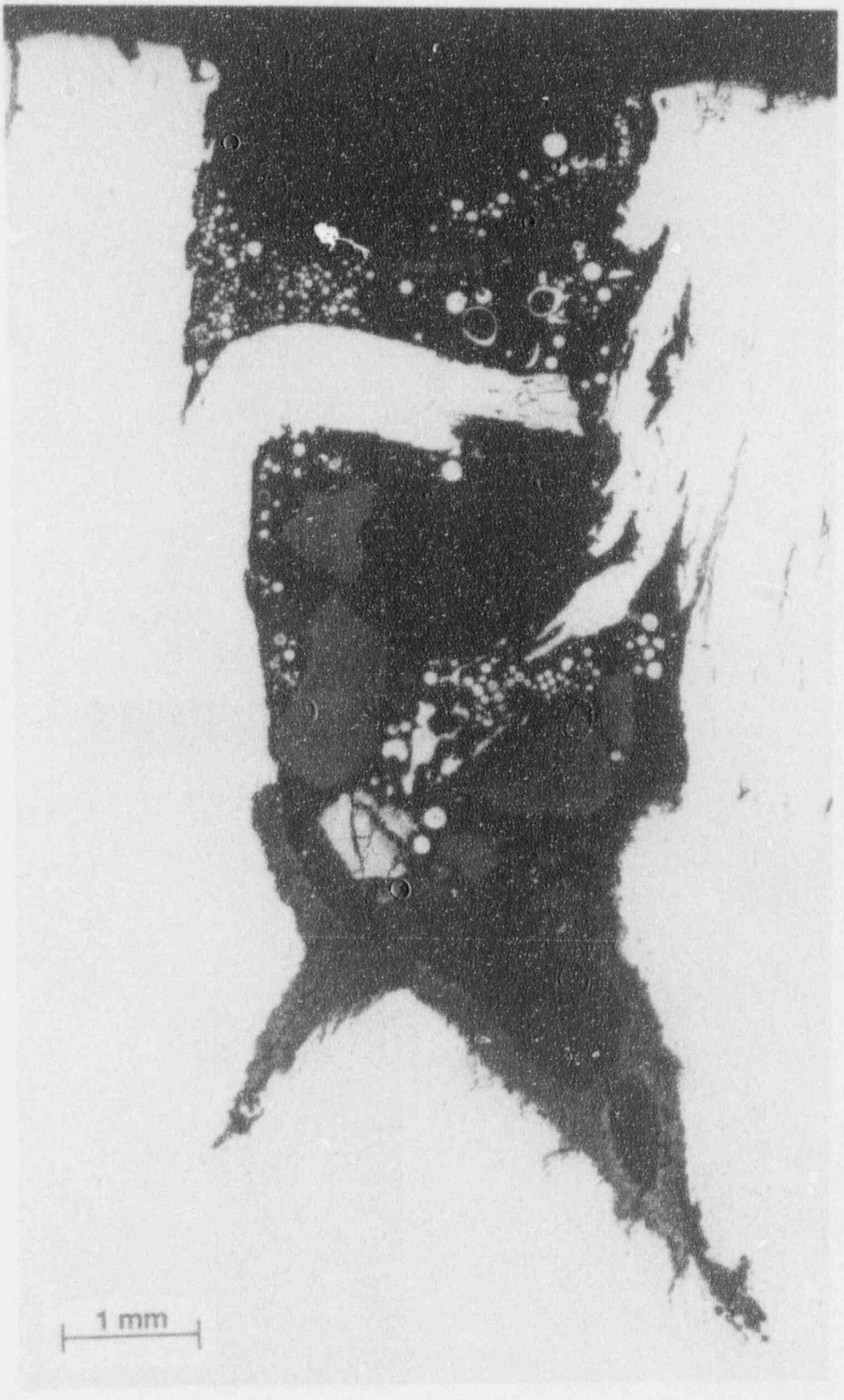

Fig. 10. Cross section through small crack in G-8. Gray masses are U-Zr "fuel;" white spheres are Fe from cutting operations. MCT 278758

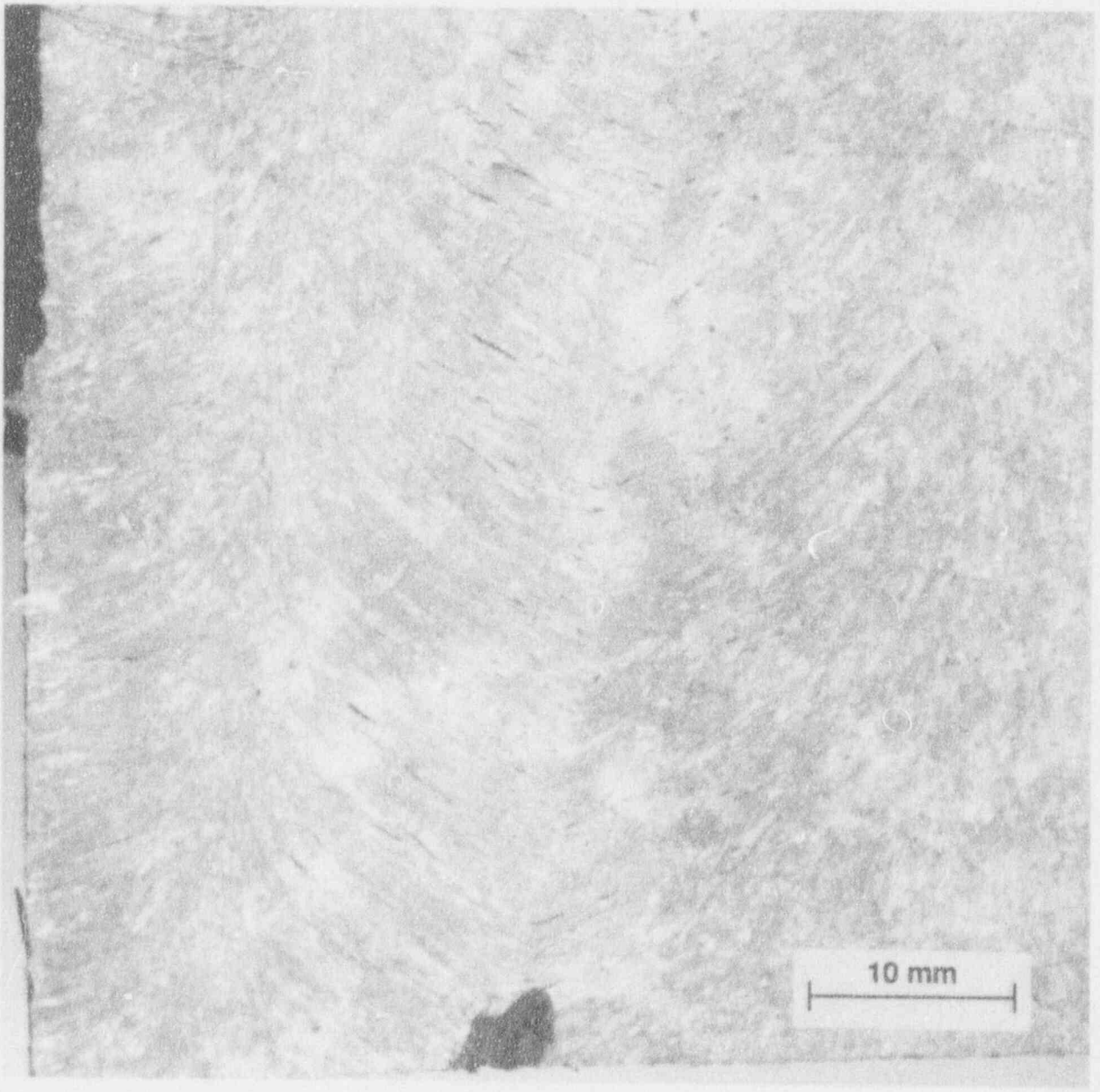

Fig. 11. Cleaned and etched surface of Sample F-10 showing small interdendritic cracks in a weld pass. MCT 278090

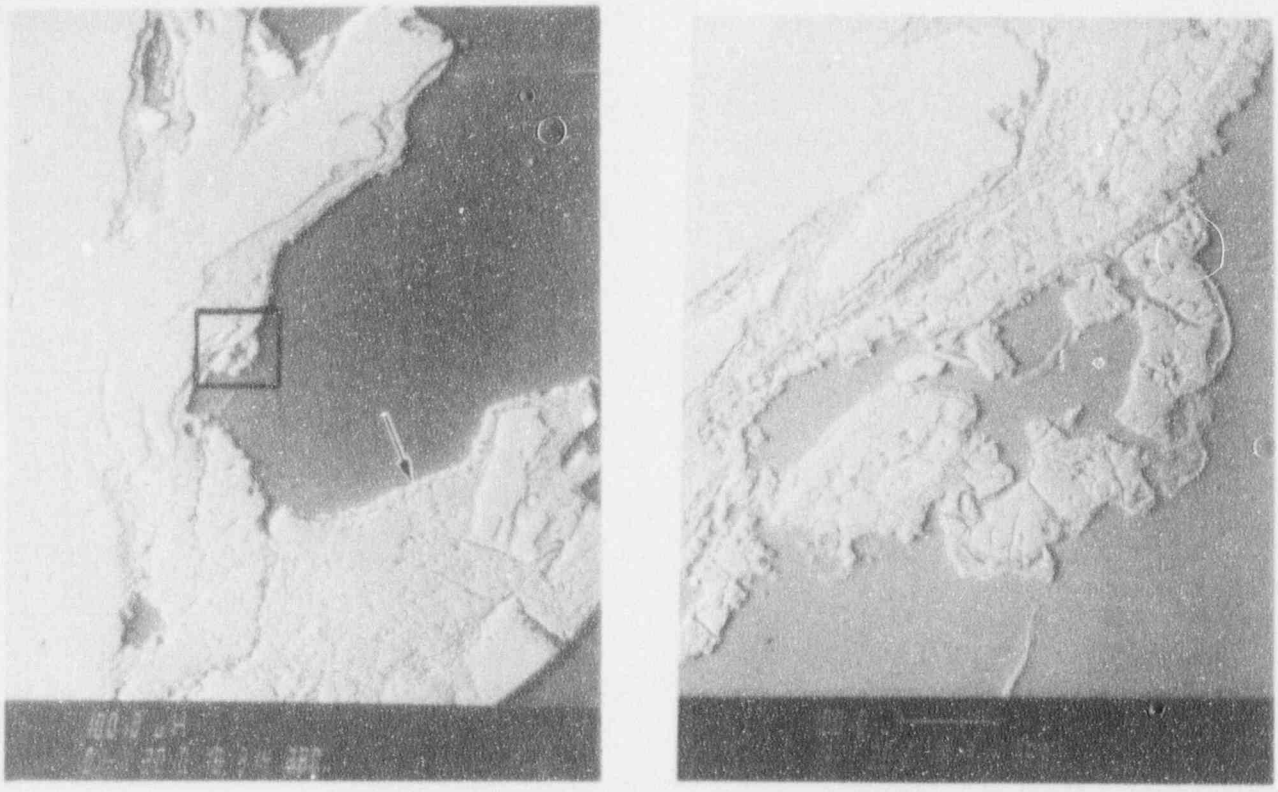

(a) (b)

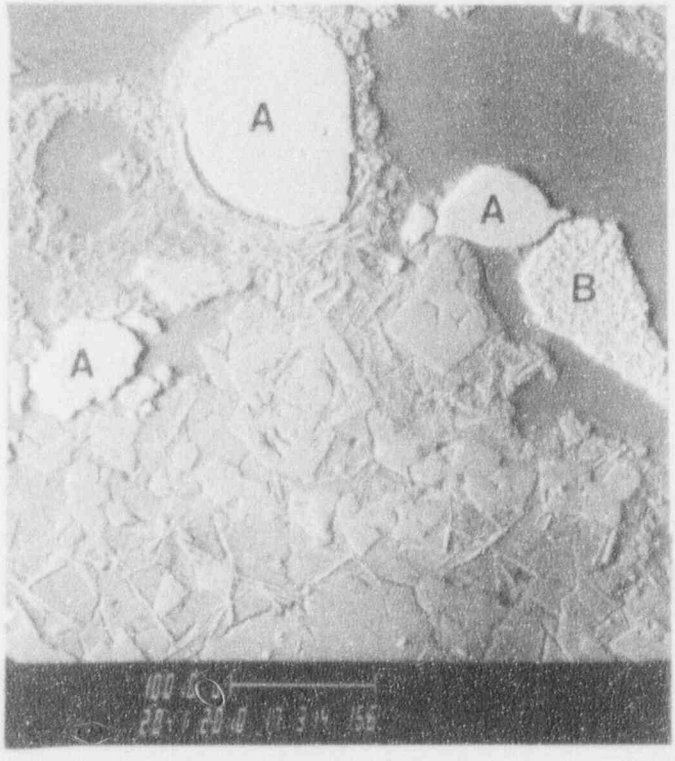

(c)

Fig. 12. SEM–BSE images of multi–layered material on crack surfaces of Sample E–6. (a) Fuel particles (white) on oxide surface (arrow); (b) area outlined in (a); and (c) In–Sn needles in Fe matrix, Ag–Cd spheroids (A), and fuel particle (B).

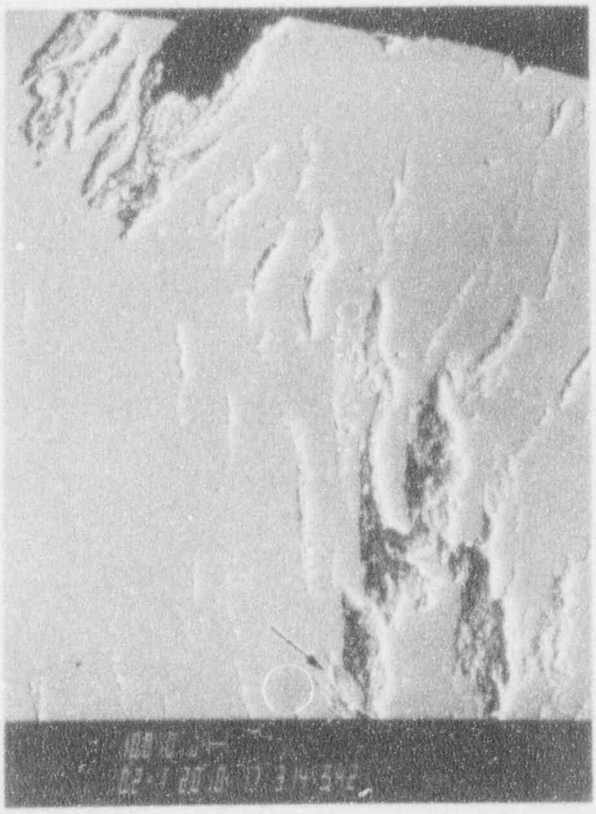

Fig. 13. Internal tears in the cladding of Sample G-8. Solidified Ag-Cd Masses are shown (arrow) ≈4 mm beneath the surface. (SEM-BSE image)

of the boat sample cladding near the crack contained several small surface penetrations that contained Ag that appeared to have penetrated intergranularly as a liquid. Solidified masses of Ag-In-Cd were also found within some tears ≈4 mm below the surface of the cladding, as shown in Fig. 13.

The materials in the crack in Sample G-8 were essentially the same as those found in the E-6 crack, except more fuel shards were present. These fragments were in a matrix of Fe oxide. Solidified masses of Ag-In-Cd and some fuel particles were found in the Fe-rich matrix within the crack extension into the vessel steel. The surface of the stainless steel cladding within the crack exhibited surface reaction layers similar to those in the E-6 crack. The upper cladding surface, however, was more ragged than that at E-6 and the intrusion of Ag-Cd stringers beneath the surface was more prevalent and obvious. The crack contained numerous pure-Fe spheroids within a thin oxide coating that apparently were from the MDM cutting operations. These spheroids were clearly independent of the core debris in the crack. Copper stringers were found in the cladding next to the crack, suggesting a reason for the hot tearing of the cladding. The Cu was occasionally combined in the stringers with Ag and In.

Small quantities of the surface debris on each boat sample were scraped from the surface for SEM–EDX analysis. However, only the scrapings from Samples E–6, E–8,

E-11, and F–10 were analyzed. On Sample F–10, the fragmented particles ranged in size from ≈10 μm to a few millimeters and consisted principally of Fe and Cr–oxides with a few flecks of U–Zr. The structure was generally inhomogeneous, and Zr, In, and Ag were also found. The particles collected from E–8 were generally angular and, basically, fragments of fuel containing U, Zr, Fe, Ni, and Cr in widely varying concentrations. On E-11, the particles were agglomerates made up of small particles from <10 to ≈300 μm. The small particles were U and Zr fuel of varying compositions, and the agglomerate matrix was essentially Fe–oxide. The scrapings from the E-6 sample consisted of spherical and angular particles on the order of 100 μm and less. The spheroids were Fe and the angular particles resembled the inhomogeneous scrapings from the Sample F–10.

In summary, the scrapings appeared to be both material laid down during the accident and adventitious material (Fe spheres) that arrived later during sample removal. The collective inhomogeneity in composition of the fuel particles on the particulate scale contrasts with the apparent gross homogeneity of the mass of "companion" material that had lain on the lower head.[3] It is not possible to determine when during the accident these fuel fragments arrived on the lower head, i.e., before or during the massive fuel relocation to the lower head.

4 Results and Discussion

4.1 Metallographic Examinations

Results from the metallographic examinations of specimens from the lower head are summarized in Table 5. With a few exceptions, the the estimates of maximum temperature by the participating laboratories are in good agreement. Samples E-6, E-8, F-10, and G-8 attained the highest temperatures (up to ≈1100°C) during the accident, and these samples, along with one end of nearby Sample H-8, comprise the so-called "hot spot" that had been identified in preliminary work at ANL[4] and confirmed by more detailed examinations conducted at INEL.[1] It also appears that portions of Sample F-5, which was near the hot spot, the maximum temperature exceeded 727°C, and a small portion of sample M-11 also may have reached or slightly exceeded 727°C. The supporting metallographic observations for these samples are summarized below.

Sample E-6. Metallographic specimens from Sample E-6 were examined at ANL and INEL. The estimates of maximum temperature obtained by INEL[1] were based upon three general microstructural features, namely (1) the dissolution (which begins after ≈10 minutes at 900°C) of a thin feathery carbide layer at the cladding/base metal interface; (2) prior austenite grain size in the ferritic steel base metal, where grain growth is observed at ≈900°C, with significant growth at temperatures in excess of ≈1000°C; and (3) spheroidization of the delta ferrite islands in the austenitic weld cladding layer, which begins to occur at 1000-1100°C. The extent of carbon diffusion into the stainless steel from the base metal that is observed at the interface was also used as an indicator, as were the measured hardnesses of the base metal and interface regions. Standards were prepared by subjecting TMI-2 lower head material to carefully controlled heat treatments and comparing the resulting microstructural features in these standards with those observed in the metallographic samples.

Table 5. Summary of results from examinations of metallographic samples from TMI-2 lower head.

Sample No., Laboratory	Specimen Number	Maximum Temperature Attained During Accident (°C)
Sample D-10		
Italy	m1	<727
ANL	m3	<727
INEL	m2	<727
Sample E-6		
ANL	402A-1 and 4	1000-1100
INEL	m1	1075-1100
Sample E-8		
Belgium	m5	>727
Finland	m4 and m10	1100 in cladding; 950 at 34 mm below clad interface
France	m7	1000-1100
FRG	m9	>850; probably >1000
Spain	m6	>1000
ANL	m2	1000-1100
INEL	m3	1075-1100
Sample E-11		
ANL	m2	<727
INEL	m3	<727
Sample F-5		
Belgium	m5	>727 to 20-30 mm below clad (?)
FRG	m6	730-850 to ≈15 mm below clad
UK	m4	>727 to 15 mm below clad; ≈727 to 40 mm below clad
ANL	m2	<727
INEL	m3	<727
Sample F-10		
UK	m4	>727
ANL	m2	900-1000
INEL	m3	1040-1060

Table 5. Summary of results from examinations of metallographic samples from TMI-2 lower head (cont'd.).

Sample No., Laboratory	Specimen Number	Maximum Temperature Attained During Accident (°C)
Sample G-8		
ANL	408P-2,3, and 4	1000-1100
INEL	m1	1040-1060
Sample H-4		
FRG	m5	<727
Italy	m4	<727
UK	m6	less than but possibly near 727
ANL	m2	<727
INEL	m3	<727
Sample H-5		
FRG	m5	<727
UK	m1	less than but possibly near 727
ANL	m3	<727
INEL	m2	<727
Sample H-8		
ANL	m3	<727
INEL	m2	>727 at one end
Sample K-7		
FRG	m6	<727
Spain	m5	<727
UK	m4	<727
ANL	m2	<727
INEL	m3	<727
Sample K-13		
Belgium	m4	<727
FRG	m5	<727
UK	m9	<727
ANL	m2	<727
INEL	m3	<727

Table 5. Summary of results from examinations of metallographic samples from TMI-2 lower head (cont'd.).

Sample No., Laboratory	Specimen Number	Maximum Temperature Attained During Accident (°C)
Sample L-9		
France	m10	<727
FRG	m9	<727
UK	m7	less than but possibly near 727
ANL	m2	<727
INEL	m3	<727
Sample M-8		
FRG	m4	<727
UK	m1	less than but possibly near 727
ANL	m2	<727
INEL	m3	<727
Sample M-11		
France	m7	<727
FRG	m5	<727
Spain	m6	<727
UK	m4	≥727 to a few mm below clad; <727 in remainder
ANL	m2	<727
INEL	m3	<727

The cladding/base-metal interface region of Sample E-6 was not examined at INEL because their metallographic laboratory can only work with nonradioactive material and they were unable to completely decontaminate the interface sample provided by ANL. Instead, a second metallographic sample from E-6, which included only the completely decontaminated base metal, was examined. This means that the interface carbide layer and the delta ferrite phase in the cladding were not examined directly at INEL. However, from their examinations of the base-metal sample and from hot-cell photomicrographs of the interface provided by ANL, INEL personnel concluded from their established criteria that Sample E-6 had reached a maximum temperature of 1075-1100°C near the surface. INEL personnel also inferred a cooling rate of 10-50°C/min from the hardness values.

The maximum temperature of between 1000 and 1100°C estimated by ANL for Sample E-6 was based upon several observations. First, a heat-affected zone produced by the weld cladding process is normally present in the base metal to a depth of ≈8 mm below the cladding/base-metal interface. The absence of this heat-affected zone

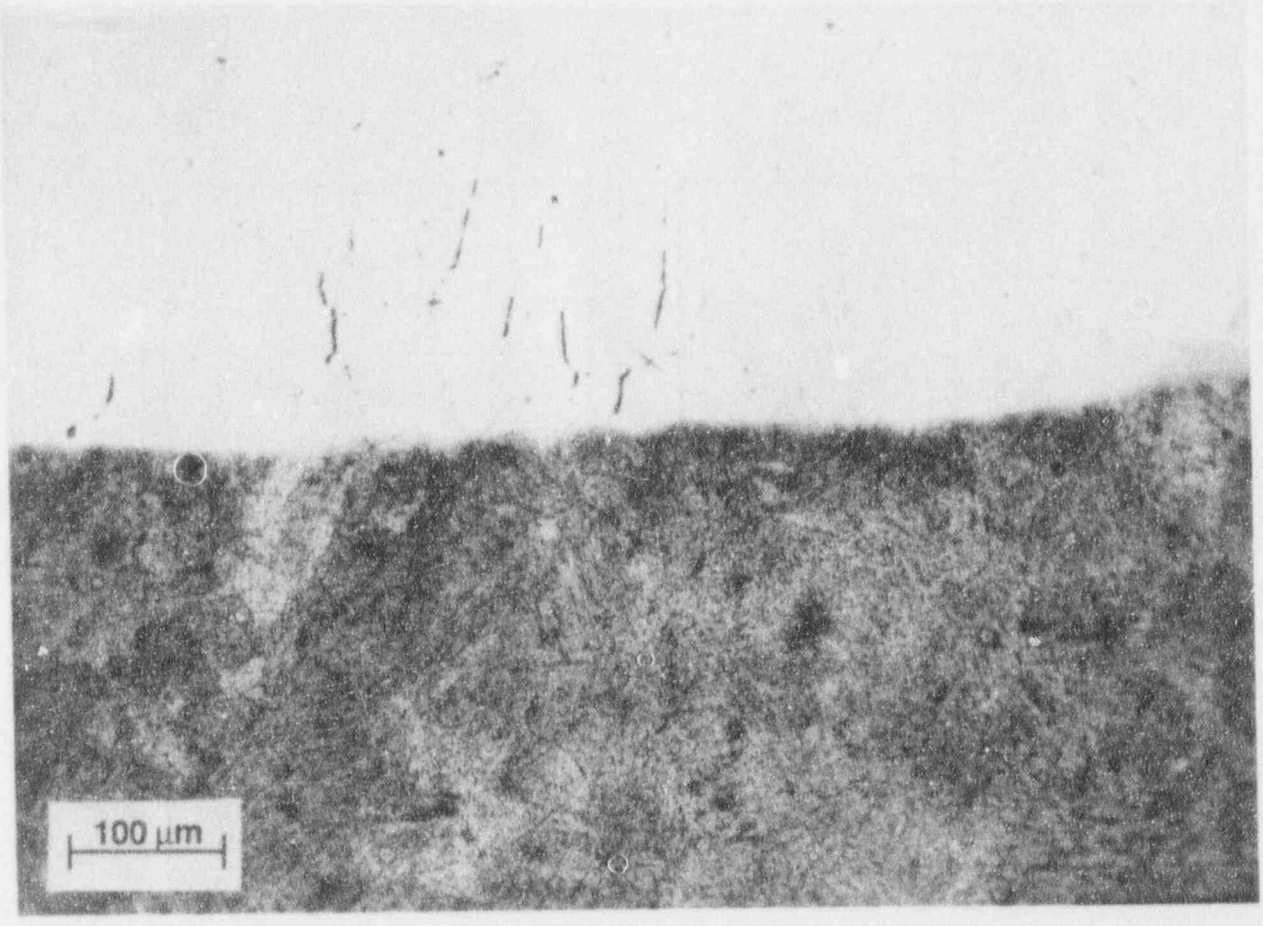

Fig. 14. Metallographic specimen from lower head sample E-6 showing absence of feathery carbide precipitate layer at cladding/base-metal interface. Note interdendritic cracking of cladding layer in upper half of micrograph.

indicates that the base metal reaustenitized during the accident. Since reaustenitization upon heating begins at 727°C and is complete at ≈830°C for A533, Grade B steel, this observation indicates a maximum temperature in excess of 727°C and probably in excess of 830°C. The absence of a feathery carbide layer at the cladding/base-metal interface suggested a maximum temperature in excess of 900°C (Fig. 14). For comparison, the intact carbide layer at the cladding/base metal interface is shown in Fig. 15 for Sample K-13, which did not exceed the ferrite-to-austenite transformation temperature of 727°C during the accident.[5] In addition, the prior austenite grain size in the bainitic microstructure of Sample E-6 near the interface corresponded to that produced in the Midland archive material by a 2-h isothermal heat treatment at 1000-1100°C. The spheroidization and partial redissolution of the delta ferrite phase in the weld cladding indicated similar maximum temperatures (Fig. 16). At 50 mm below the interface, the grain size corresponded to that produced by a similar heat treatment at 900-1000°C. The observed hardness of 250-260 VHN in the base metal suggested a cooling rate of between 10 and 100°C/min from the austenitizing temperature.

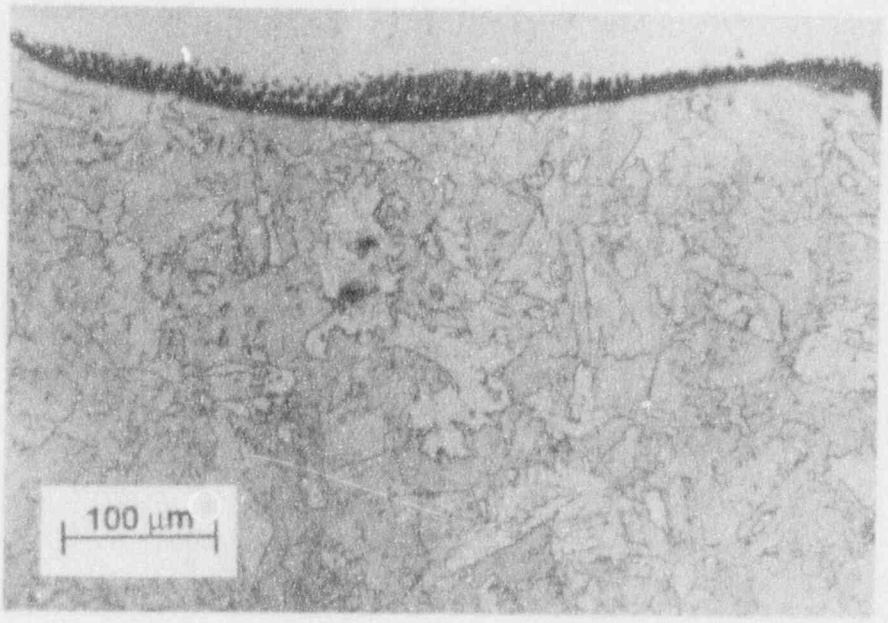

Fig. 15. Metallographic specimen from lower head Sample K-13 showing presence of feathery carbide precipitate layer at cladding/base-metal interface. The maximum temperature did not exceed 727°C at this location during the accident. (From Ref. 5).

Sample E-8. Lower Head Sample E-8 was also examined at INEL and ANL. In addition, this sample was examined at the Study Centre for Nuclear Energy (SCK/CEN) in Belgium,[5] the Technical Research Centre (VTT) of Finland,[6] the Centre d'Etudes Nucleaires de Saclay (CEN) in France,[7] the Staatliche Materialprüfungsanstalt (MPA) in the Federal Republic of Germany (FRG),[8] and Equiptos Nucleares S. A. (ENSA) in Spain.[9]

Based upon comparisons with standard microstructures produced in both heat-treated Midland archive material and samples of lower head material, INEL researchers concluded that the maximum temperature attained in Sample E-8 was between 1075 and 1100°C at the interface, assuming a time-at-temperature of 30 min. They further estimated that the maximum temperature at 45 mm below the interface was ~50-150°C lower than the peak interface temperature. A cooling rate of 10-50°C/min was again inferred. The examination at ANL indicated a maximum temperature of 1000-1100°C for this sample, based upon prior austenite grain size in the bainite and the spheroidization of the delta ferrite phase in the weld cladding. The cooling rate was again estimated to be between 10 and 100°C/s.

The examination conducted at the SCK/CEN in Belgium revealed the absence of a heat-affected zone in the base metal, spheroidization and partial dissolution of the delta ferrite phase in the cladding, and austenite grain growth near the interface (Figs. 17 and 18). These observations, coupled an the observed increase in hardness throughout the base metal, led to the conclusion that the maximum temperature of this specimen during the accident was substantially above 727°C.

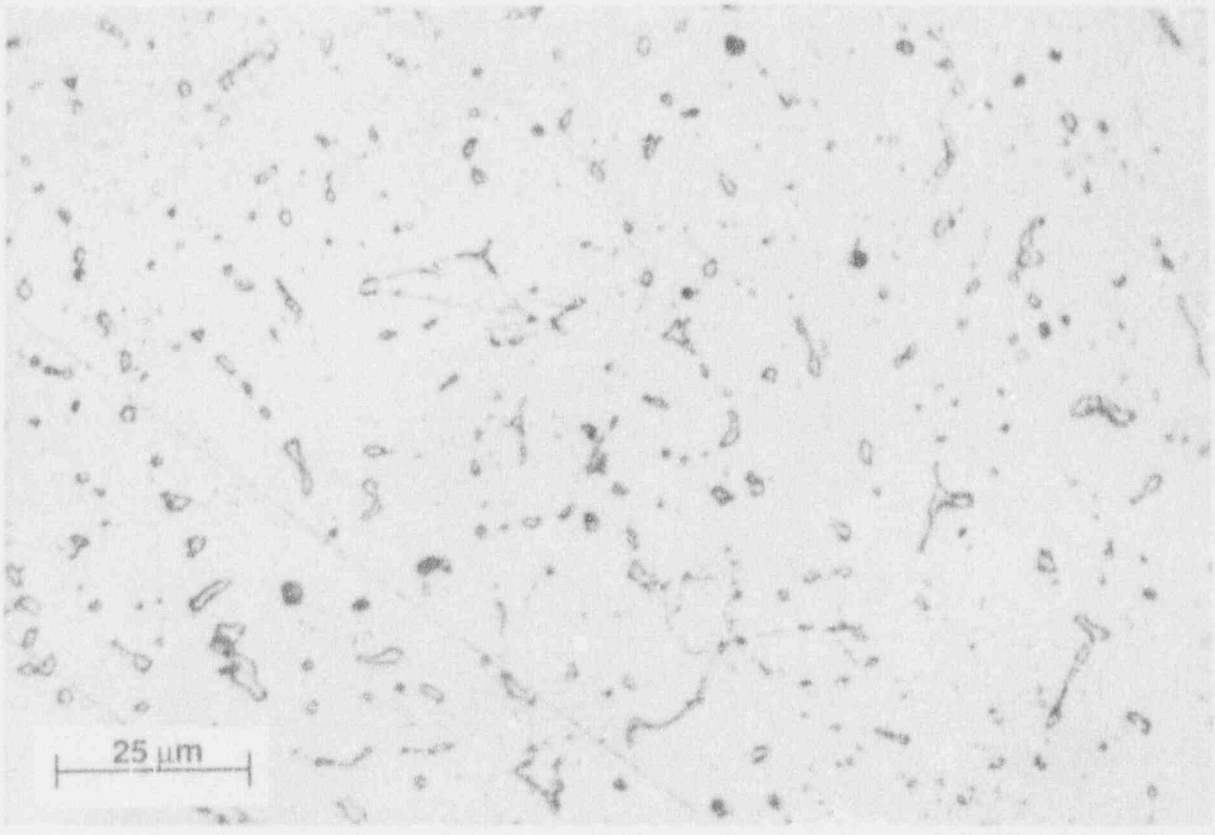

Fig. 16. Metallographic specimen from lower head Sample E-6 showing spheroidization of delta ferrite phase in Type 304L weld cladding layer.

The VTT of Finland conducted detailed optical metallographic and SEM examinations of two specimens from Sample E-8. They noted the same microstructural features as had been seen in the SCK/CEN investigation and estimated a maximum temperature of 1100°C in the cladding (Fig. 19), 1050°C at 2 mm below the interface, 1000°C at 21 mm below the interface, and 950°C at 34 mm below the interface. No cooling rate was estimated, but the study revealed that the cooling was sufficiently fast to produce full hardening through the specimen thickness but slow enough to permit some carbide precipitation and austempering of the bainite.

The examination conducted by the CEN in France similarly deduced maximum base-metal temperatures of 1000-1100°C, based upon the absence of a heat-affected zone, the observed austenite grain size, and measured hardnesses. They estimated the cooling rate to be much faster than the 1°C/min that they used in their simulation experiments, and probably of the order of 50-100°C/min.

Personnel at the MPA in FRG also observed the absence of a heat-affected zone in the base metal of Sample E-8, the dissolution of carbides at the interface, and hardnesses characteristic of complete austenitization during the accident. They estimated the maximum temperature to have exceeded 850°C and probably 1000°C.

Fig. 17. Metallographic specimen from lower head Sample E-8 showing spheroidization of delta ferrite phase in cladding. (From Ref. 5)

The examination conducted at ENSA in Spain likewise observed the absence of a heat-affected zone in the base metal, the elimination of the thin carbide layer at the interface, the larger prior austenite grain size in the base metal, and a reduction in the amount of delta ferrite in the weld overlay (Fig. 20). From this evidence, they deduced a maximum temperature >1000°C.

Sample F-10. Sample F-10 was examined at INEL, ANL, and Harwell Laboratory in the U.K.[10] Using examination techniques similar to those described above for Sample E-8, INEL personnel estimated the maximum temperature of this sample to have been between ≈1040 and 1060°C at the interface, and the cooling rate was again placed at between 10 and 50°C/min. The examination at ANL suggested a slightly lower maximum temperature of between 900 and 1000°C, based primarily on the somewhat smaller prior austenite grain size as compared with Samples E-6 and E-8. The Harwell examination indicated that the maximum temperature had been "considerably above the A1" (727°C), based upon both microstructural evidence and observed hardness values (Fig. 21).

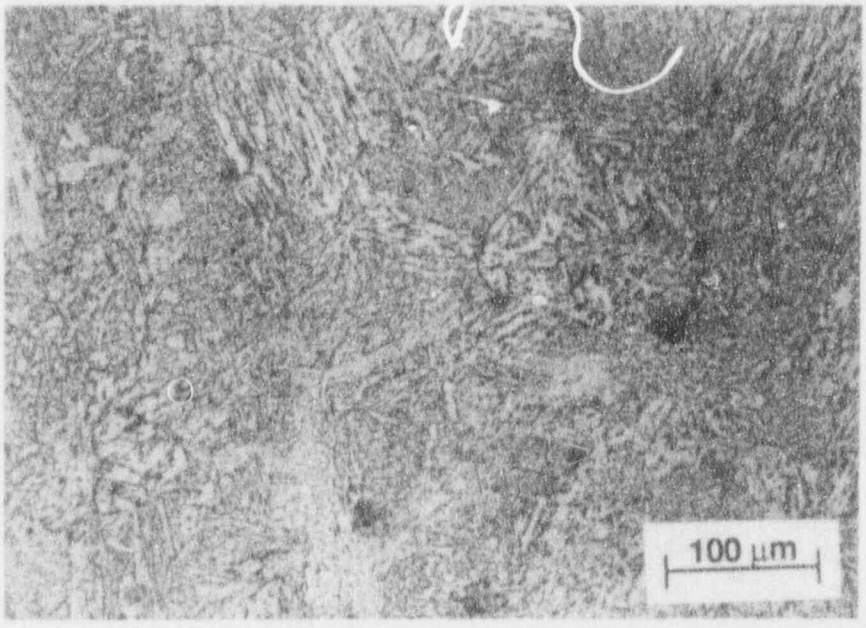

(a)

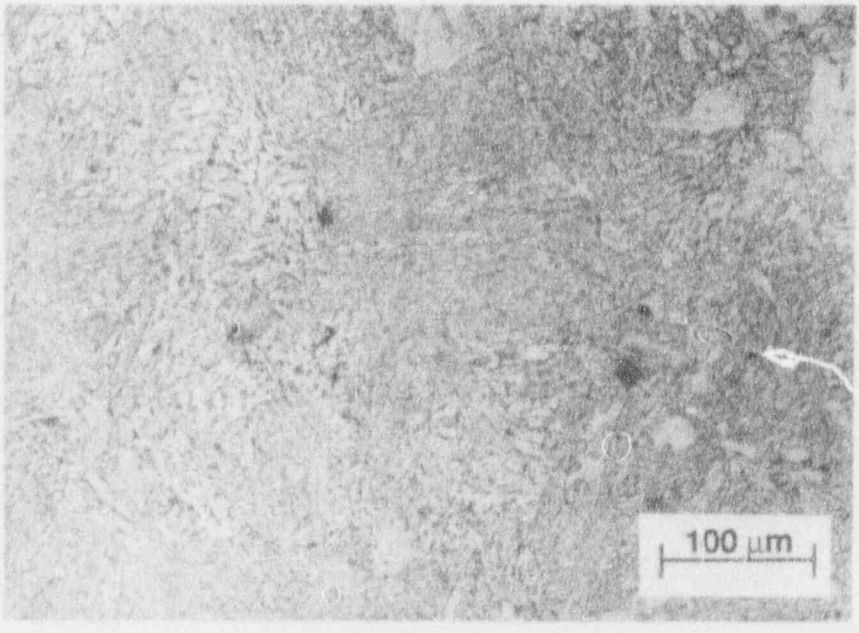

(b)

Fig. 18. Metallographic specimen from lower head Sample E-8 showing austenite grain growth in base metal (a) 1 mm below cladding/base-metal interface and (b) 3 mm below interface. (From Ref. 5)

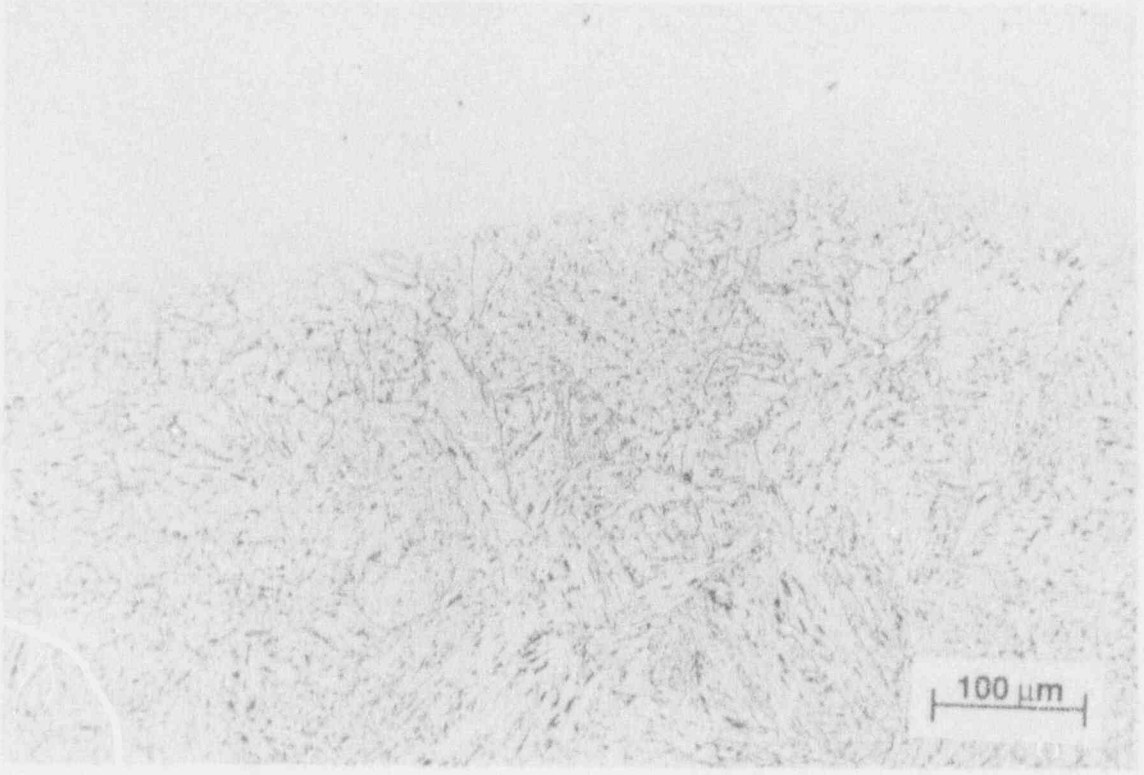

Fig. 19. Metallographic specimen from lower head Sample E-8 showing absence of carbide layer at cladding/base-metal interface. (From Ref. 6)

Sample G-8. Sample G-8 was the last of the four lower head samples that were entirely within the lower head hot spot. Metallographic specimens from this sample were examined at INEL and ANL. Because of extensive cladding cracking and the penetration of these cracks by core material, it was again not possible to obtain for INEL a completely decontaminated metallographic specimen that included the cladding and interface regions. Instead, worker at INEL inferred the maximum temperature of this sample from prior austenite grain size in the base metal. Because the microstructure was similar to that present in Sample F-10, they estimated the maximum temperature to be between 1040 and 1060°C. The examination at ANL placed the maximum temperature in the range of 1000-1100°C. The cooling rate was again estimated to be between 10 and 50°C/min by INEL and between 10 and 100°C/min by ANL.

Sample F-5. Sample F-5 was adjacent to one end of the "hot spot" identified near the bottom of the TMI-2 lower head. While ANL and INEL found that their metallographic specimens had not exceeded 727°C, observations at Belgium, FRG, and the U.K. on adjacent metallographic specimens (see Appendix A) suggested a maximum temperature slightly in excess of 727°C, although the results from Belgium were somewhat ambiguous.

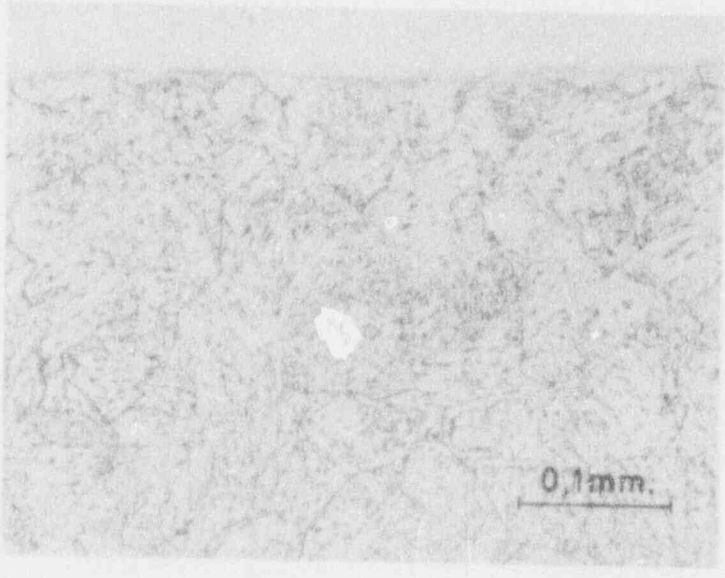

(a)

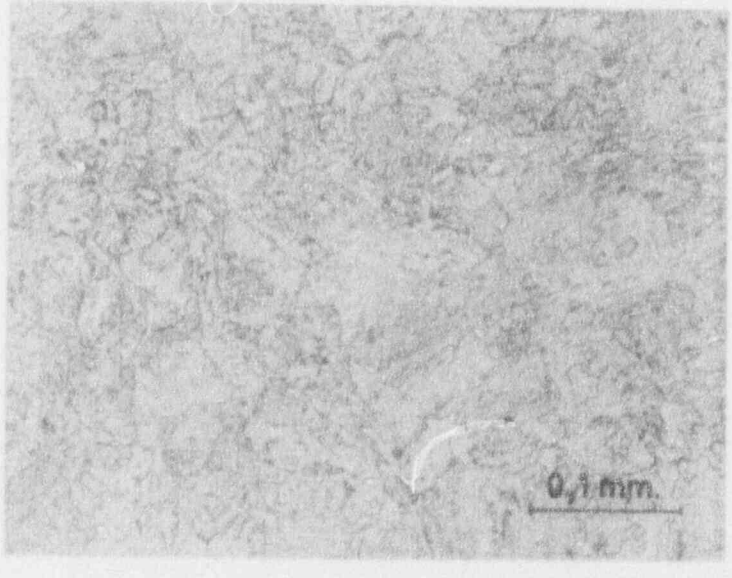

(b)

Fig. 20. Metallographic specimen from lower head Sample E-8 showing (a) absence of carbide layer at cladding/base-metal interface and (b) austenite grain growth in base metal 4 mm below interface. (From Ref. 9)

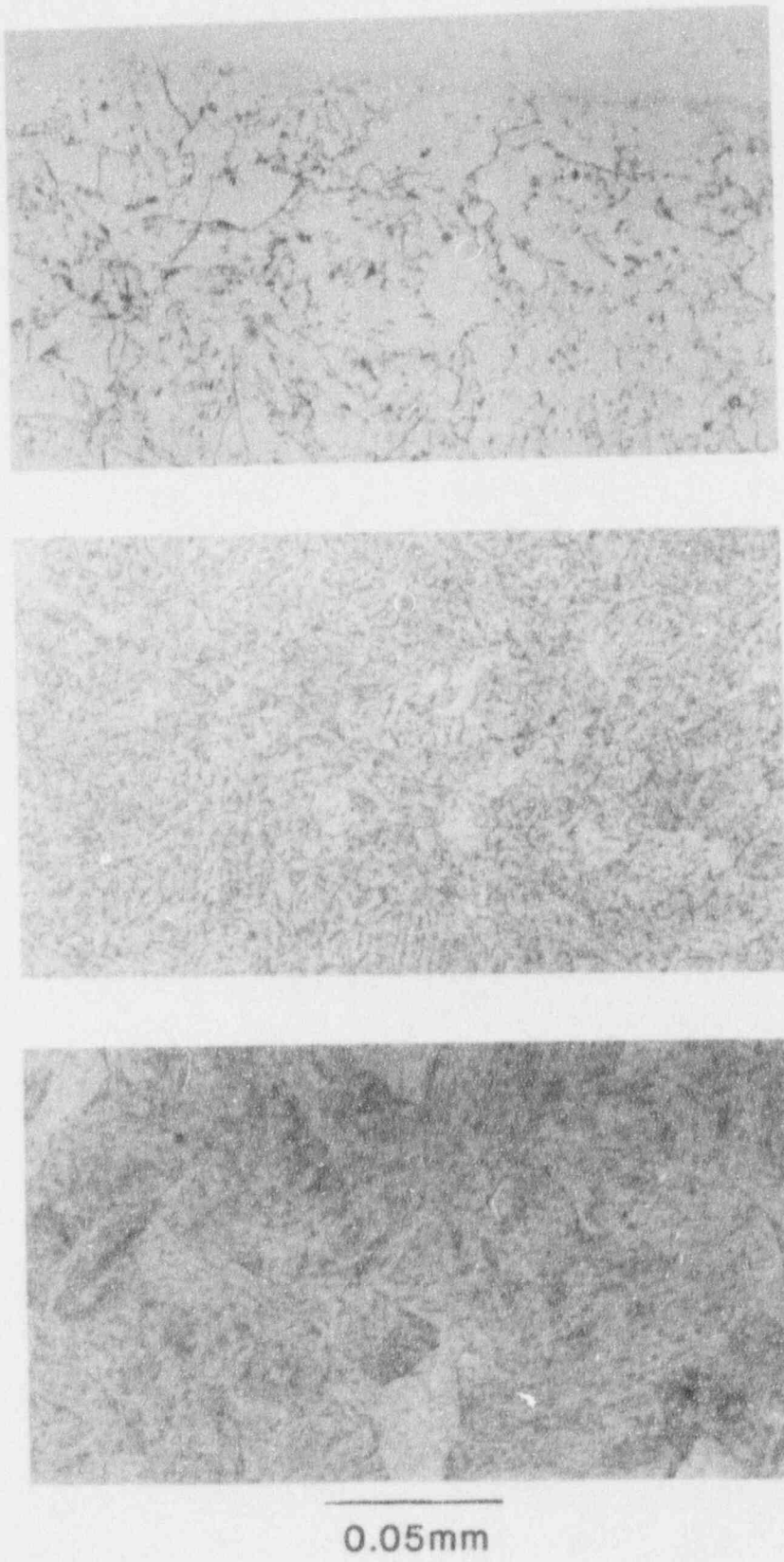

Fig. 21. Metallographic specimen from lower head Sample F-10 showing absence of carbide layer at cladding/base-metal interface (a) and austenite grain growth in base metal 1 mm (b) and 5 mm (c) below interface. (From Ref. 10)

The conclusion at INEL and ANL that the maximum temperature of Sample F-5 was <727°C was based primarily upon hardness measurements and the observation that the heat-affected zone in the base metal produced by the weld cladding was still present. After the European laboratories reported maximum temperatures somewhat in excess of 727°C, hardness measurements were repeated at INEL on the reverse side of their specimen, thinking that perhaps a temperature gradient might be present through the thickness. However, these measurements again indicated a maximum temperature of <727°C.

At SCK/CEN in Belgium, a significant increase in hardness of the base metal to a depth of ≈30 mm below the cladding/base-metal interface was noted. This hardness increase corresponded roughly to a region of coarser, larger grained bainite that was present to a depth of ≈20 mm below the interface, suggesting that the temperature of the base metal had exceeded 727°C to a depth of 20-30 mm during the accident. However, the heat-affected zone in the base metal produced by the weld-cladding process was still clearly visible, as noted in the previous paragraph. As an alternate explanation, the Belgian researchers speculated that the transformation evidence observed in the first 20-30 mm of the base metal may have been produced by some unspecified local overheating after the vessel was heat treated but before the weld cladding was applied.

Investigators at the MPA in FRG noted an increase in hardness of the base metal to a depth of ≈15 mm below the interface. They found that the microstructure in this region corresponded to that produced by a partial reaustenitization (Fig. 22), and therefore concluded that the maximum temperature was between ≈730 and 850°C (the two-phase ferrite plus austenite region) during the accident.

The metallographic study conducted at Harwell Laboratory in the U.K. also revealed microstructural evidence of partial transformation to a depth of ≈15 mm below the interface. In addition, increased hardness was observed to a depth of ≈30 mm. Based upon these observations, the investigators concluded that the base metal temperature had exceed 727°C (but probably not 850°C) to a depth of ≈15 mm below the clad and had approached 727°C to a depth of ≈40 mm.

It should be noted that the hardness profiles determined for Sample F-5 by the SCK/CEN, the MPA, and Harwell all showed peak hardness of the order of 230-250 VHN extending for distances of 15-30 mm below the cladding/base-metal interface. This contrasts with the hardness profile obtained at INEL, where peak hardness of ≈210 VHN extended for only ≈5 mm below the interface. Thus, it appears that the observed transformations were quite localized in this sample, in keeping with its location near the perimeter of the lower head hot spot.

Sample H-8. Limited material for metallographic specimens was also available from Sample H-8, and examinations were conducted at INEL and ANL. As can be seen in the initial sectioning diagram for Sample H-8 in Appendix A, the metallographic specimens m2, examined by INEL, and m3, examined by ANL, were adjacent to each other at one end of the boat sample. This was the end most distant from the hot spot, and both samples were found not to have exceeded 727°C during the accident. Metallographic specimen m5 from the opposite end of Sample H-8 was subsequently

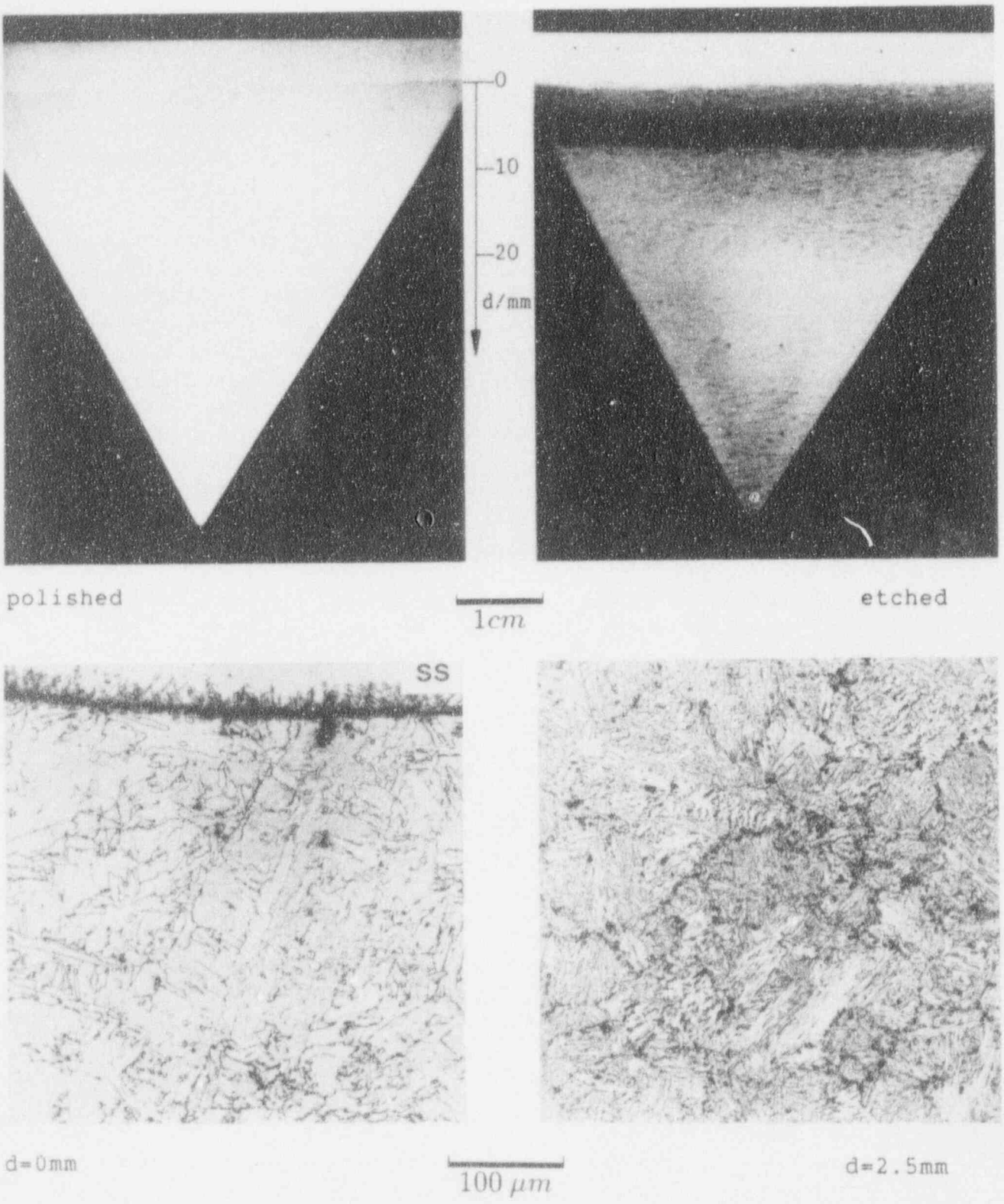

Fig. 22. Metallographic specimen from lower head Sample F-5 showing evidence of partial reaustenitization of base metal to a depth of ≈15 mm below the cladding/base-metal interface. (From Ref. 8)

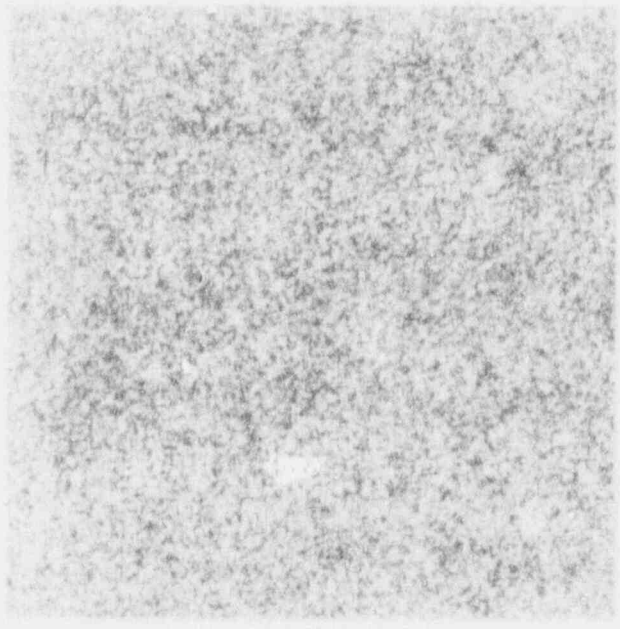

d=7mm 100 μm

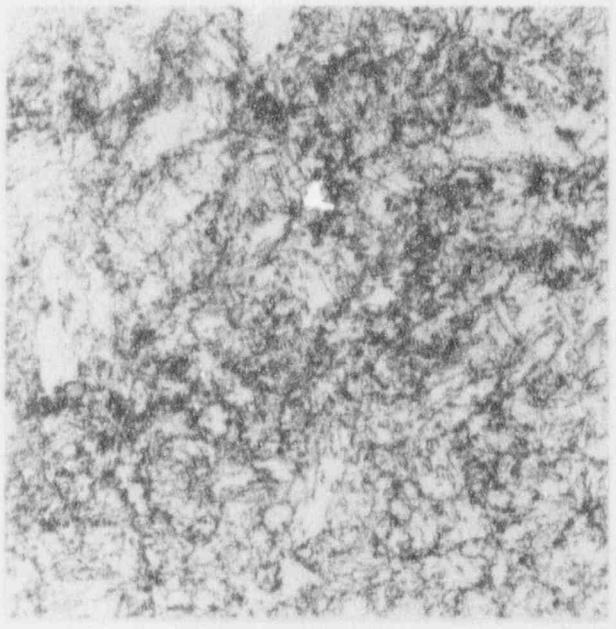

100 μm d=11mm

d=20mm 400 μm

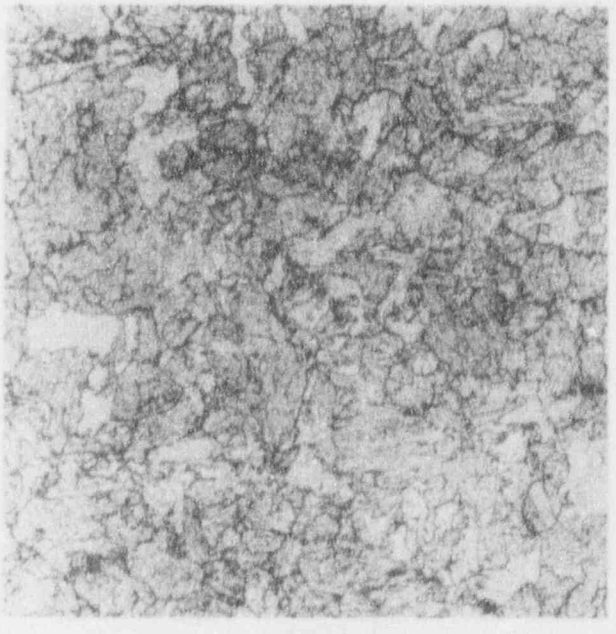

100 μm d=20mm

Fig. 22. (Cont'd.)

sent to INEL for examination to see if a temperature gradient existed along the sample length. Unfortunately, this specimen contained embedded radioactive contamination that INEL was unable to remove, so it could not be examined.

Longitudinal strips remaining after the tensile specimens were cut from Sample H-8 were then sent to INEL for metallographic and hardness studies. These strips are indicated in the second sectioning diagram for Sample H-8 (Appendix A) as pieces x3, x4, x5, x9, x10, and x15. Hardness measurements indicated that three of the strips had exceeded a temperature of 727°C near the end adjacent to Sample G-8 and the hot spot. The observed distances from the end nearest G-8 over which transformation had occurred were ~15 mm for specimens x15 and x10 and ≈25 mm for specimen x4. Specimen x15 was from the bottom of the sample and x10 and x4 were from the same side. As expected, the transformation distance was greatest for specimen x4, which was nearest the surface. The orientation of Sample H-8 relative to the hot spot suggests that the side containing specimens x3, x5, and x9 should have been slightly closer to the high-temperature region. However, none of these three samples was found to have exceeded 727°C over any portion of its length. In any case, it seems clear that the end of Sample H-8 nearest the hot spot did exceed 727°C during the accident.

Sample M-11. Metallographic specimens from Sample M-11 were examined at INEL, ANL, CEN in France, MPA in FRG, ENSA in Spain, and Harwell in the U.K. Results obtained at the first five laboratories indicated that the maximum temperature at this location had not exceeded 727°C. However, the examination conducted by Harwell in the U.K. revealed subtle microstructural evidence near the interface that suggested that the base metal had attained or slightly exceeded the A1 transformation temperature of 727°C for a distance of 5 mm or less below the interface with the cladding (Fig. 23). Because Sample M-11 was located ≈1.5 m from the center of the hot spot, this finding suggests that portions of the lower head away from the hot spot still reached rather high temperatures during the accident and that, locally, these temperatures may have approached or even slightly exceeded 727°C near the interface.

Other Samples. Metallographic and hardness results from the remaining lower head samples, including results from examinations performed in Italy that were not described above,[11] indicated that none of the samples exceeded 727°C during the accident. However, researchers at the Harwell Laboratories noted significant tempering of the bainite microstructure in the base metal of Samples H-4, H-5, M-8, and L-9, suggesting that the temperature in these samples probably approached 727°C, at least near the surface.

4.2 Tensile Tests

The results of the tensile tests conducted on the lower head specimens are presented in Table 6 for the base-metal specimens and Table 7 for the cladding specimens. These tests, carried out at ANL as well as in Belgium,[5] France,[7] and Spain,[12] were conducted in general accordance with ASTM Standards E8 and E8M, and all elevated-temperature tests were conducted in an Ar or He environment. The strain rate for the elastic portion of the loading was $\leq 5 \times 10^{-4}$ s^{-1}, and the strain rate during plastic loading was 4×10^{-4} s^{-1} $\pm 1 \times 10^{-4}$ s^{-1}. The reported yield strength values

Fig. 23. Microstructure of lower head Sample M-11 at cladding/base metal interface (a), 2 mm below interface (b), and 6 mm below interface (c) showing evidence of partial reaustenitization. (From Ref. 10)

were obtained by the 0.2% offset method, except where discontinuous yielding occurred; in these cases, the observed upper yield strength is reported.

The base-metal tensile and yield strength data of Table 6 are plotted in Fig. 24, together with average values reported by the the Japanese National Research Institute for Metals (NRIM) for five other heats of A533, Grade B steel.[13] The NRIM data were obtained at a strain rate of 5×10^{-5} s^{-1} up to yield and 1.25×10^{-3} s^{-1} for the remainder of the test. The NRIM tensile strength data suggest a strain-aging effect between 100 and 300°C, resulting in a local tensile strength minimum at ≈150°C. Both the tensile and yield strengths of this alloy are strongly temperature dependent; the room-temperature values are reduced by more than a factor of 2 at 600°C and by more than a factor of 10 at 900°C.

The data for specimens taken from lower head samples E-6 and E-8 are plotted separately in Fig. 24, and these data lie significantly above the best-fit curve to the remaining data. Both of these samples were heated to maximum temperatures of ≈1000-1100°C during the accident, followed by a relatively rapidly cooling. The resulting hardening has produced significant increases in strength at both room temperature and 600°C. On the other hand, no perceptible strengthening is seen in specimens from sample M-11, which came from a location where the maximum temperature may have approached or slightly exceeded 727°C near the surface.

Limited tensile data obtained on the stainless steel cladding material are reported in Table 7. Additional tests were not performed because it was determined that the analysts were not planning to include any structural contribution by the cladding layer to the mechanical behavior of the lower head.

4.3 Creep Tests

The creep test results are summarized in Table 8 and the stress-vs.-time-to-failure data are plotted in Fig. 25. These tests were carried out at ANL and in Belgium,[5] France,[7] and Spain,[14] and they were conducted in general accordance with ASTM Standard E139. The tests were conducted in an Ar or He environment except those conducted by the SCK/CEN in Belgium. All but one of the Belgian tests was conducted in vacuum, as indicated in the table; a single test at 800°C and 30 MPa was conducted in an Ar environment. Strain-vs.-time curves from the creep tests of Table 8 are presented in Appendix B. However, no curves are available for the three creep tests conducted in France at 1100°C.

Materials with slightly different thermal histories were tested at both 600 and 700°C. At 600°C, tests were conducted on specimens from Sample K-13, for which the maximum temperature during the accident did not exceed 727°C, as well as on specimens from Sample F-5, for which the maximum temperature was apparently somewhat >727°C over a portion of the sample. No significant difference in time to failure is observed in Fig. 25. This lack of an effect may be attributed to the fact that the maximum temperature probably did not significantly exceed the transformation temperature of 727°C in F-5, particularly in the bottom half of the sample from which the creep test specimens were taken. Similarly at 700°C, specimens from Sample M-11, for which the maximum temperature may have approached or slightly exceeded

Table 6. Summary of tensile data obtained from base-metal specimens of the TMI-2 lower head.

Test Temp.; Country	Sample No.	Max. Temp. (°C)	Specimen No.	Tensile Strength (MPa)	Yield Strength (MPa)	Uniform Elong. (%)	Total Elong. (%)	Reduct. of Area (%)
Room Temperature								
Belgium	K-13	<727	t7	594	414	11	24	72
France	M-11	~727	t7	581	408	11	22	65
Spain	K-7	<727	t7	600	426	13	29	63
U.S.	L-9	<727	t18	592	423	15	24	67
	E-6	~1050	-	773	650	9.0	16	62
Belgium	E-8	~1100	t8	778	653	4.5	14	50
Spain	E-8	~1100	t7	769	633	9.2	18	51
600°C								
Belgium	K-13	<727	t11	257	253	0.8	25	72
France	M-11	~727	t8	239	224	1.2	33	75
Spain	K-7	<727	t8	247	238	3.2	48	81
U.S.	L-9	<727	t5	256	231	1.6	44	91
	E-6	~1050	-	382	344	4.0	40	74
700°C								
Belgium	K-13	<727	t12	120	106	1.7	77	90
France	M-11	~727	t9	146	136	1.6	42	66
Spain	K-7	<727	t9	110	89	4.8	83	87
U.S.	H-8	~727	t4	137	126	2.8	50	86
800°C								
France	L-9	1000[a]	t7	79	44	18	64	43
U.S.	G-8	~1050	t5	77	52	15	80	65
900°C								
Belgium	F-5	1000[a]	t10	49	38	13	43	31
Spain	L-9	1000[a]	t15	40	29	13	36	27
1000°C								
U.S.	H-8	~727	t5	30	20	14	42	35
France	L-9	<727	t12	32	21	9	23	23
1100°C								
Belgium	F-5	~727	t7	20	14	13	124	97
Spain[b]	L-9	<727	t16	19	11	13	(110)	-
1200°C								
U.S.	H-8	~727	t9	12.0	7.6	12	93	99
France[c]	L-9	<727	t11	18	13	7	>40	99

[a]Specimen heat treated by holding at 1100°C for 2 h and cooling to room temperature at 10-50°C/min to simulate severed damage.

[b]Test conducted at 1070°C because of experimental difficulties.

[c]Test conducted at 1150°C.

Table 7. Summary of tensile data obtained from cladding specimens of the TMI-2 lower head.

Test Temp.; Country	Sample No.	Max. Temp. (°C)	Specimen No.	Tensile Strength (MPa)	Yield Strength (MPa)	Uniform Elong. (%)	Total Elong. (%)	Reduct. of Area (%)
Room Temperature								
Belgium	F-5	~727	t2	553	330	37	40	30
U. S.	F-5	~727	t3	551	322	28	30	34
1100°C								
Belgium	F-5	~727	t1	30	29	0.8	16	14

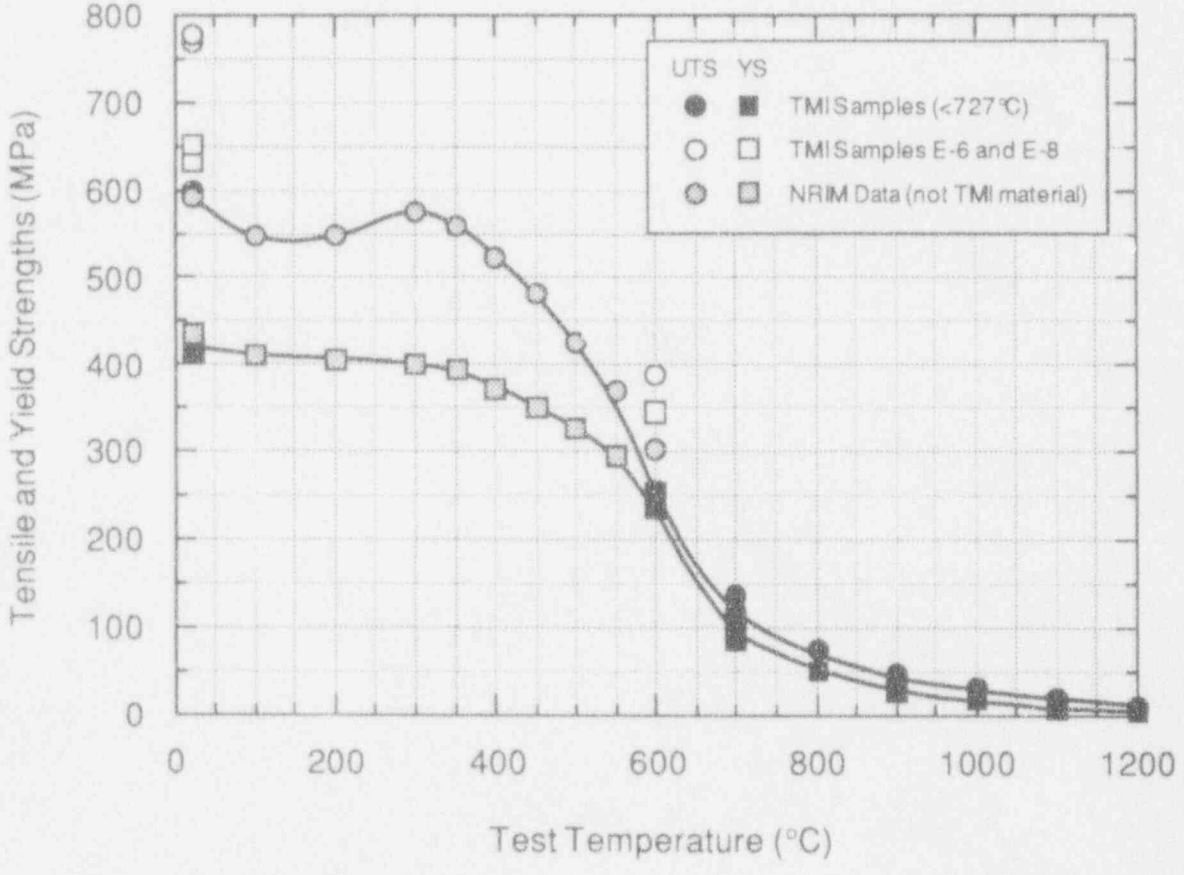

Fig. 24. Tensile and yield strengths of TMI-2 lower head material compared with Japanese National Research Institute for Metals (NRIM) data for other heats of A533, Grade B steel.

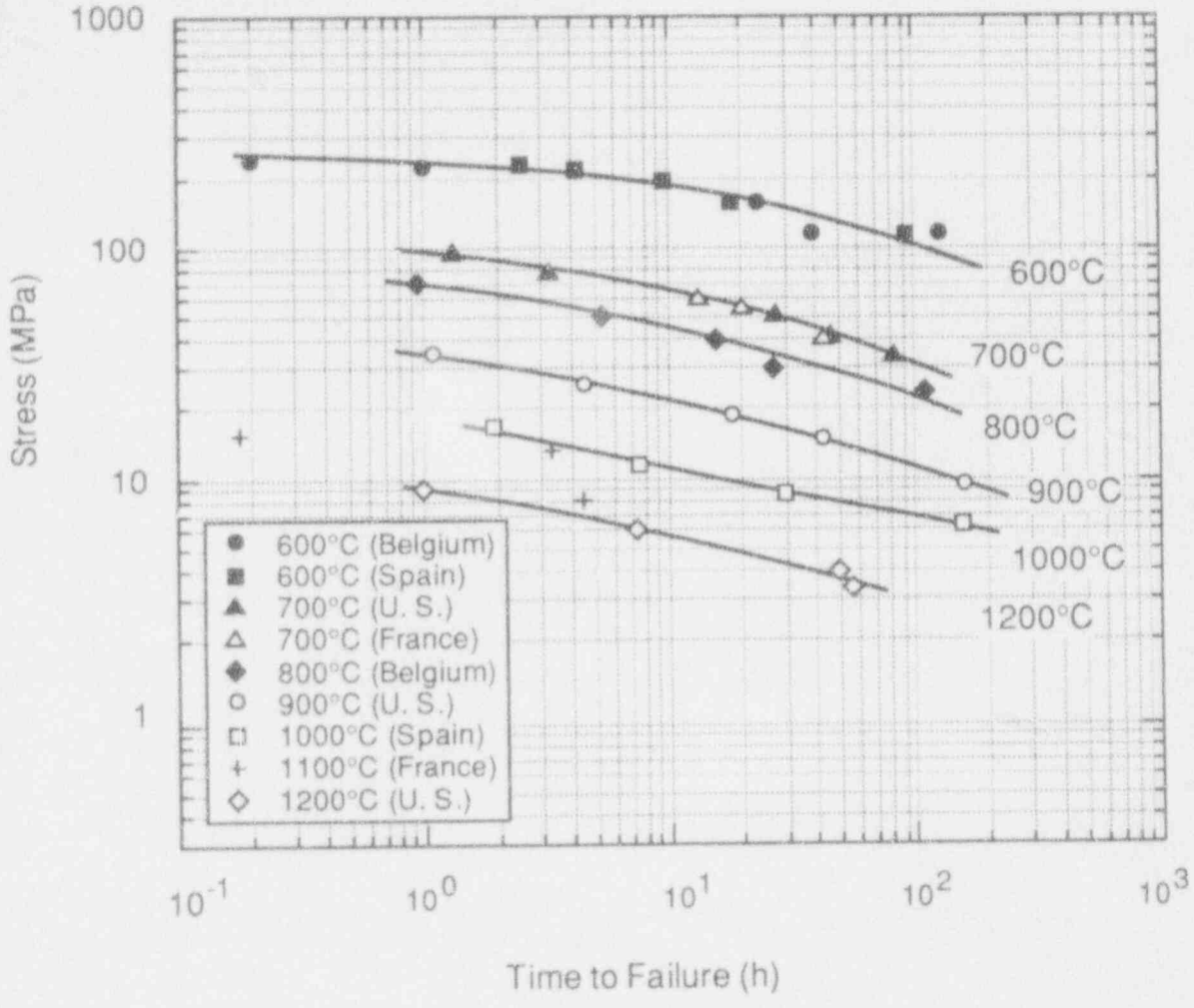

Fig. 25. Stress vs. time to rupture data from creep tests conducted on TMI-2 lower head material with estimated best-fit curves.

727°C, show no difference in behavior when compared with specimens from Sample H-8, for which the maximum temperature remained below 727°C.

The best-fit curves to the creep data from the lower-head specimens of Fig. 25 are replotted in Fig. 26 together with data previously obtained from the Midland archive material in OECD round-robin tests. The agreement between the 600°C data and that obtained in the round-robin tests is reasonably good. However, at higher temperatures, the best-fit curves to the lower-head data fall noticeably above time-to-failure data from tests on the archive material. These differences may be caused in part by differences in the microstructure and prior thermal-processing history of the two materials, but it seems unlikely that prior thermal history would have any effect in tests conducted at temperatures of 1000°C and greater.

Two time-temperature correlations were explored in an attempt to fit the creep data of Table 8. The first of these was the Larson-Miller parameter L[15]

Table 8. Summary of creep data obtained on specimens from TMI-2 lower head.

Test Temp.; Country	Sample No.	Max. Temp. (°C)	Specimen No.	Stress (MPa)	Time to Failure (h)	Elong. at Failure (%)	Reduct. of Area (%)
600°C							
Belgium	K-13	<727	t8[a]	240	0.2	36	81
			t13[a]	225	1.0	43	84
			t10[a]	155	23.1	37	33
			t9[a]	115	39	32	71
			t14[a]	115	128	23	22
Spain	F-5	~727	t14	232	2.47	42	73
			t18	221	4.14	57	76
			t15	194	9.47	47	65
			t16	157	17.75	51	73
			t17	114	92.8	51	41
700°C							
France	M-11	~727	t10	60	13.5	54.4	-
			t9	55	20	72.9	-
			t11	40	43	41.6	-
U.S.	H-8	~727	t17	95.1	1.34	34	85
			t16	80.0	3.27	33	82
			t13	52.1	27.6	73	89
			t14	41.6	46.0	77	93
			t15	34.5	81.6	96	90
800°C							
Belgium	F-5	1000[b]	t13[a]	70	0.95	67	44
			t11[a]	50	5.4	46	31
			t9[a]	40	15.5	45	29
			t8[a]	30	27	39	23
			t12[a]	23.7	111	43	23
900°C							
U.S.	H-5	1000	t16	35.0	1.09	41	30
			t15	26.0	4.55	36	30
			t14	19.0	18.1	39	45
			t11	14.8	42.3	40	30
			t12	9.51	159.5	33	30

Table 8. Summary of creep data obtained on specimens from TMI-2 lower head (cont'd.).

Test Temp.; Country	Sample No.	Max. Temp. (°C)	Specimen No.	Stress (MPa)	Time to Failure (h)	Elong. at Failure (%)	Reduct. of Area (%)
1000°C							
Spain	K-7	<727	t11	16.9	1.90	38	48
			t10	11.5	7.54	32	66
			t12	8.7	29.64	22	73
			t13	6.3	152.8	30	40
1100°C							
France	L-9	<727	t12	15.0	0.17	9.6	-
			t11	13.0	3.3	24.1	-
			t10	8.0	4.33	3.3	-
1200°C							
U.S.	M-8	<727	t6	9.0	0.98	96	99
			t5	6.0	7.26	115	99
			t4	4.0	48.2	99	99
			t7	3.4	55.1	81	99

[a]Tests conducted in vacuum; remaining tests were conducted in an Ar or He environment.

[b]Specimen heat treated by holding at 1100°C for 2 h and cooling to R.T. at 10-50°C/min to simulate severe damage.

$$L = T[C + \log_{10}(t_f)],$$

where T is temperature in Kelvin, t_f is time to failure in hours, and C is a fitting constant. A least squares analysis determined that the optimum value of C for the present data base was 12.5, and stress σ was related to the Larson-Miller parameter by the relation

$$\log_{10}(\sigma) = 4.3406 - 0.00018767 \cdot L, \qquad (1)$$

where the applied stress σ is in MPa. Figure 27 shows the present data plotted in the form of log(σ) vs. the calculated Larson-Miller parameter, assuming C = 12.5. The calculated coefficient of correlation r for this fit is 0.98277.

The creep data of Table 8 are replotted in Fig. 28 in the usual format, along with the Larson-Miller best-fit curves obtained as described above. The fit is only fair, with the straight-line fits inherent in the Larson-Miller correlation deviating noticeably from the actual data, particularly at the lower temperatures.

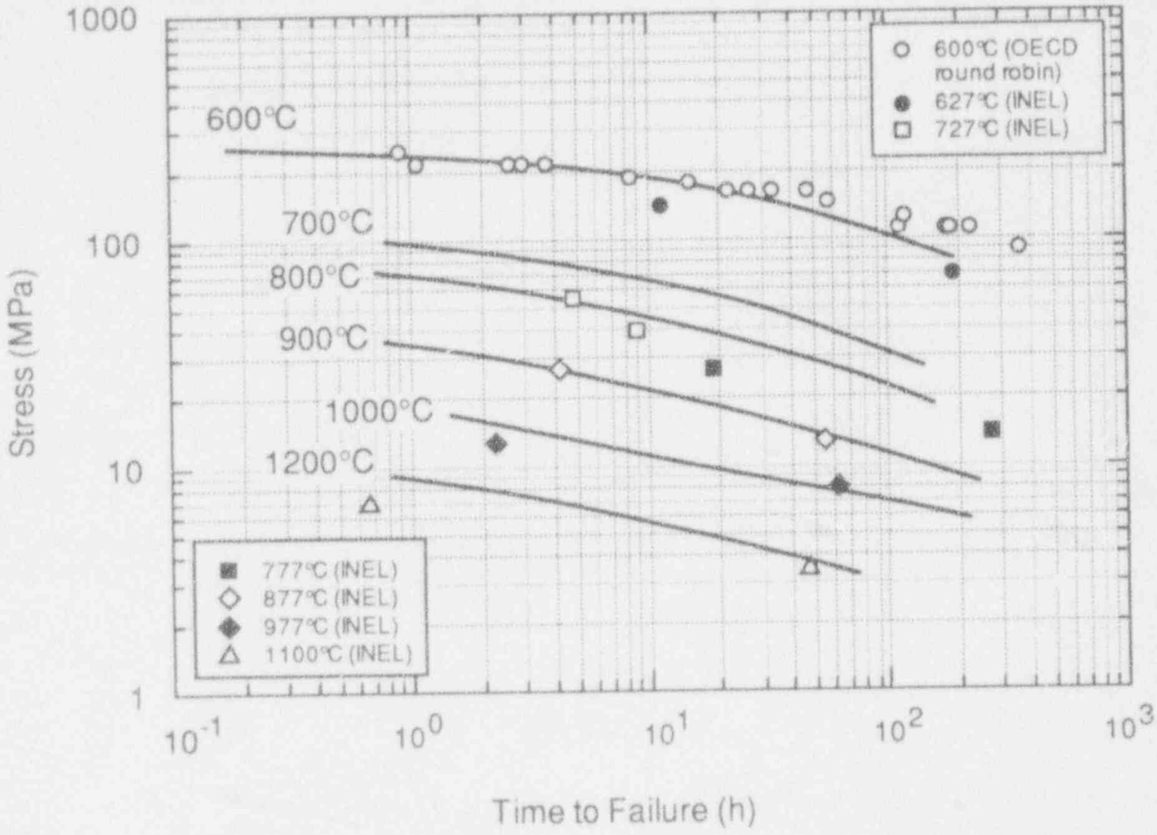

Fig. 26. Best-fit curves to data of Fig. 25 plotted vs. data previously obtained for Midland archive material in OECD round-robin tests.

The Manson-Haferd time-temperature correlation[16] was also evaluated in an attempt to obtain a better fit to the data. The Manson-Haferd parameter M has the form

$$M = \frac{\log_{10}(t_f) - t_a}{T - T_a},$$

where t_f is time to failure in h, T is test temperature in Kelvin, and t_a and T_a are fitting constants. A least squares analysis was again carried out, and the optimum values for t_a and T_a were found to be 7.57 and 520 respectively. The plot of log(σ) vs. M for the present data is shown in Fig. 29, and the best fit curve is the second order polynomial

$$\log_{10}(\sigma) = -0.80467 - 261.41 \cdot M - 5291.25 \cdot M^2. \qquad (2)$$

The calculated coefficient of correlation for this fit is 0.99347.

A comparison of the resulting best fit curves with the actual σ vs. t_f data in Fig. 30 shows an improved fit when compared to the Larson-Miller correlation. However,

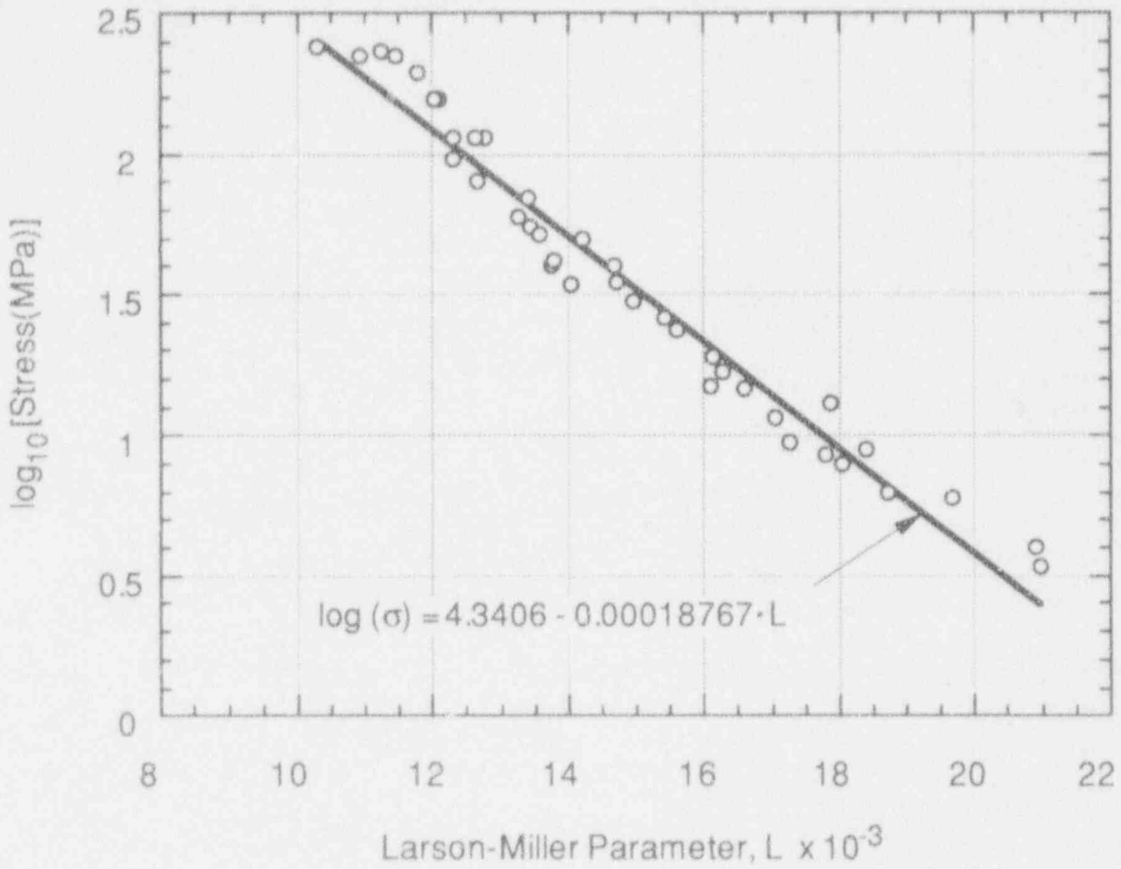

Fig. 27. Plot of log(σ) vs. Larson-Miller parameter (C = 12.5) for TMI-2 lower head material creep data.

systematic departures of the best-fit curves from the actual data are noted in the 700-900°C region. This problem may be associated, in part, with the ferrite-to-austenite phase transformation that occurs over the temperature regime from 727 to ~850°C.

4.4 Impact Tests

The Charpy V-notch impact data obtained in Italy[17] on specimens from the lower head are summarized in Table 9, and the absorbed impact energy is plotted as a function of test temperature in Fig. 31. The three groups of test specimens for which the maximum temperature did not exceed 727°C show similar behavior, with an upper shelf energy of ~170 J and a transition temperature of the order of 20°C. However, the data from specimens of Sample F-10, for which the maximum temperature was as high as ~1050°C, stand in marked contrast. The F-10 material shows a significantly higher ductile-to-brittle transition temperature of ~70°C, as well as a lower upper-shelf energy of ~120 J. These differences reflect the reduced ductility and impact resistance of that s produced in this material by the high temperatures and relatively rapid cooling associated with the accident.

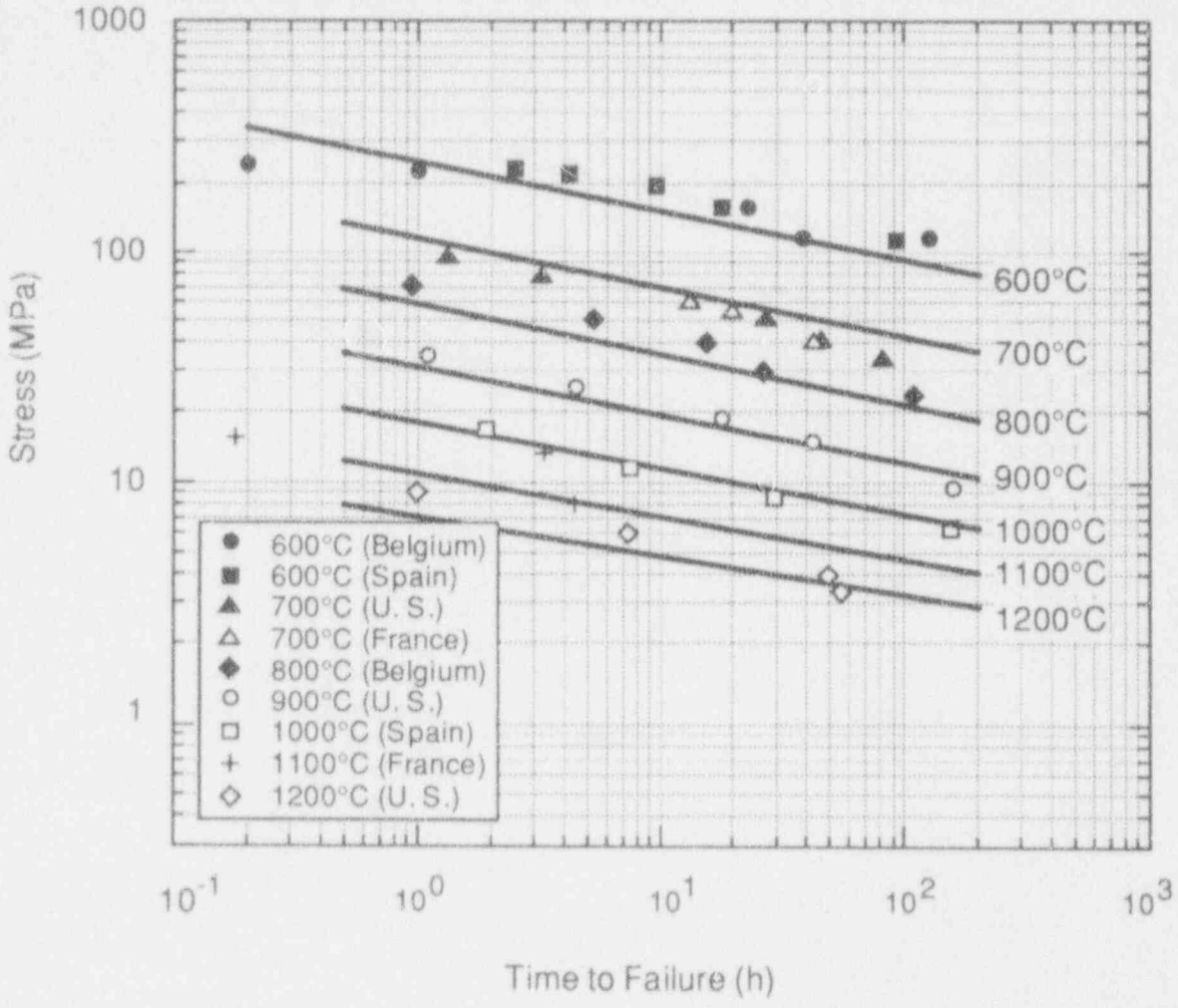

Fig. 28. Stress vs. time to rupture data from creep tests conducted on TMI-2 lower head material compared with best-fit curves from the Larson-Miller time-temperature correlation.

4.5 Cladding Cracks

Examination of Samples E–6 and G–8 suggests that the cladding failed by a process similar to hot tearing, causing extensive cracking along interdendritic boundaries. The precise nature of the loading that produced the cracks is not clear, but it apparently was caused by thermal stresses imposed as a result of the accident, probably during cooling. Microstructural examination of the underlying base metal and the results of tensile and hardness tests indicate that both samples reached temperatures of ≈1000-1100°C during the accident and then cooled rapidly. Temperatures of this magnitude would be expected to impose significant thermal stresses on the cladding and base metal during a transient event, reduce the resistance of Type 308L weld cladding alloy to hot tearing, and cause recrystallization of the base metal, thereby erasing any

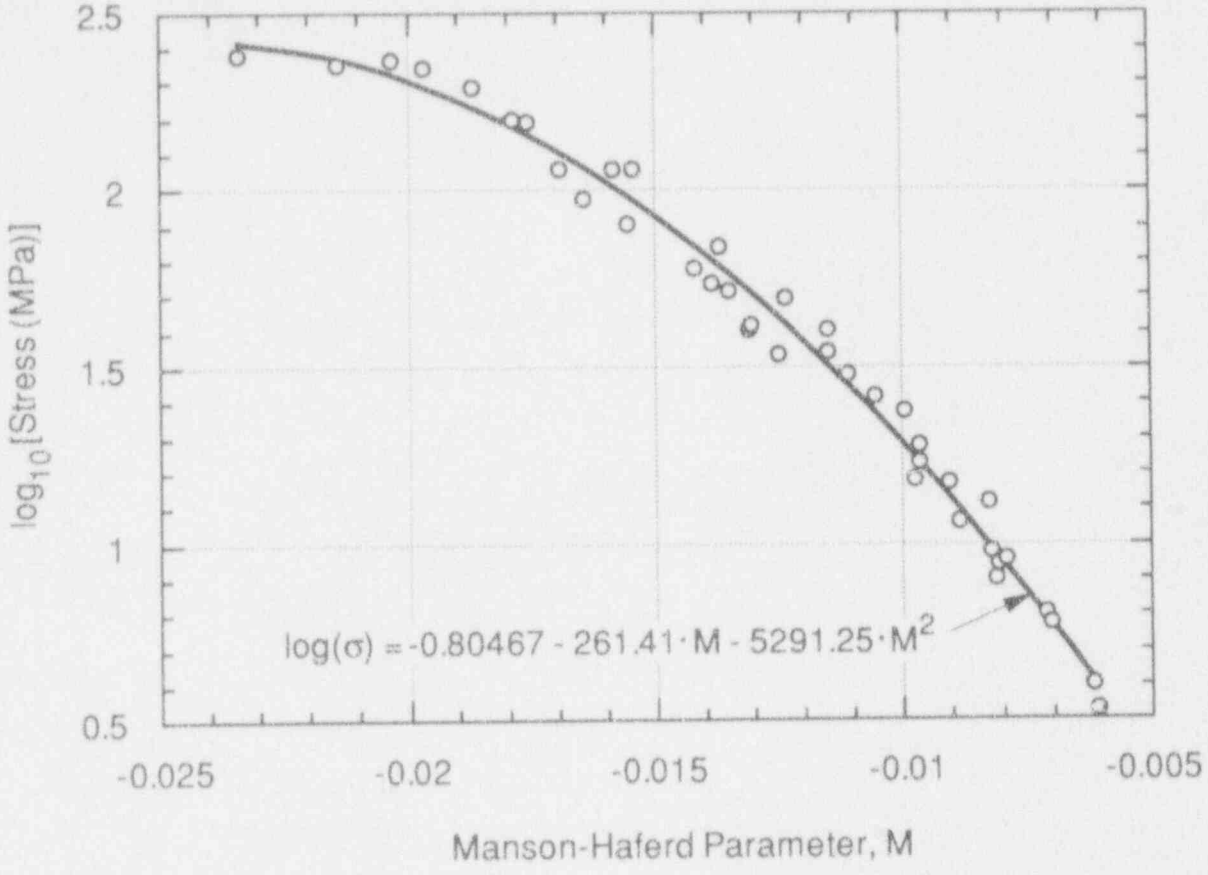

Fig. 29. Plot of log(σ) vs. Manson-Haferd parameter (t_a = 7.57, T_a = 520) for TMI-2 lower head material creep data.

evidence of deformation. Although the observed cladding cracking may have been produced by thermal shock during initial contact with the hot core materials, it is more likely that it occurred during the early stages of cooldown when the still-hot cladding layer was placed into tension because of thermal contraction of the underlying base metal. This latter process is analogous to hot tearing during welding, and produces cracks similar to those found in the F-10 sample. Because the cooling rate from the maximum temperature was relatively high (on the order of 10 to 100°C per min), significant thermal stresses would be expected. The cracking at the F-10 location was apparently less severe because the location was only at the periphery of what is believed to have been the hot spot in the vessel wall.

The composition and superposition of the reaction layers on the crack surfaces provide some clues to the sequence of events that took place during the accident. The crack surfaces in the stainless steel are covered by previously molten Fe–Cr-rich oxide layers that also contain In and Sn, and Ag–Cd precipitates. The molten In–Sn phase in the grain boundaries of the oxide in the ferritic steel also indicates that there was a source of the molten material when the high-temperature oxide was formed, probably very shortly after crack formation. Fuel particles were present only on top of these

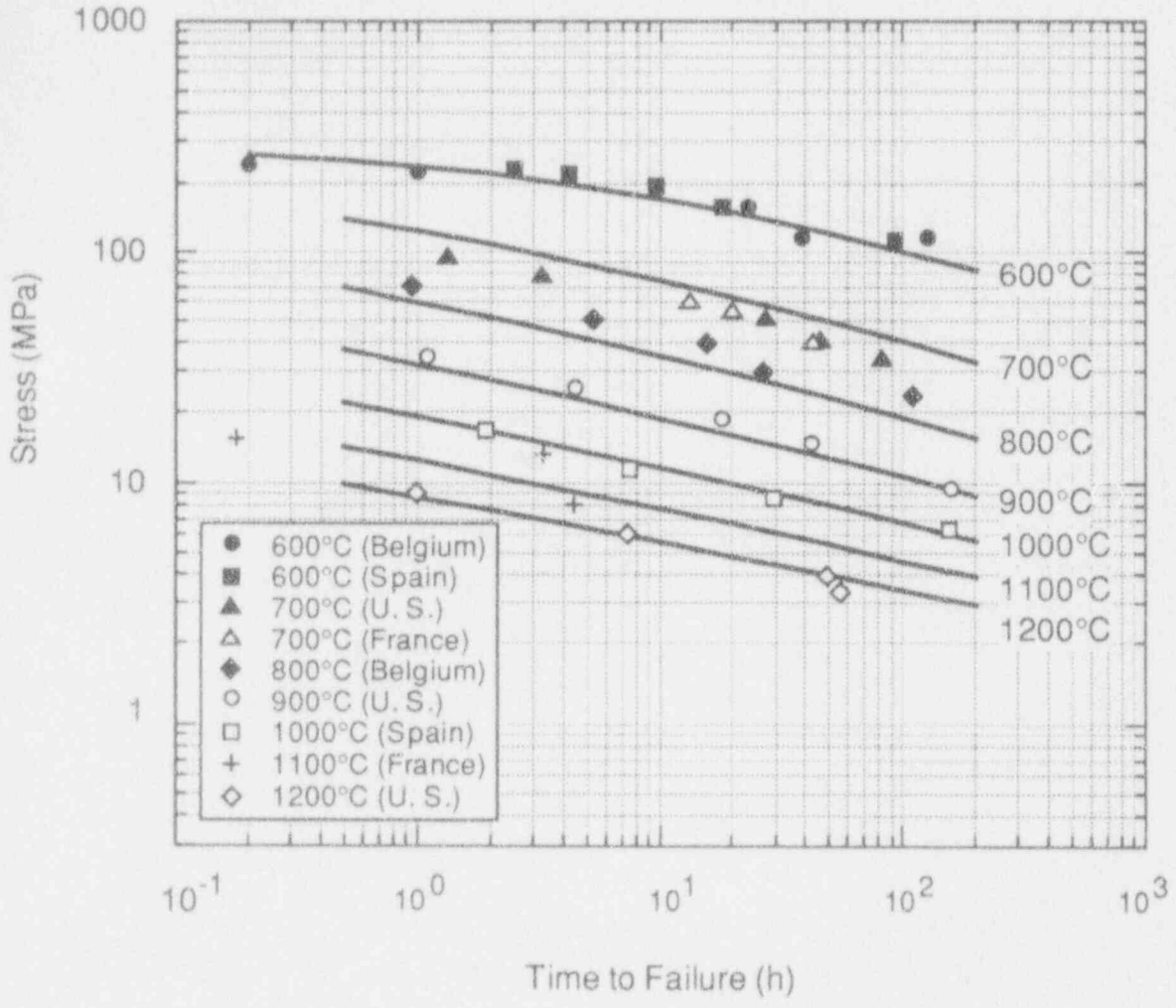

Fig. 30. Stress vs. time to rupture data from creep tests conducted on TMI-2 lower head material compared with best-fit curves from the Manson-Haferd time-temperature correlation.

solidified oxides or as very minor constituents in them. The absence of significant quantities of fuel that solidified in situ and reacted with the molten oxides on the stainless steel indicates that the massive flow of fuel to the lower head was not the source of these liquid materials. However, this massive flow could have been the source of the solidified-fuel shards found in the cracks atop the solidified oxides. This fuel would have solidified when it came into contact with the lower head, if not earlier in its movement from the core region.

The finding of numerous surface cracks and internal tears in the cladding that contained solidified Ag–Cd masses indicates that a molten source of these materials was on the lower head when the cracks formed. It is also quite likely that penetration of these liquid materials interdendritically into the cladding contributed to the hot-tearing of the cladding.

Table 9. Summary of Charpy V-notch impact data on specimens from TMI-2 lower head.

Specimen Number	Test Temperature (°C)	Energy (J)	Ductility (%)	Lateral Expansion (mm)	Hardness (HV)
Sample D-10 (maximum temperature <727°C)					
k3	-20	31.35	10	0.38	179
k4	0	99.82	30	0.75	181
k1	10	108.26	40	0.76	183
k2	22	117.69	55	0.80	183
k6	100	170.29	100	1.1	186
k5	200	185.84	100	1.02	180
Sample H-4 (maximum temperature <727°C)					
k10	-20	66.83	10	0.36	190
k4	0	85.37	25	0.70	184
k8	10	118.82	55	0.70	199
k1	22	127.69	50	0.87	189
k7	35	130.67	90	0.85	198
k2	50	167.83	100	0.98	183
k5	100	173.67	100	1.04	190
k6	200	171.24	100	1.09	192
k12	300	160.26	100	1.04	187
Sample E-11 (maximum temperature <727°C)					
k2	22	100.68	55	0.75	186
k1	35	143.38	90	1.02	211
k3	50	135.47	95	0.98	182
Sample F-10 (maximum temperature ~1050°C)					
k3	0	28.00	0	0.23	246
k1	22	53.61	30	0.44	246
k5	22	40.72	20	0.41	242
k7	35	43.79	20	0.42	250
k2	50	48.88	50	0.52	247
k11	75	99.51	80	0.70	245
k8	100	112.53	100	0.86	246
k10	200	123.24	100	0.94	243
k12	300	110.43	100	0.90	248

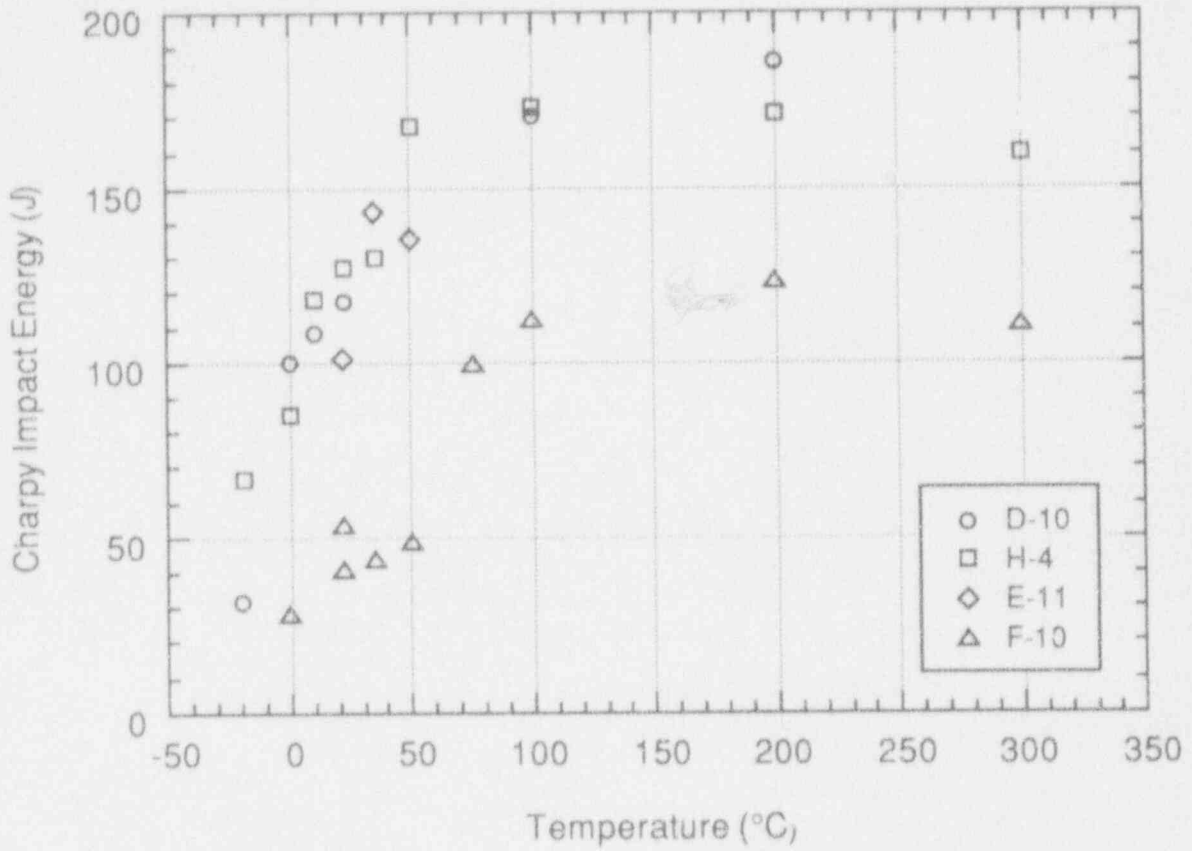

Fig. 31. Absorbed impact energy vs. test-temperature data from Charpy V-notch impact tests on specimens from TMI-2 lower head.

These observations on core materials suggest that the first material from the core to reach the lower head was from control assemblies that failed early in the accident. When the massive fuel flow reached the lower head, this layer of control-assembly materials would have re-melted and then penetrated the cladding in the vessel hot-spot region. After the cracks formed, instantaneous oxidation of the crack surfaces and the ferritic vessel probably occurred in the presence of trapped superheated water vapor, which also would have oxidized constituents in the liquid metal, leaving the more noble Ag-Cd unoxidized in the liquid oxide. The reacted crack surfaces and the jagged surface of the G-8 sample suggest that this liquid oxide was corrosive to the stainless steel. The fact that there is essentially no registry of the mating surfaces across the cracks suggests loss of material, perhaps by a dissolution process. It may be noted in Fig. 8 that the bent-over ligament of cladding in the crack would extend above the cladding surface if it were set upright. This indicates that the cladding surface in the vicinity of the crack was dissolved away to some extent in a manner similar to that of the seemingly lost material in the crack. The cladding surfaces of the F-10 and E-6 samples did not exhibit a similar jagged appearance, suggesting that such erosion was very dependent on local conditions. The fact that the cracks in these samples were not filled with a solidified liquid suggests that the liquid was held out by either gas pressure or surface tension.

The composition of the scrapings taken from the surface of the boat samples offers no real clue to the nature of the surface material that was originally in contact with the vessel. These materials were a heterogeneous mix of fuel and control-assembly constituents, generally in an Fe-oxide matrix. This morphology is similar to that found for the scale on a number of the instrument nozzles.[18] It could be concluded that the original control assembly debris was consumed into the larger mass of fuel debris that arrived later.

5 Summary and Conclusions

Microstructural characterizations and mechanical tests have been conducted by ANL and the OECD partner laboratories on material from 15 locations in the lower head of the pressure vessel of the TMI-2 nuclear reactor. The microstructural characterizations were conducted by conventional optical metallography, hardness measurements, scanning electron microscopy (SEM) on etched specimens and surface replicas, and analytical transmission electron microscopy on thin foils and carbon extraction replicas. The mechanical tests consisted of tensile tests at room temperature, tensile and creep tests at 600-1200°C, and Charpy impact tests at -20-300°C. The specimens tested were taken from locations where the maximum temperature had not exceeded 727°C during the accident and from locations where the maximum temperature had been as high as 1100°C. The results of these investigations lead to the following conclusions:

1. Metallographic specimens from Samples E-6, E-8, F-10, and G-8 were all found to have reached maximum temperatures in the range of 1000-1100°C during the accident. These specimens were all from the so-called "hot spot" in the lower head that had been identified earlier. The cooling rate from the peak temperature was estimated to be ≈10-100°C/min for these specimens.

2. Metallographic specimens from Sample F-5, which was near the hot spot, were found by investigators in Belgium, FRG, and the U.K. to have slightly exceeded 727°C near the surface. However, examinations at ANL and INEL on adjacent specimens did not detect any evidence of transformation, which would have occurred at temperatures >727°C.

3. Metallographic specimens from Sample H-8 were found to have exceeded 727°C near the end of this sample closest to the hot spot, but the remainder of the sample remained below this temperature.

4. Subtle evidence of maximum temperatures slightly in excess of 727°C near the surface in a specimen from Sample M-11 was observed by investigators in the U.K. Five other laboratories examining adjacent specimens did not report indications of a phase transformation.

5. Researchers at the Harwell Laboratories in the U.K. noted significant tempering of the bainite microstructure in the base metal of Samples H-4, H-5, M-8, and L-9, indicating that the temperature in these samples probably approached 727°C, at least near the surface.

6. The results of tensile tests conducted on base-metal specimens for which the maximum temperature during the accident (T_{max}) did not exceed 727°C agree well with with literature data for A533B steel and show a dramatic drop in strength at temperatures above 600°C.

7. Tensile specimens from samples for which T_{max} exceeded 727°C showed significantly higher strengths at room temperature and 600°C when compared to specimens for which the temperature did not exceed 727°C.

8. Creep tests at 600 and 700°C indicated no significant difference in behavior between base-metal specimens for which T_{max} was of the order of 727°C and those for which it was well below this value. Fifty-hour stress-rupture stresses were found to be ≈8 MPa at 1100°C and <4 MPa at 1200°C.

9. The stress-rupture data for the lower head material was found to be in good agreement with data previously obtained on archive material from the Midland reactor at 600°C. However, the lower head material was found to be substantially stronger in creep than the Midland material at higher temperatures.

10. The stress-rupture data obtained from base-metal specimens could be more accurately fit with a Manson-Haferd time-temperature parameter than a Larson-Miller parameter.

11. Charpy V-notch impact tests conducted on lower head base-metal material noted a substantial difference between specimens from Sample F-10, for which T_{max} was as high as ≈1050°C, as compared with specimens from samples for which T_{max} was <727°C. The F-10 material showed a significantly higher ductile-to-brittle transition temperature as well as a lower upper-shelf energy value.

12. Cracks through the stainless steel cladding of Samples E-6 and G-8 appear to have been hot tearing phenomena, probably assisted by interdendritic penetration of liquid Ag-Cd.

13. Materials in the cladding cracks suggest the presence of control-assembly debris on the lower head before the massive flow of fuel arrived.

References

1. G. E. Korth, *Metallographic and Hardness Examinations of TMI-2 Lower Pressure Vessel Samples*, TMI V(92) EG01, Idaho National Engineering Laboratory (January 1992).

2. D. R. Diercks, *TMI-2 Vessel Investigation Project (VIP) Metallurgical Program, Progress Report October 1989—June 1990*, NUREG/CR-5524, Vol. 2, ANL-90-34, Argonne National Laboratory (November 1990).

3. D. Akers, S. M. Jensen, and B. K. Schuetz, *Companion Sample Examinations*, EGG-OECD-9810, (April 1992).

4. D. R. Diercks, *Decontamination and Examination of TMI-2 Lower Head Samples*, TMIV(90) AL05, presented at TMI-2 VIP Program Review Meeting, Jackson Hole, WY, November 27, 1990.

5. W. Vandermeulen and W. Hendrix, *Examination Report of the Samples of the TMI-2 RPV Received by SCK/CEN (Belgium)*, SCK/CEN, Mol (March 1992).

6. Reijo Pelli, *Metallographic Examinations of TMI-2 RPV Lower Head Sample E-8 and the Archive Material of Midland Reactor*, TMIV(92) SF01, VTT Technical Research Centre of Finland, Espoo (April 1992).

7. F. Le Naour, *CEA Contribution to the TMI-2 Vessel Material Investigation Project*, N.T. SRMA 92-1956, Centre d'Etudes de Saclay (May 1992).

8. H. Ruoff, K.-H. Katerbau, and D. Sturm, *Metallographic Examination of TMI-2 Lower Pressure Vessel Head Samples*, TMIV(91) D001, Staatliche Materialprüfungsanstalt, Stuttgart (September 1991).

9. L. Pedrero and P. Veron, *Metallographic Investigation of TMI-2 Lower Pressure Vessel Head Samples*, TMIV(92) E002, Equiptos Nucleares S. A., Miliaño (April 1992).

10. J. M. Titchmarsh and R. Cooke, *AEA-Technology Examinations of TMI-VIP Lower Head Samples*, TMIV(91) UK2, AEA Technology, Harwell (September 1991).

11. A. Masperoni and P. P. Milella, *Metallographic Examinations of Archive Material (Midland Reactor) and TMI-2 RPV Lower Head Samples D-10 and H-4*, TMIV(93) I01, ENEA, Rome (April 1993).

12. M. J. Callejas Cano, *OECD TMI-2 VIP Program Tensile Test*, TMIV(92) E003, CIAT, Madrid (February 1992).

13. *Data Sheets on the Elevated-Temperature Properties of 1.3 Mn-0.5 M0-0.5 Ni Steel Plates for Boilers and Other Pressure Vessels (SBV 2)*, NRIM Creep Data Sheet No. 18B, National Research Institute for Metals, Tokyo (1987).

14. A. Ballesteros, *TMI-2 Vessel Investigation Project Creep Tests*, TMIV(92) E004, Tecnatom, S. A., Madrid (May 1992).

15. F. R. Larson and J. Miller, Trans. ASME, vol. 74, pp. 765-771 (1952).

16. S. S. Manson and A. M. Haferd, NACA Tech. Note 2890 (March 1953).

17. P. P. Milella and F. Bigagli, *Charpy V Testing of Specimens of the TMI 2 Vessel Lower Head*, TMIV(92) I01, ENEA, Rome (May 1992).

18. L. A. Neimark, et al., *TMI-2 Instrument Nozzle Examinations at Argonne National Laboratory*, TMI(93)AL01, February 1993.

Appendix A:

Sectioning Diagrams for TMI-2 Lower Head Samples

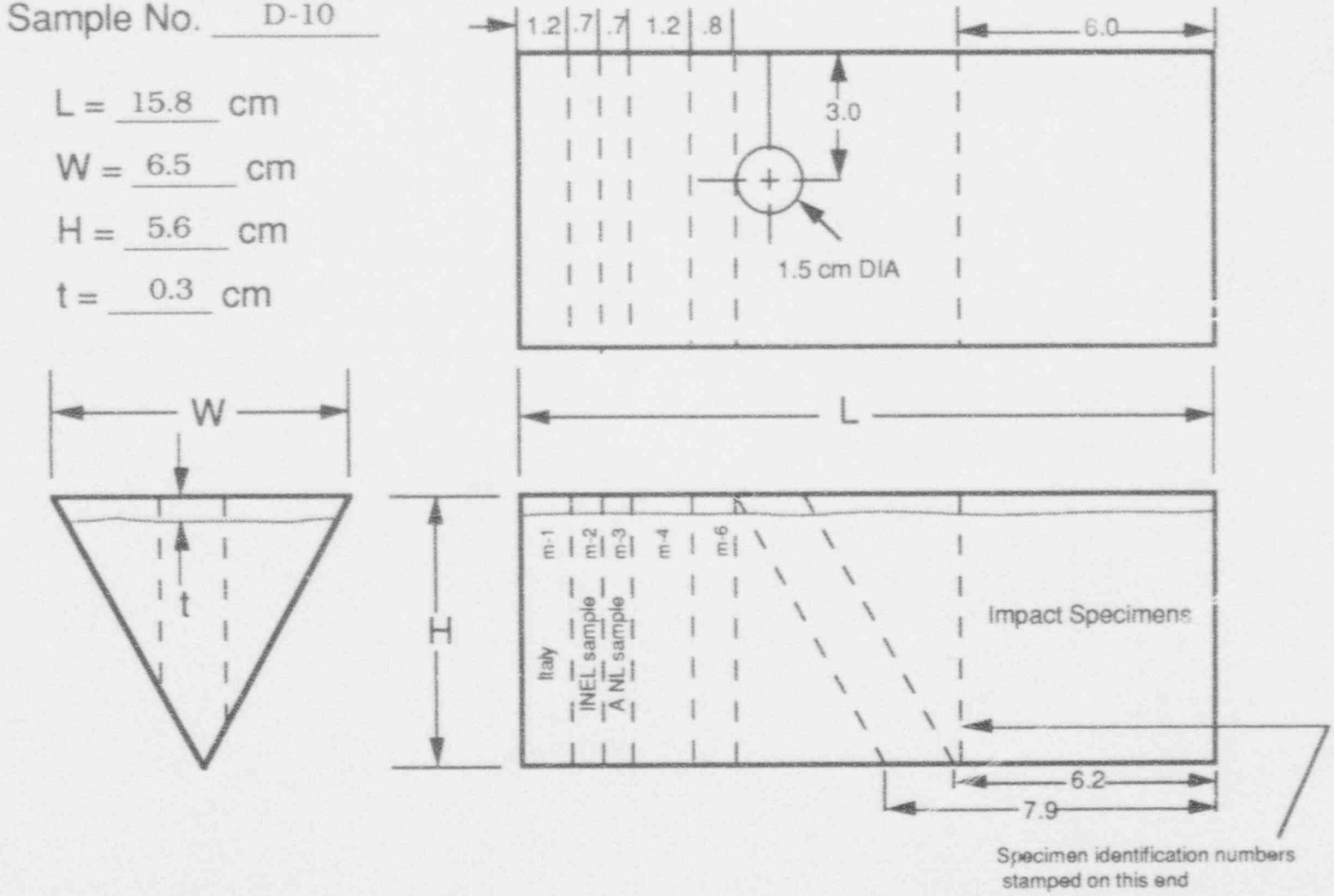

Fig. A1. Dimensions and initial sections from TMI-2 lower head Sample D-10.

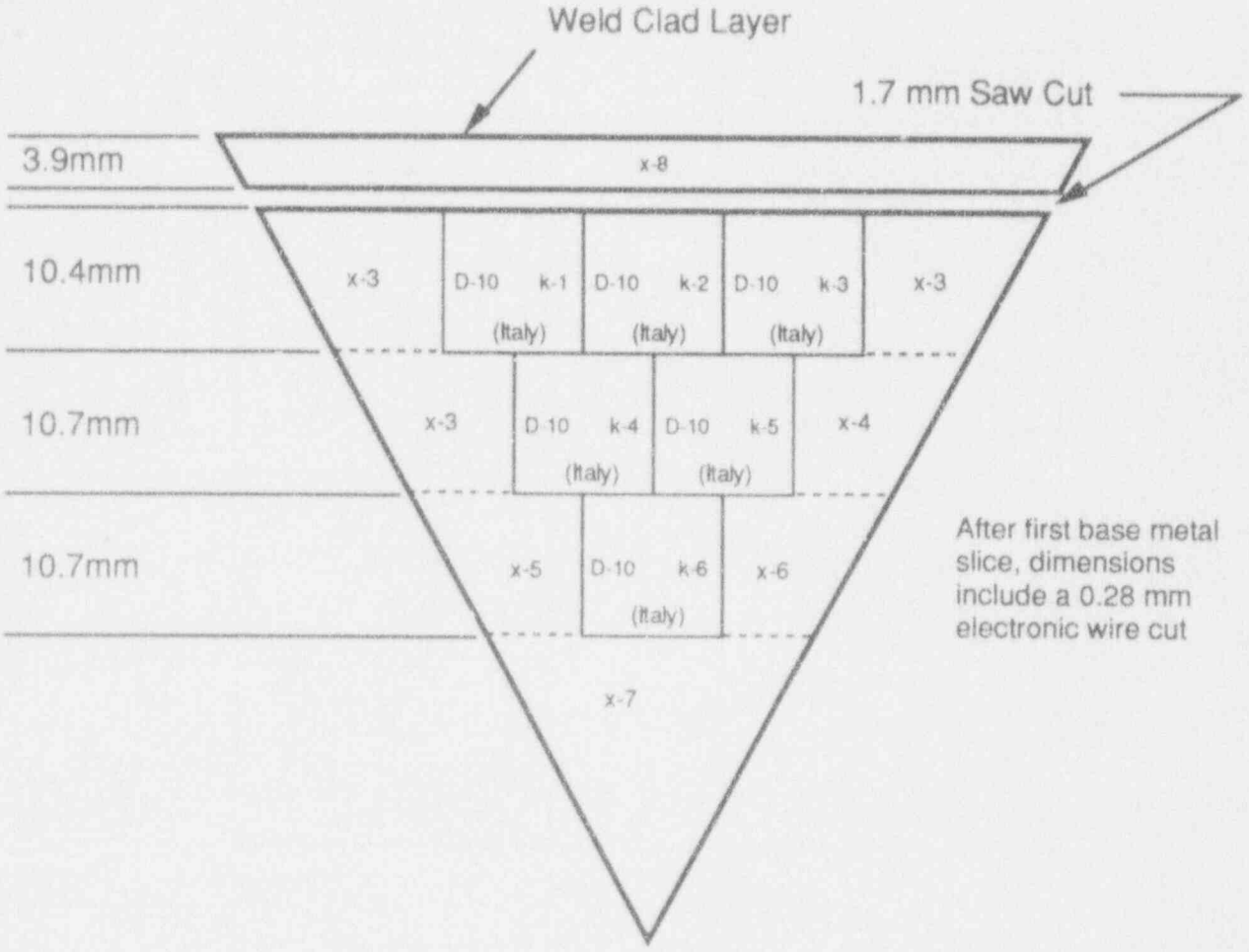

Fig. A2. Locations of mechanical test specimens cut from Sample D-10.

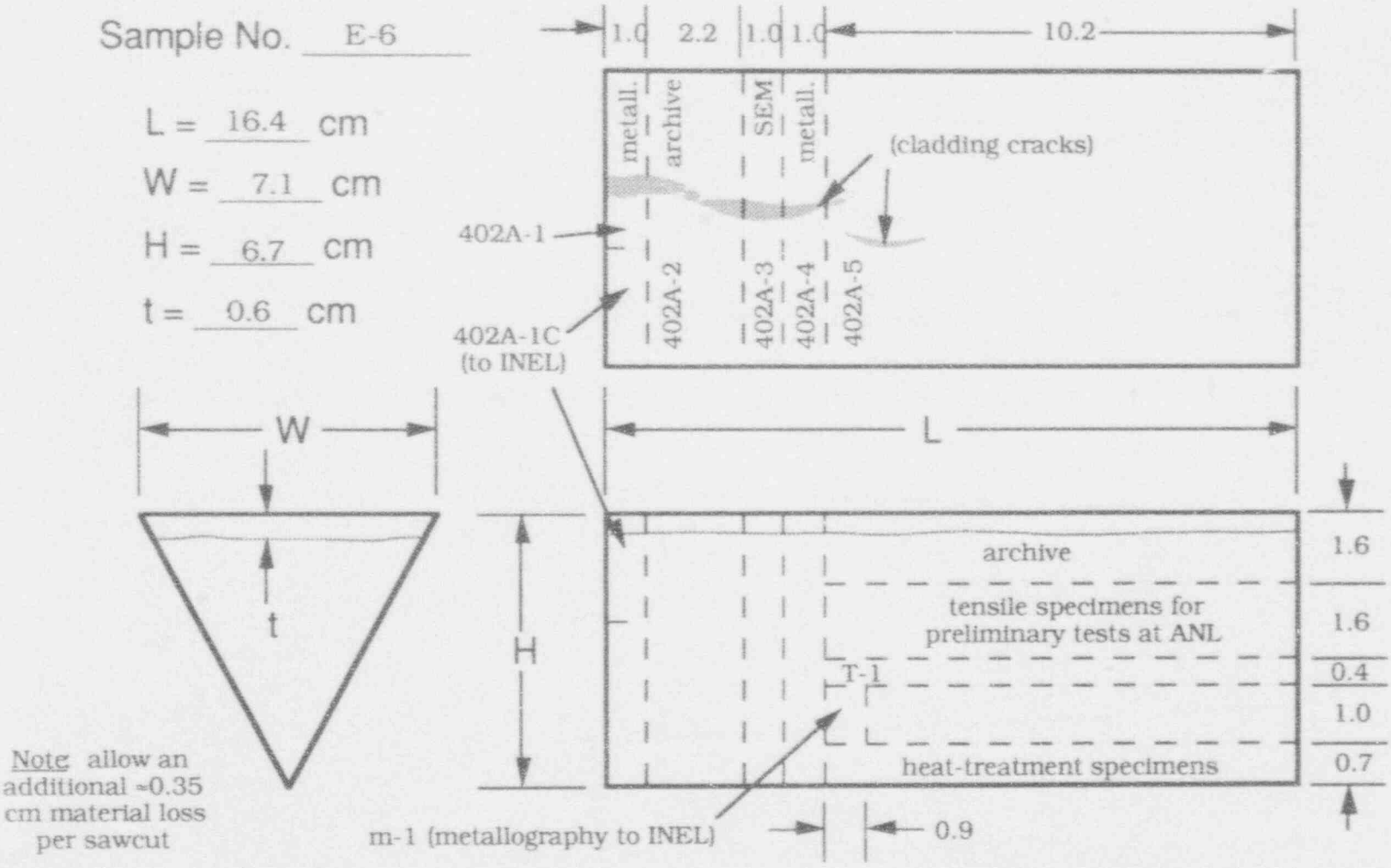

Fig. A3. Dimensions and initial sections from TMI-2 lower head Sample E-6.

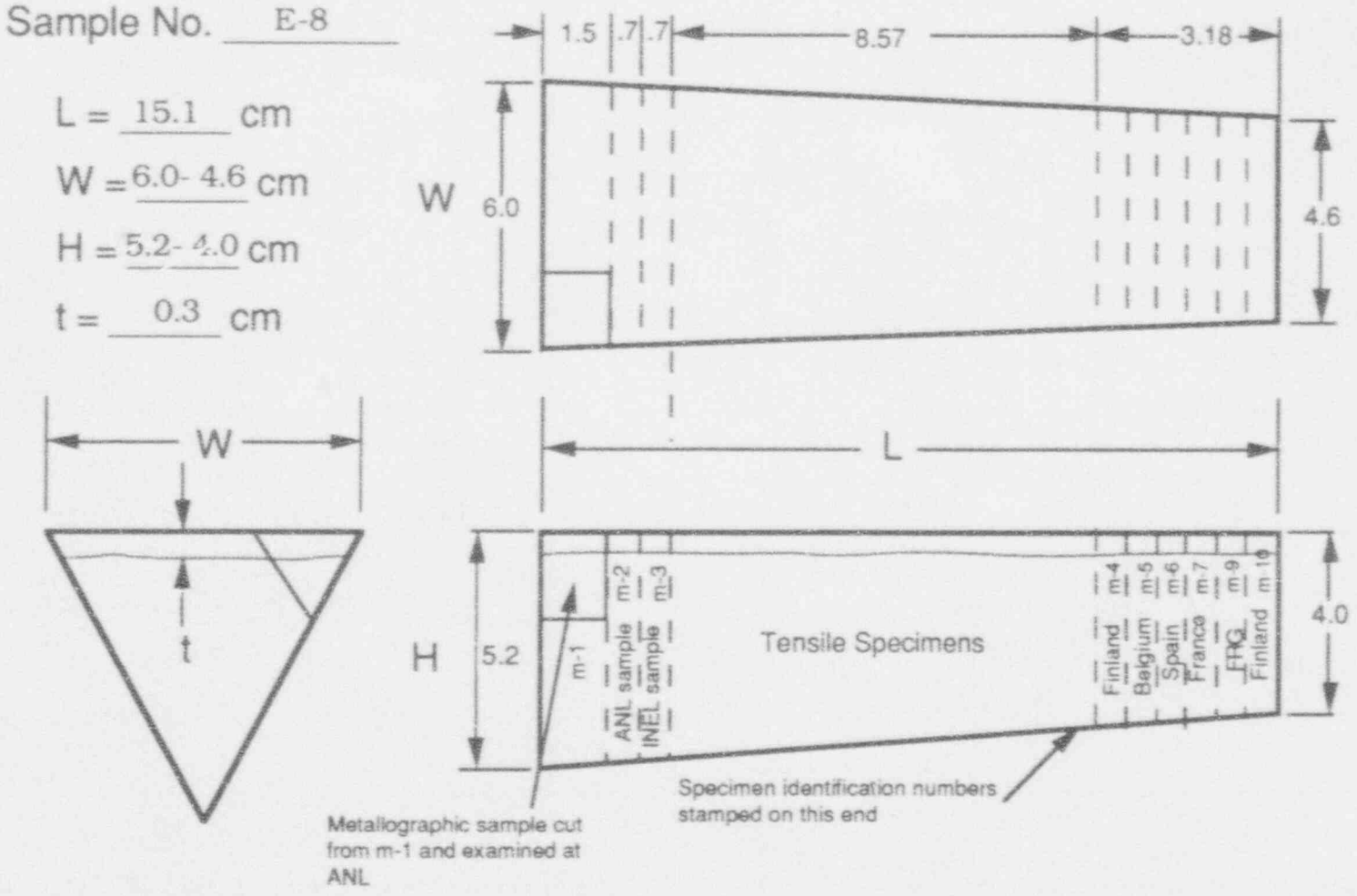

Fig. A4. Dimensions and initial sections from TMI-2 lower head Sample E-8.

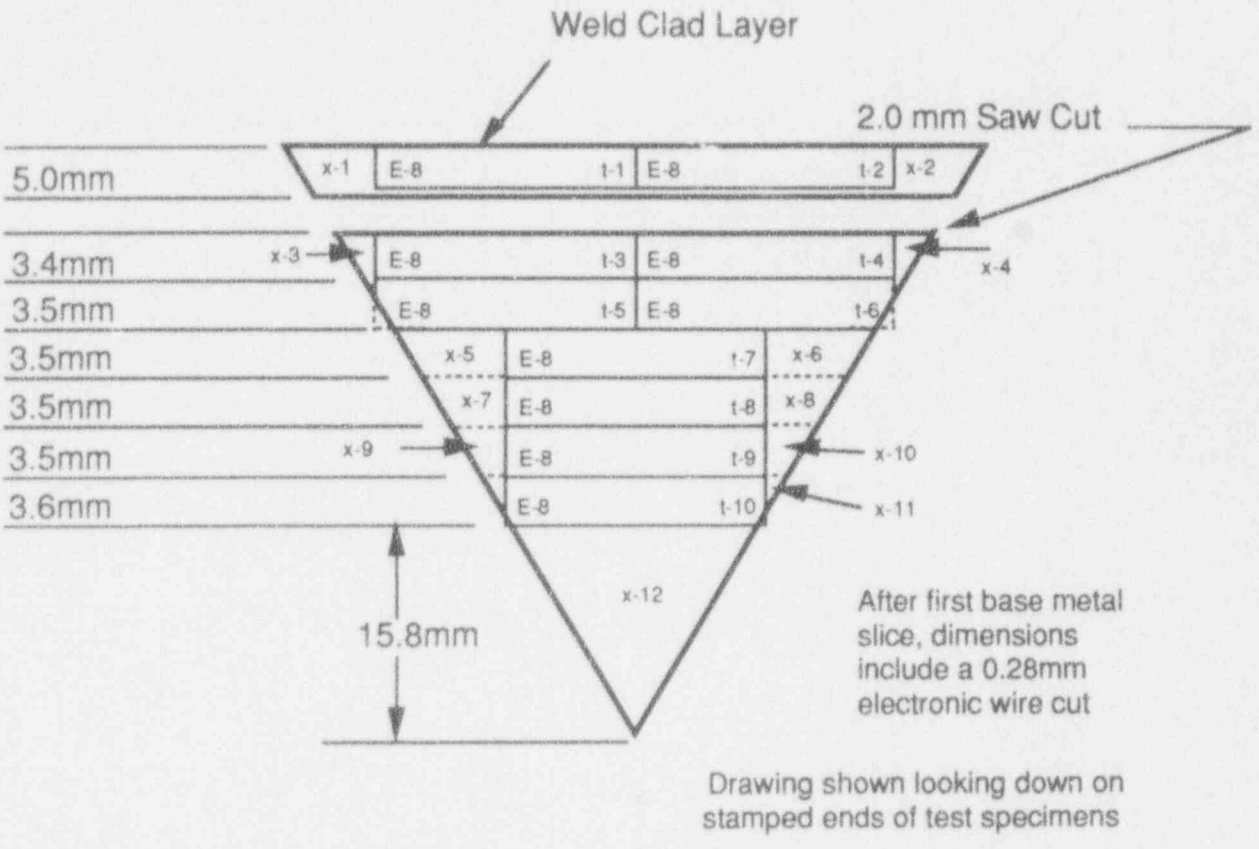

Fig. A5. Locations of mechanical test specimens cut from Sample E-8.

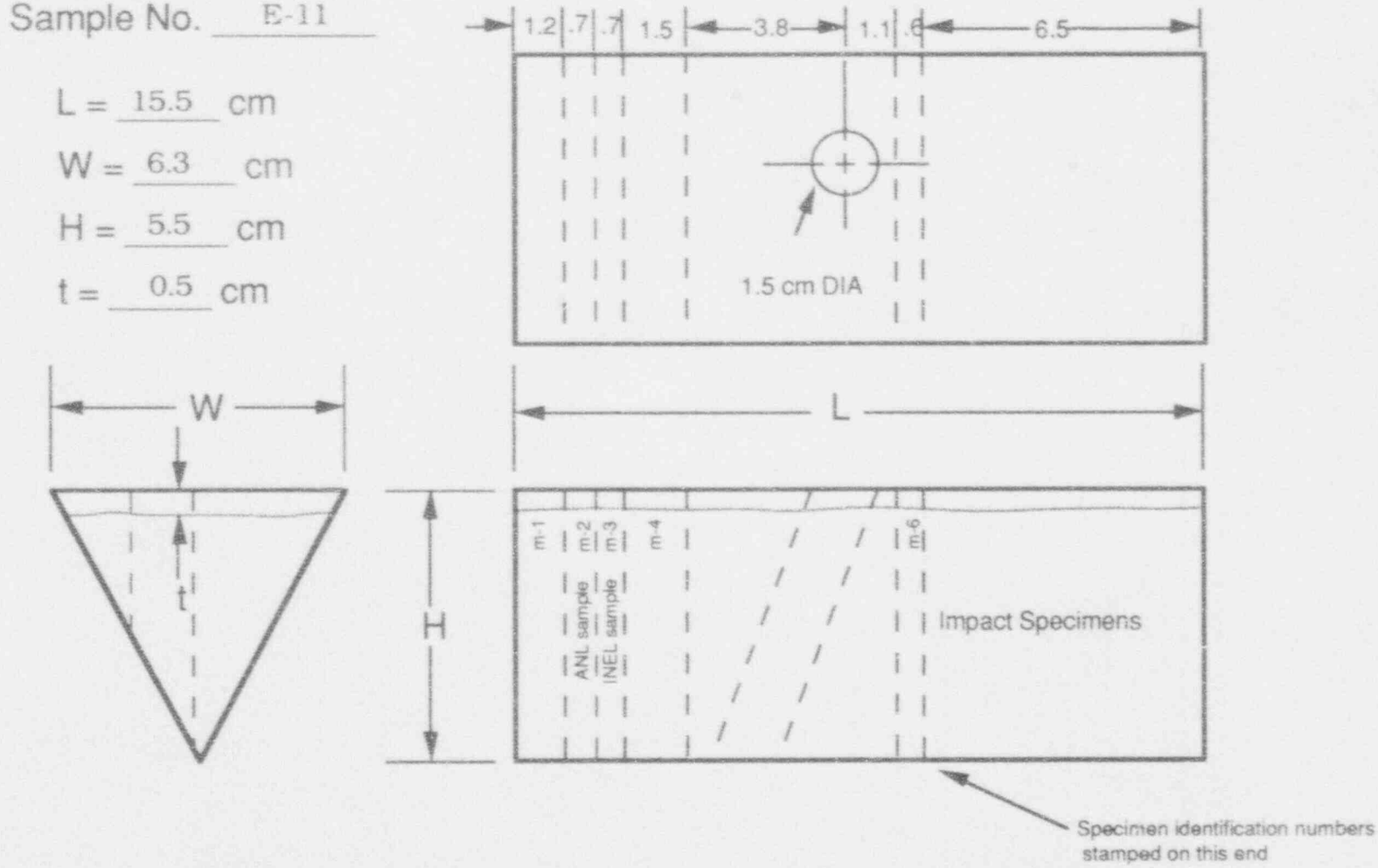

Fig. A6. Dimensions and initial sections from TMI-2 lower head Sample E-11.

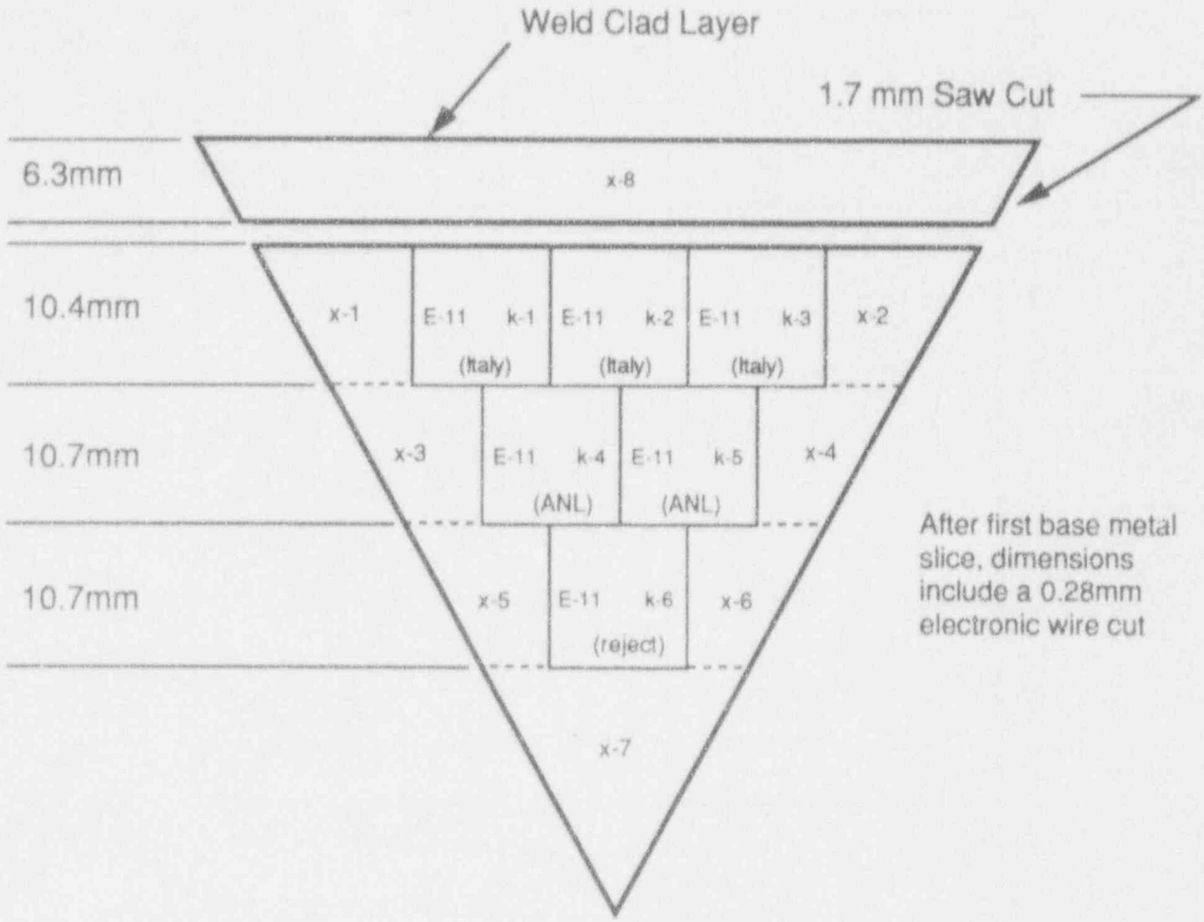

Fig. A7. Locations of mechanical test specimens cut from Sample E-11.

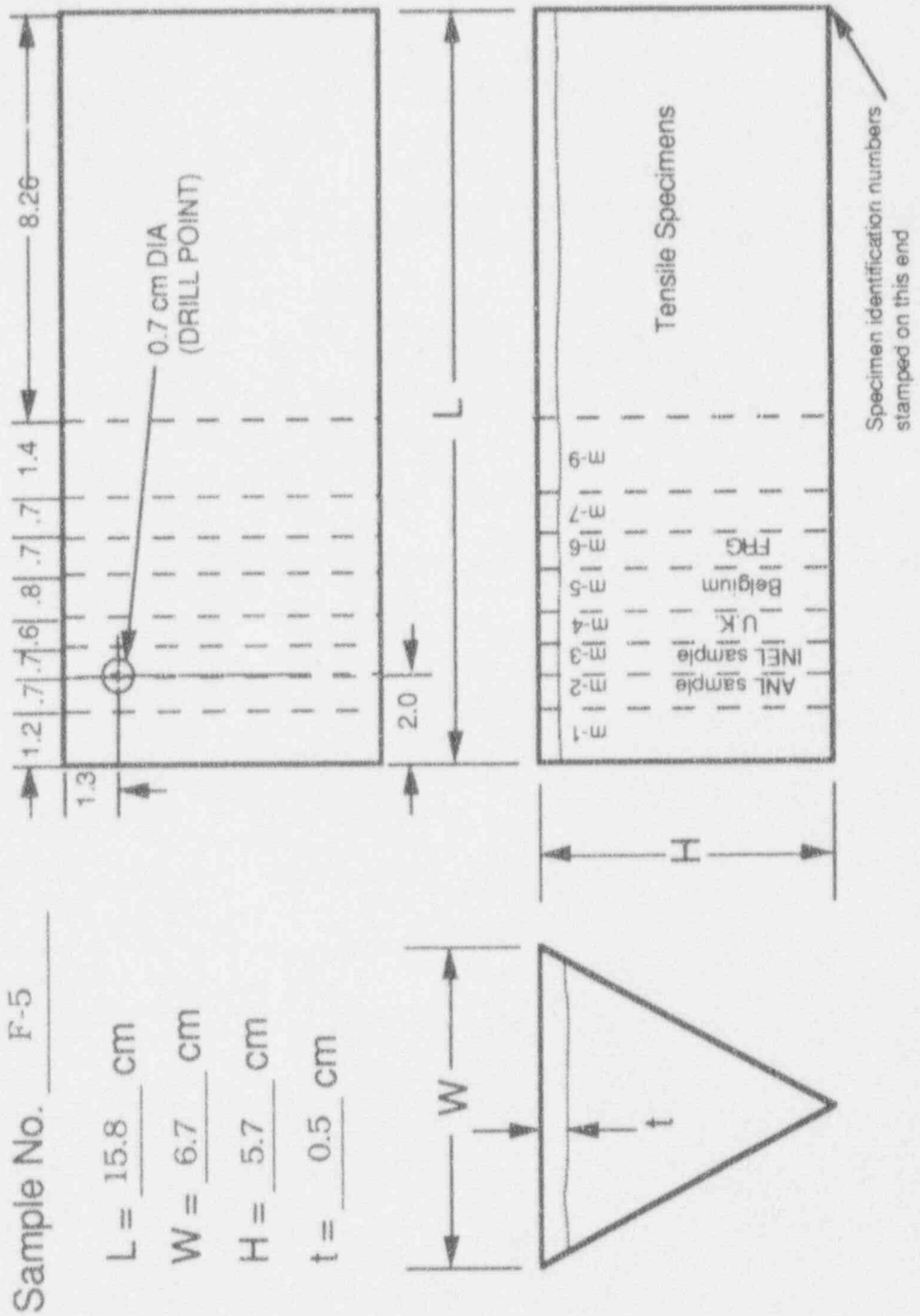

Fig. A8. Dimensions and initial sections from TMI-2 lower head Sample F-5.

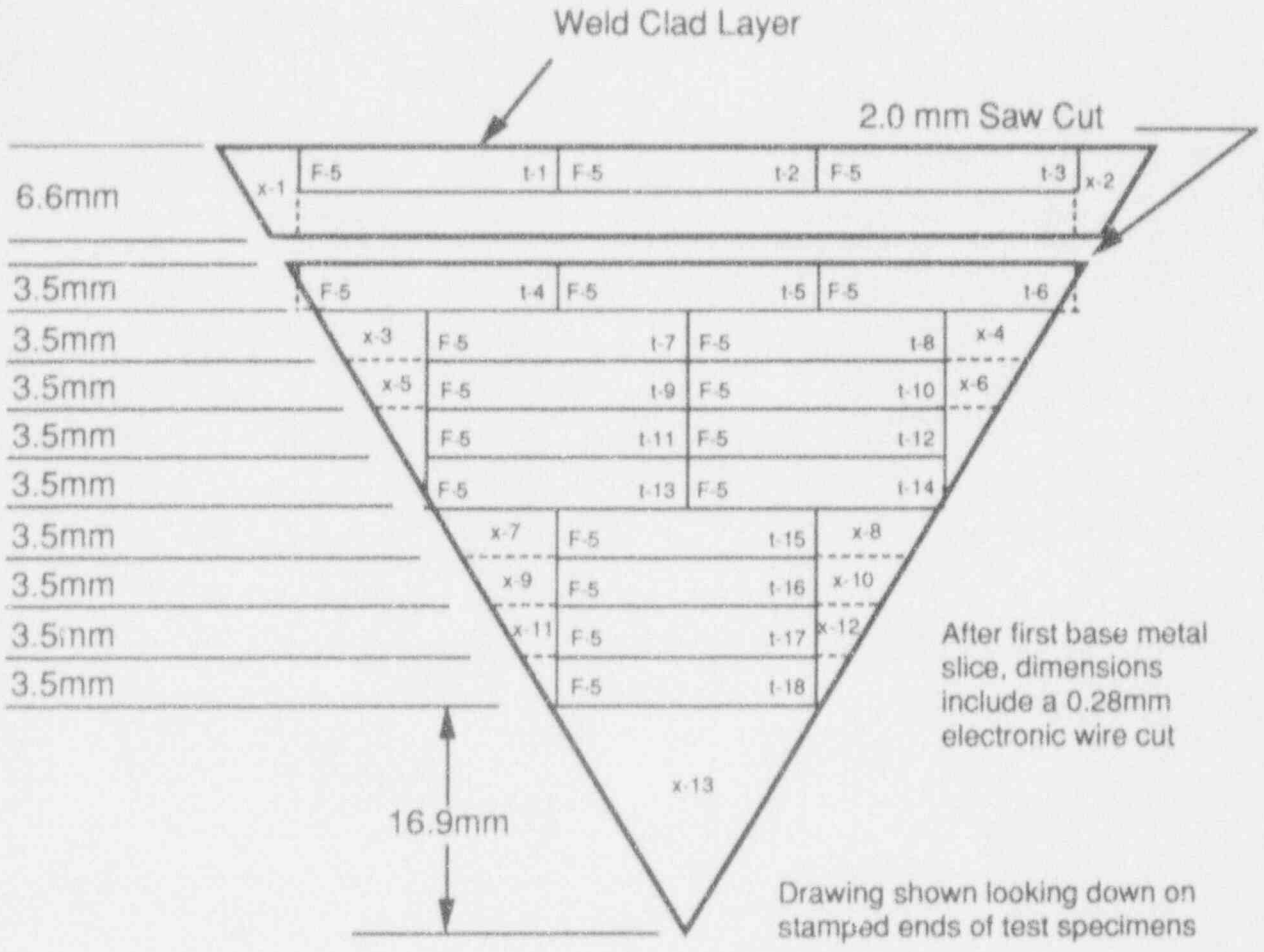

Fig. A9. Locations of mechanical test specimens cut from Sample F-5.

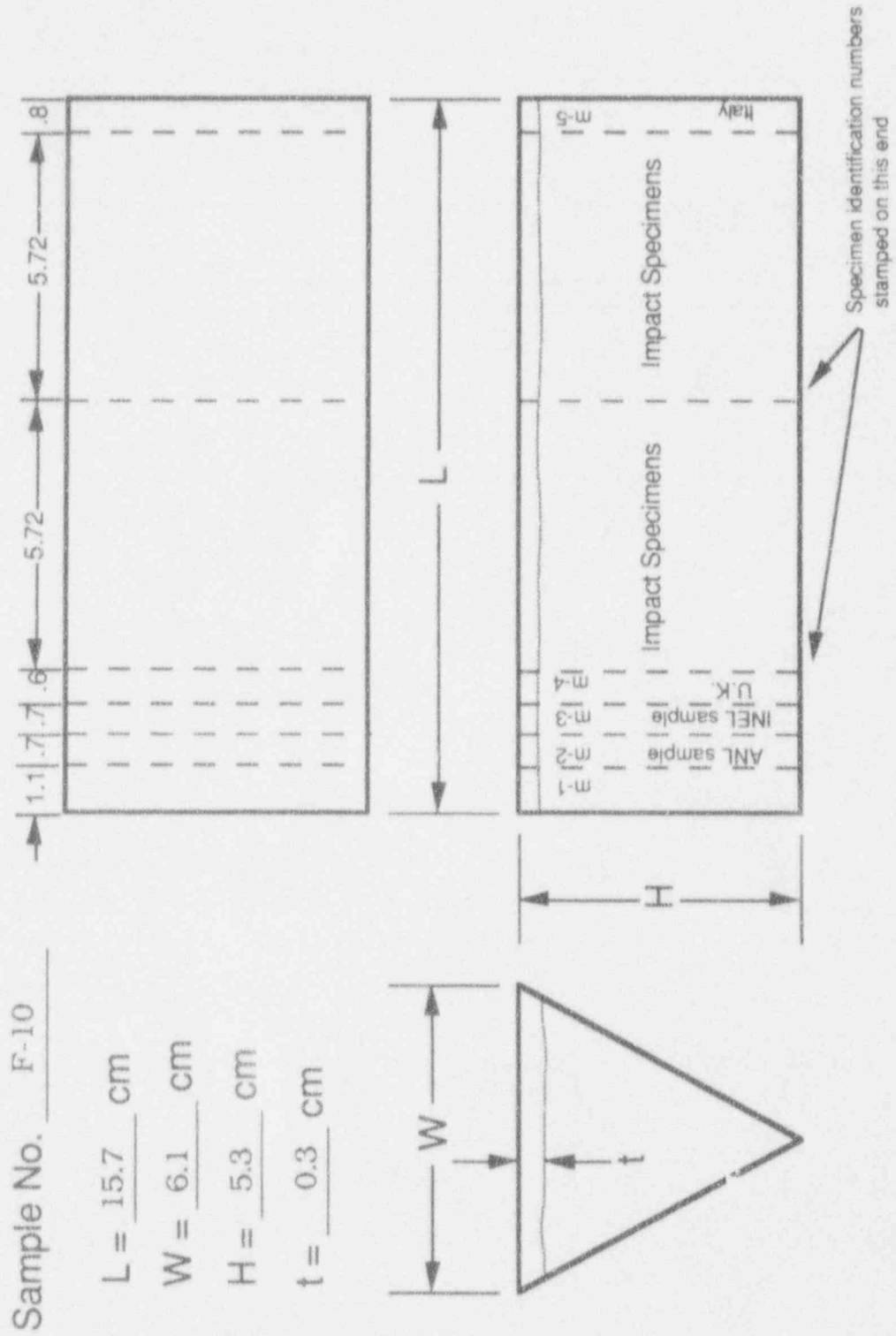

Fig. A10. Dimensions and initial sections from TMI-2 lower head Sample F-10.

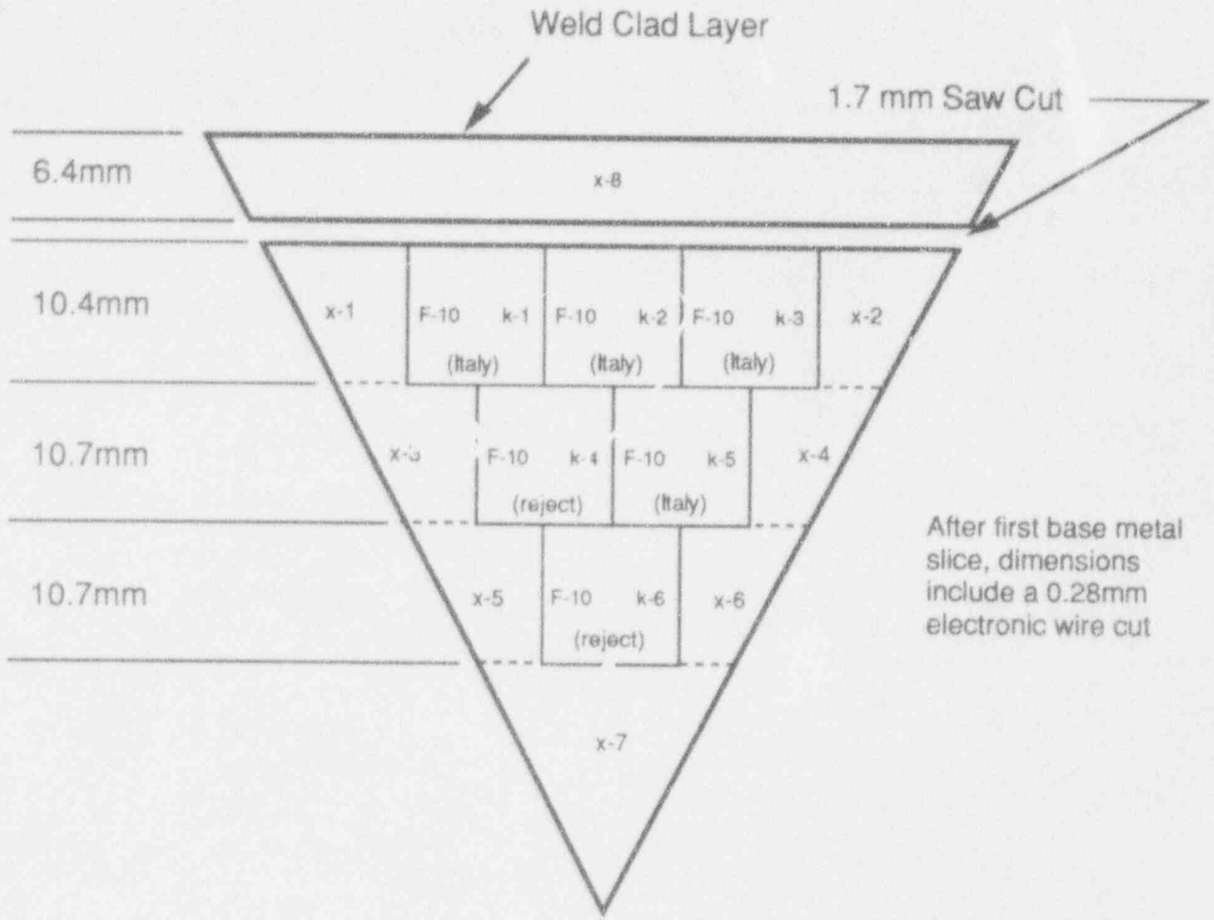

Fig. A11. Locations of mechanical test specimens k1 through k6 cut from Sample F-10.

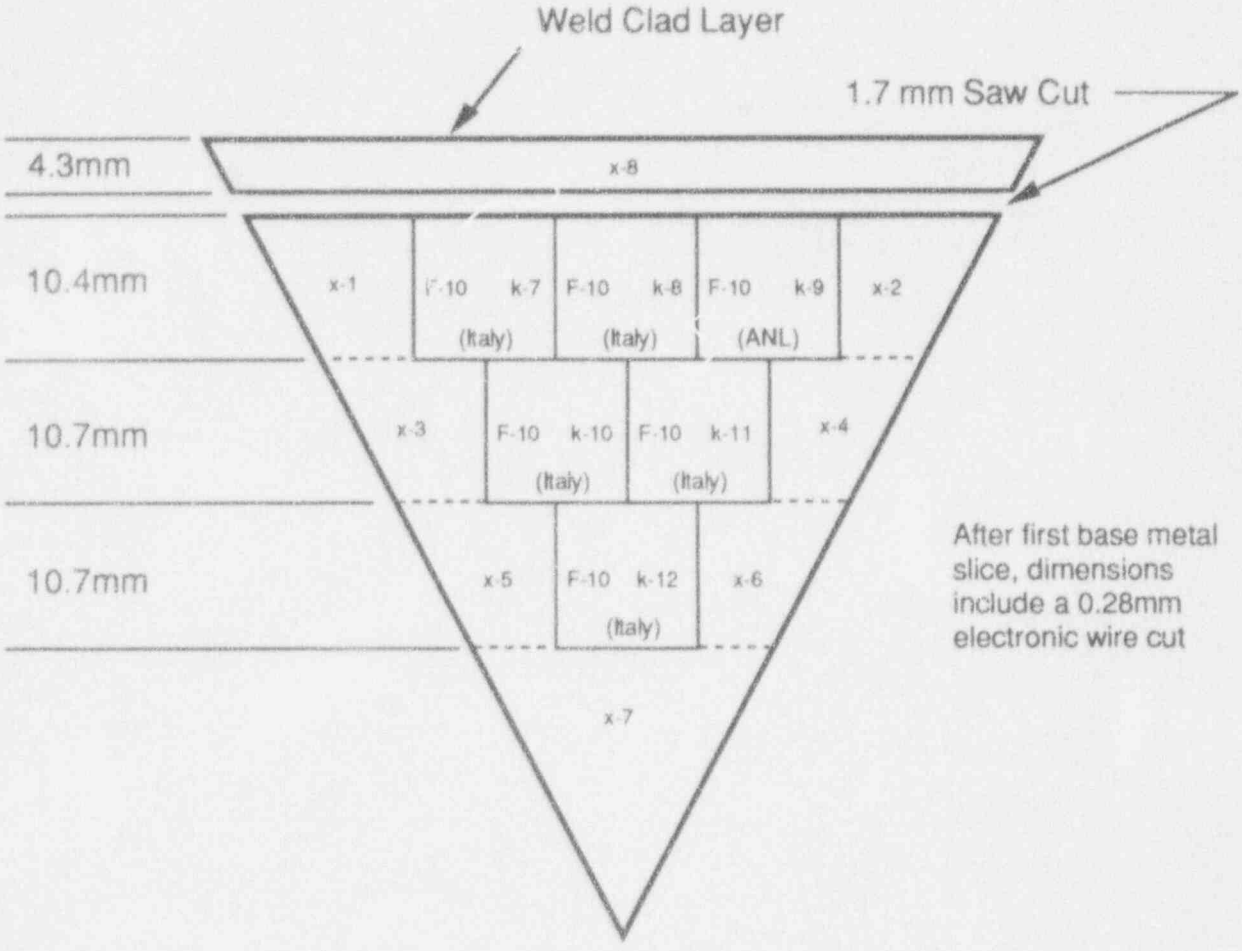

Fig. A12. Locations of mechanical test specimens k7 through k12 cut from Sample F-10.

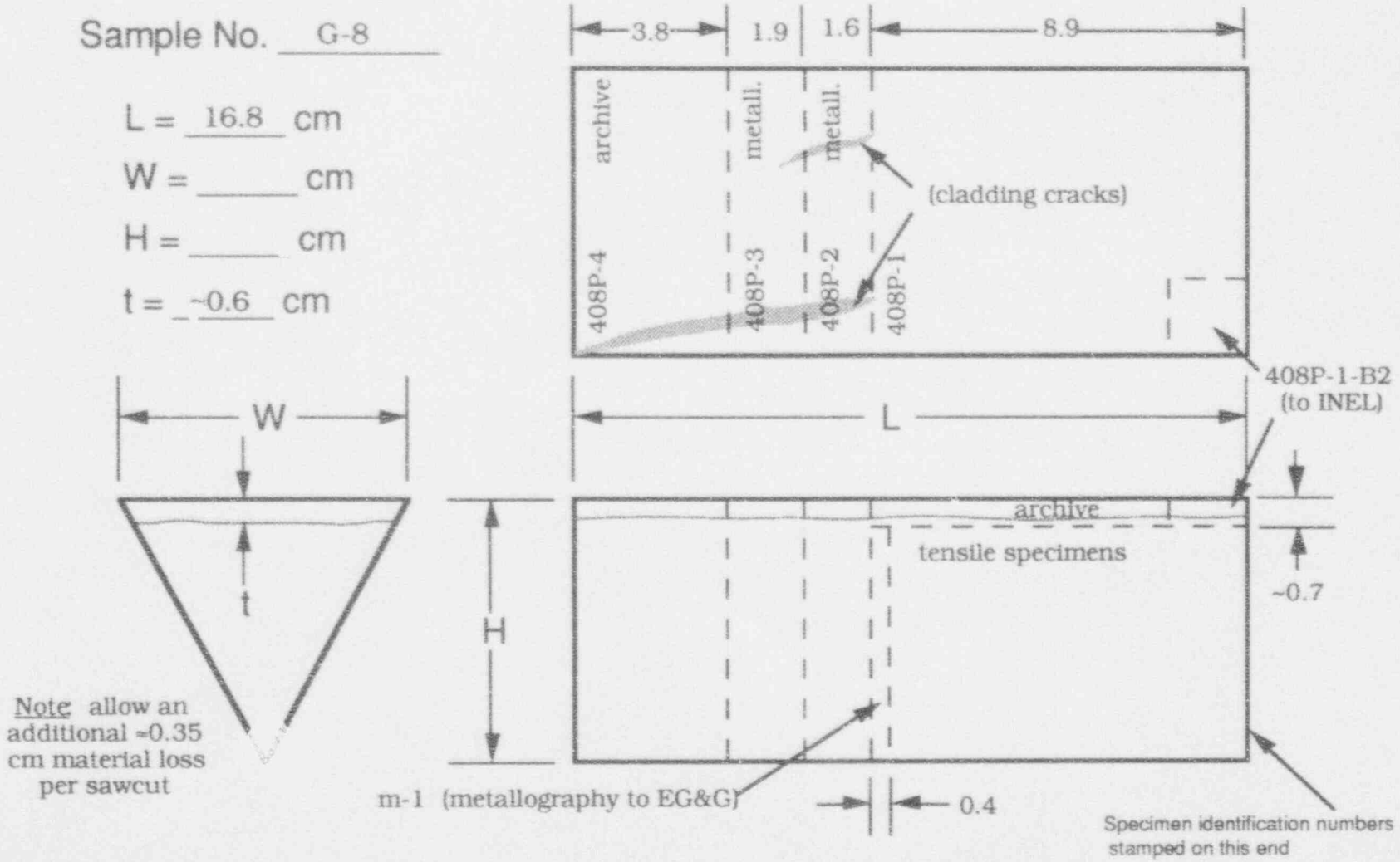

Fig. A13. Dimensions and initial sections from TMI-2 lower head Sample G-8.

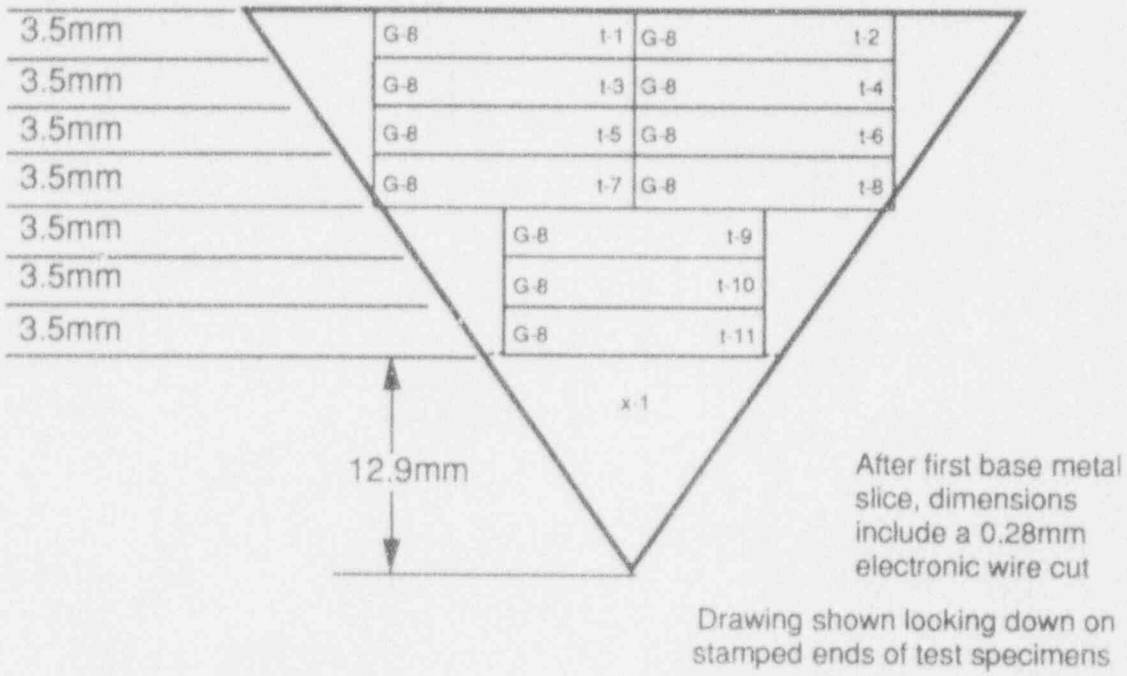

Fig. A14. Locations of mechanical test specimens cut from Sample G-8.

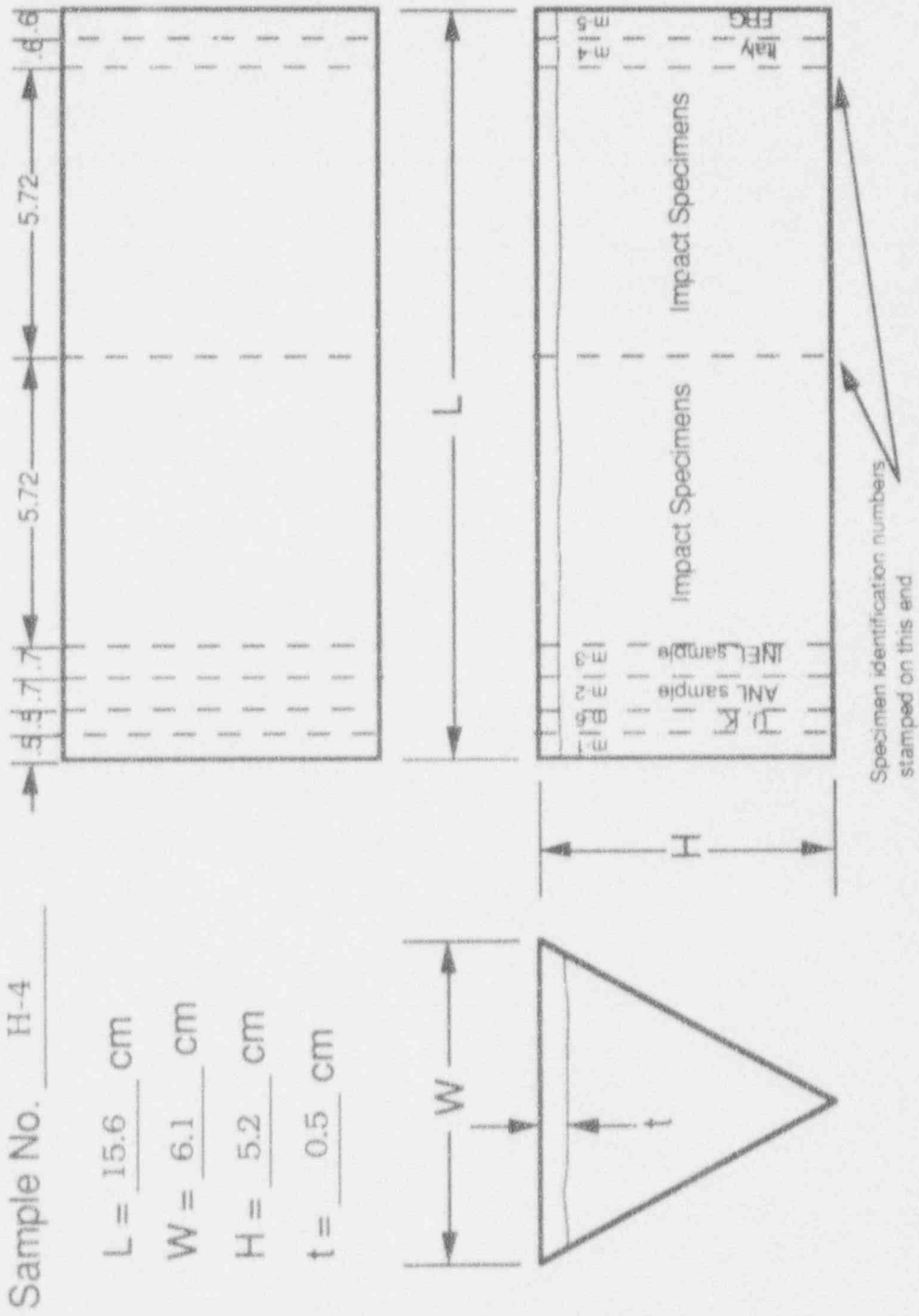

Fig. A15. Dimensions and initial sections from TMI-2 lower head Sample H-4.

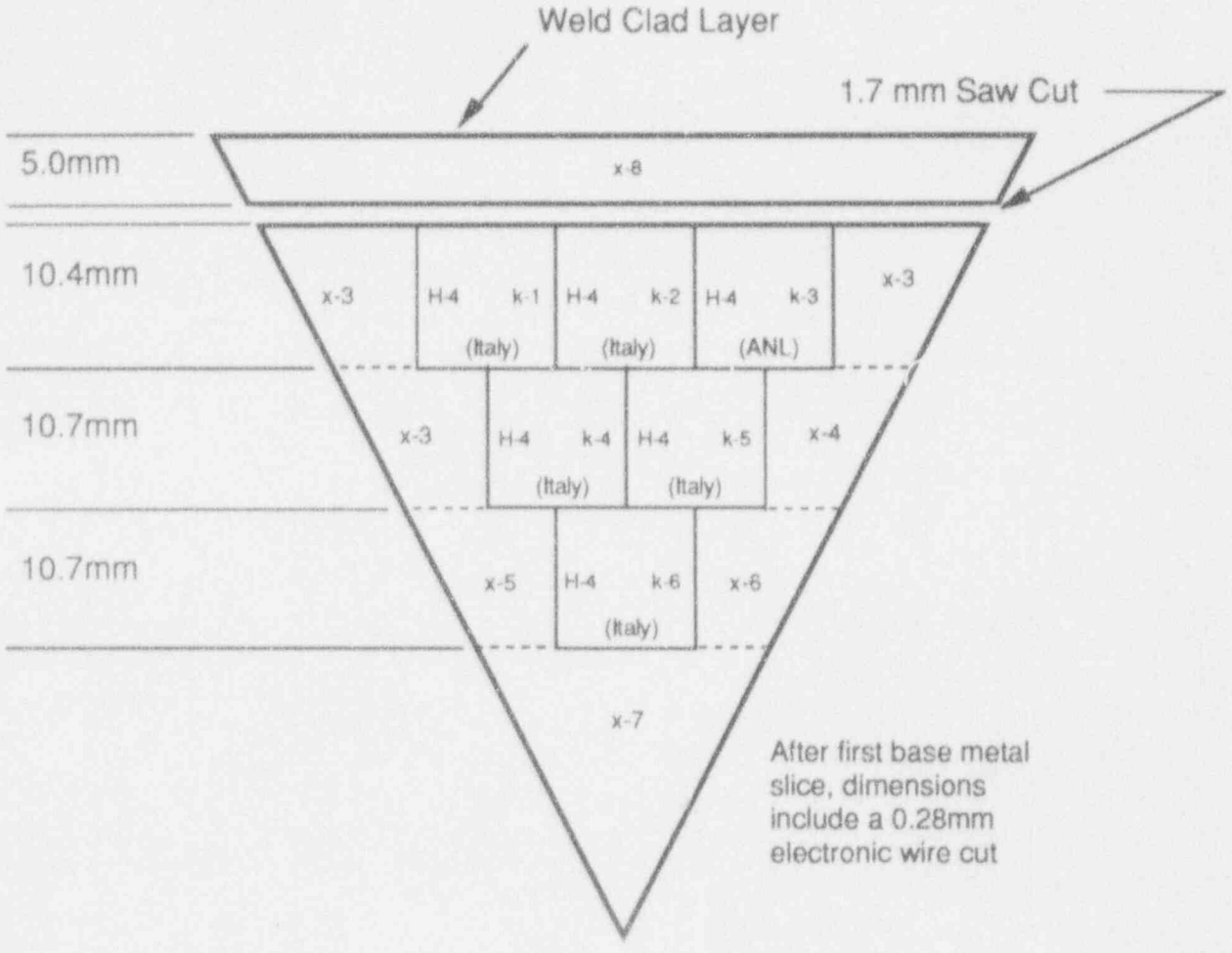

Fig. A16. Locations of mechanical test specimens k1 through k6 cut from Sample H-4.

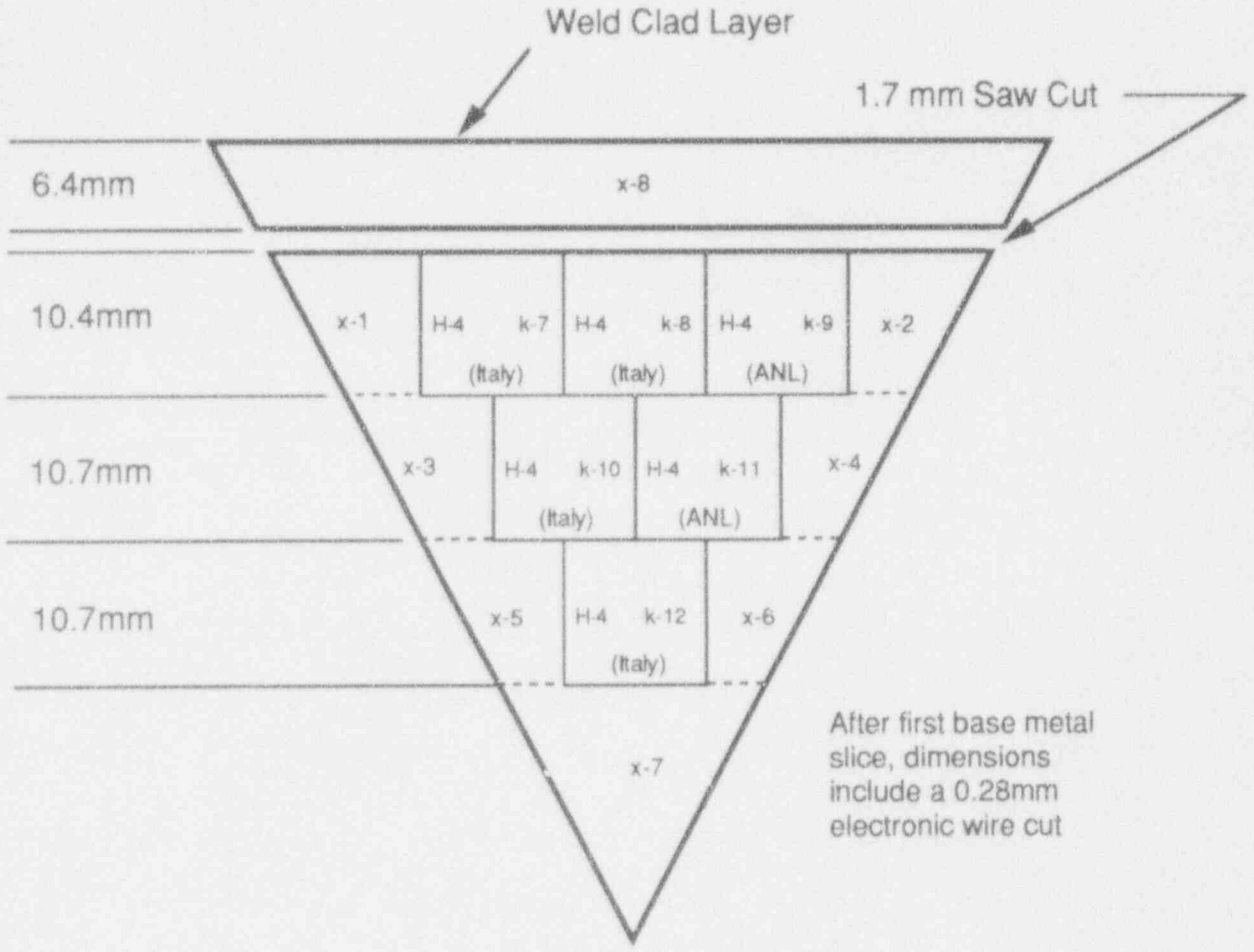

Fig. A17. Locations of mechanical test specimens k7 through k12 cut from Sample H-4.

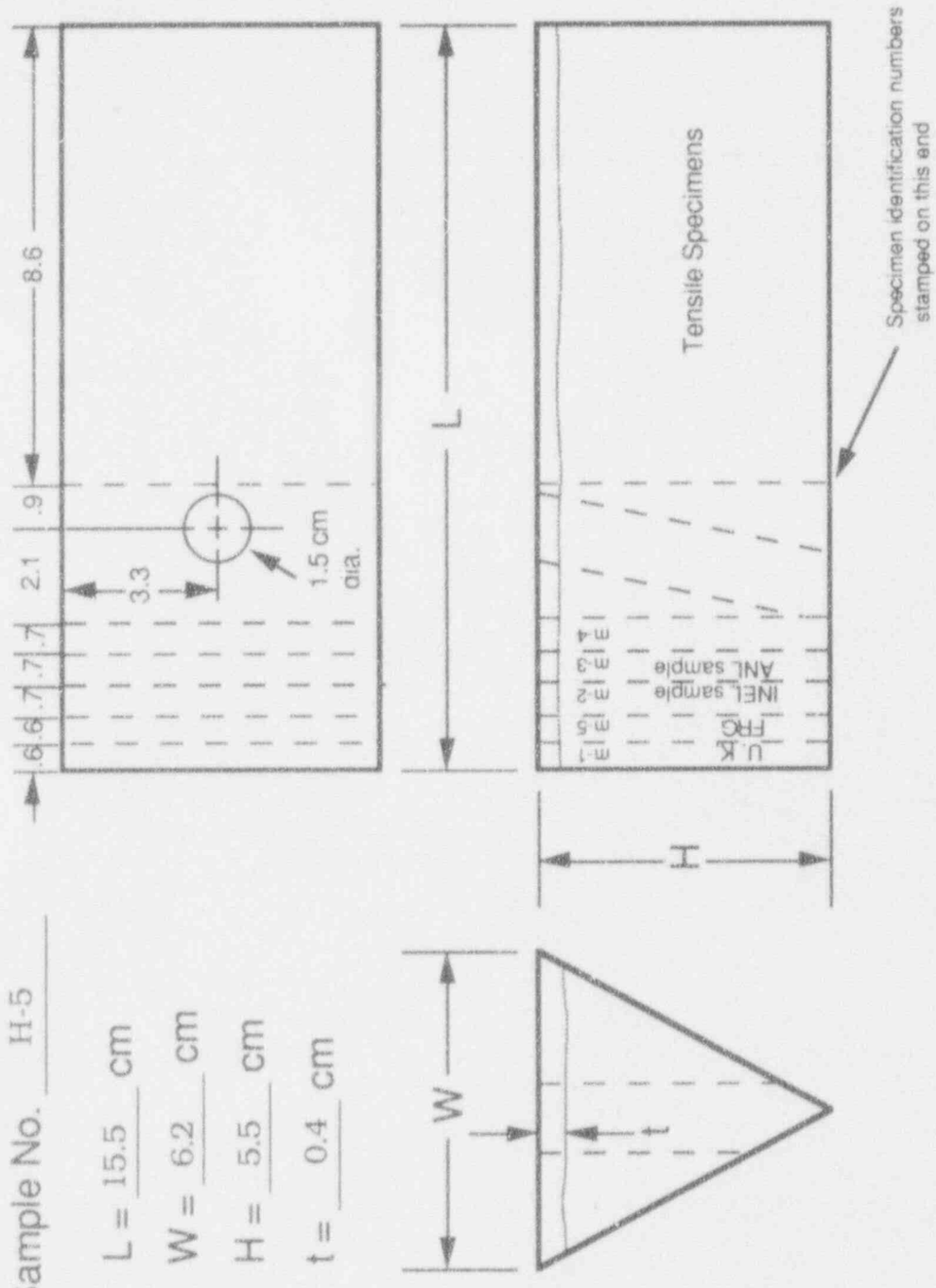

Fig. A18. Dimensions and initial sections from TMI-2 lower head Sample H-5.

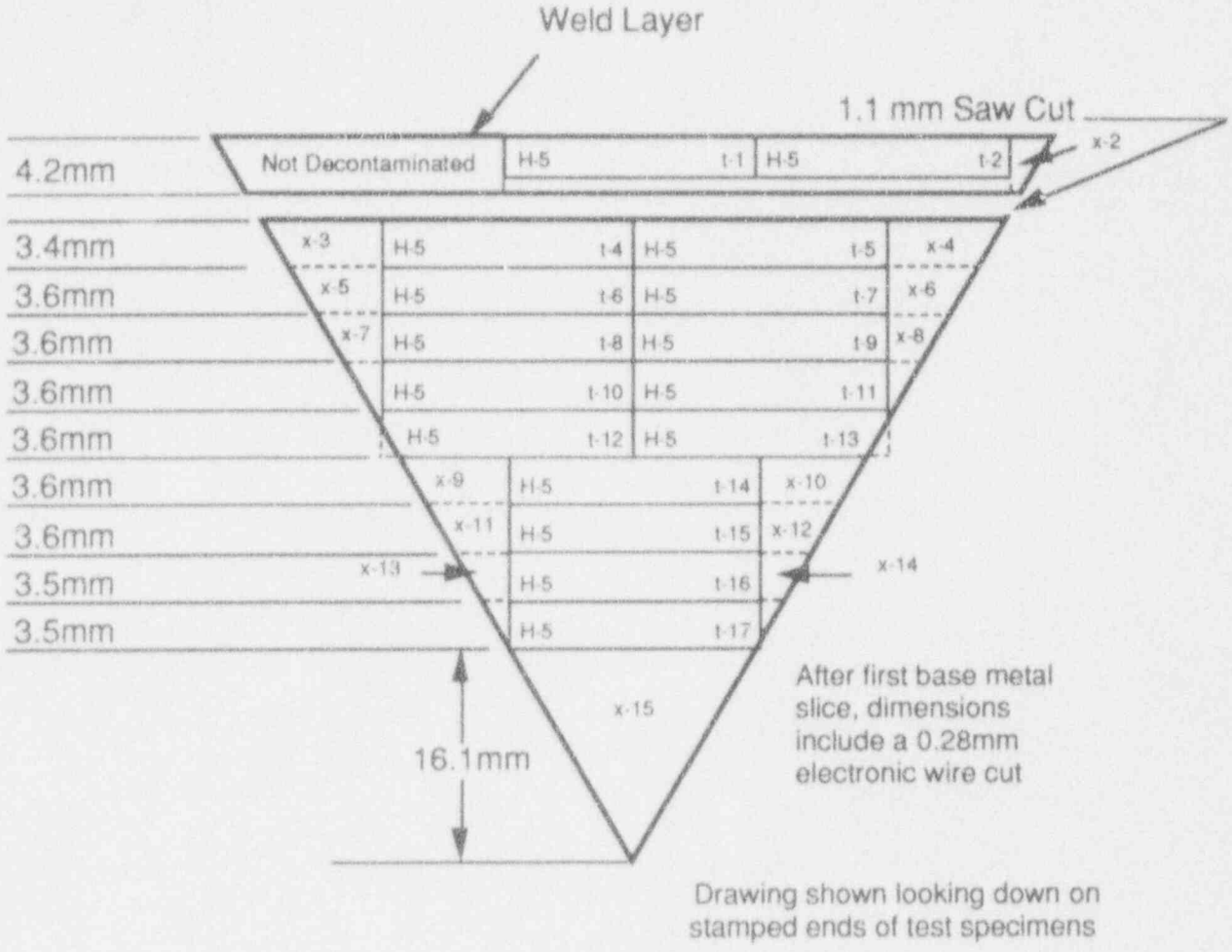

Fig. A19. Locations of mechanical test specimens cut from Sample H-5.

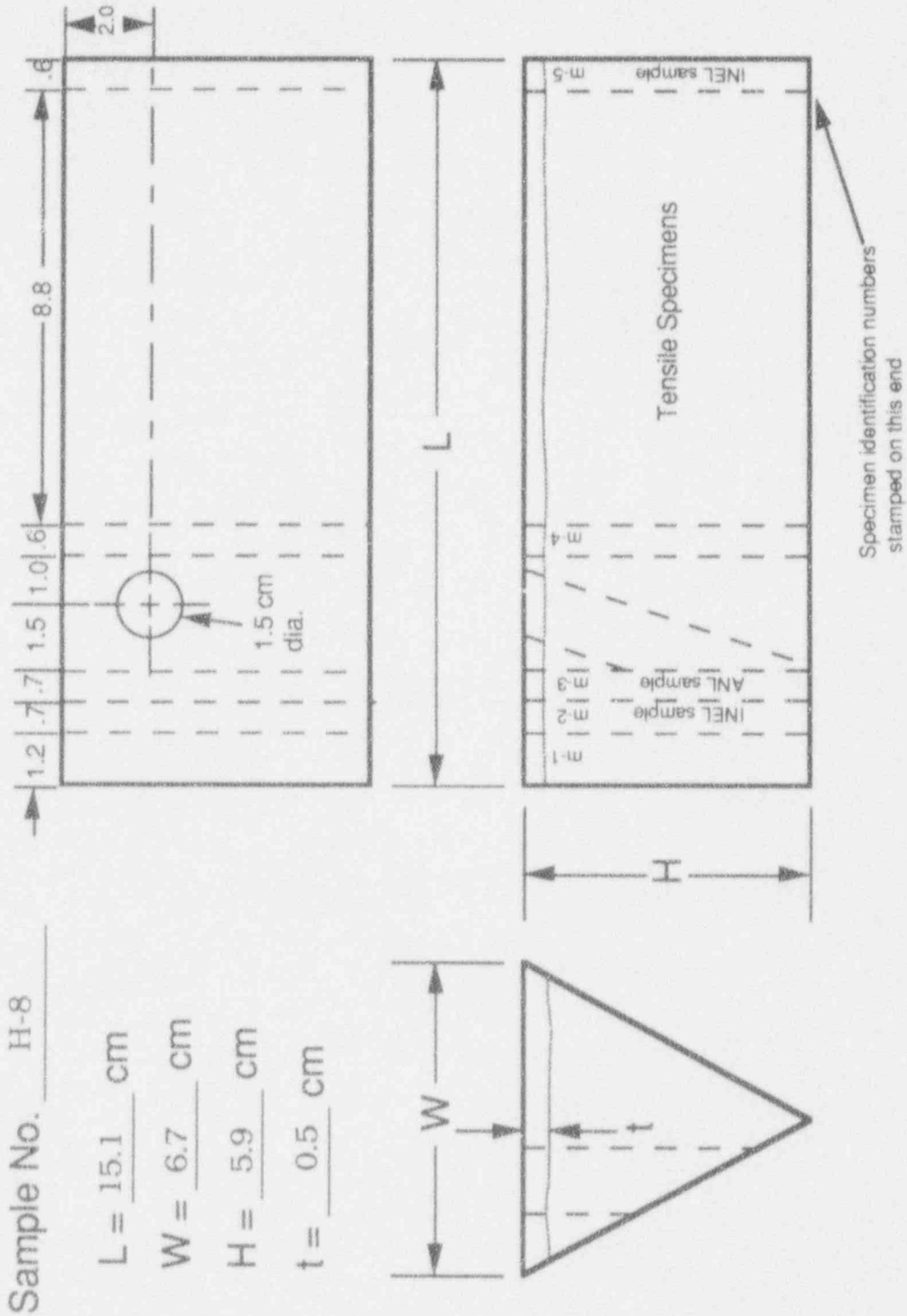

Fig. A20. Dimensions and initial sections from TMI-2 lower head Sample H-8.

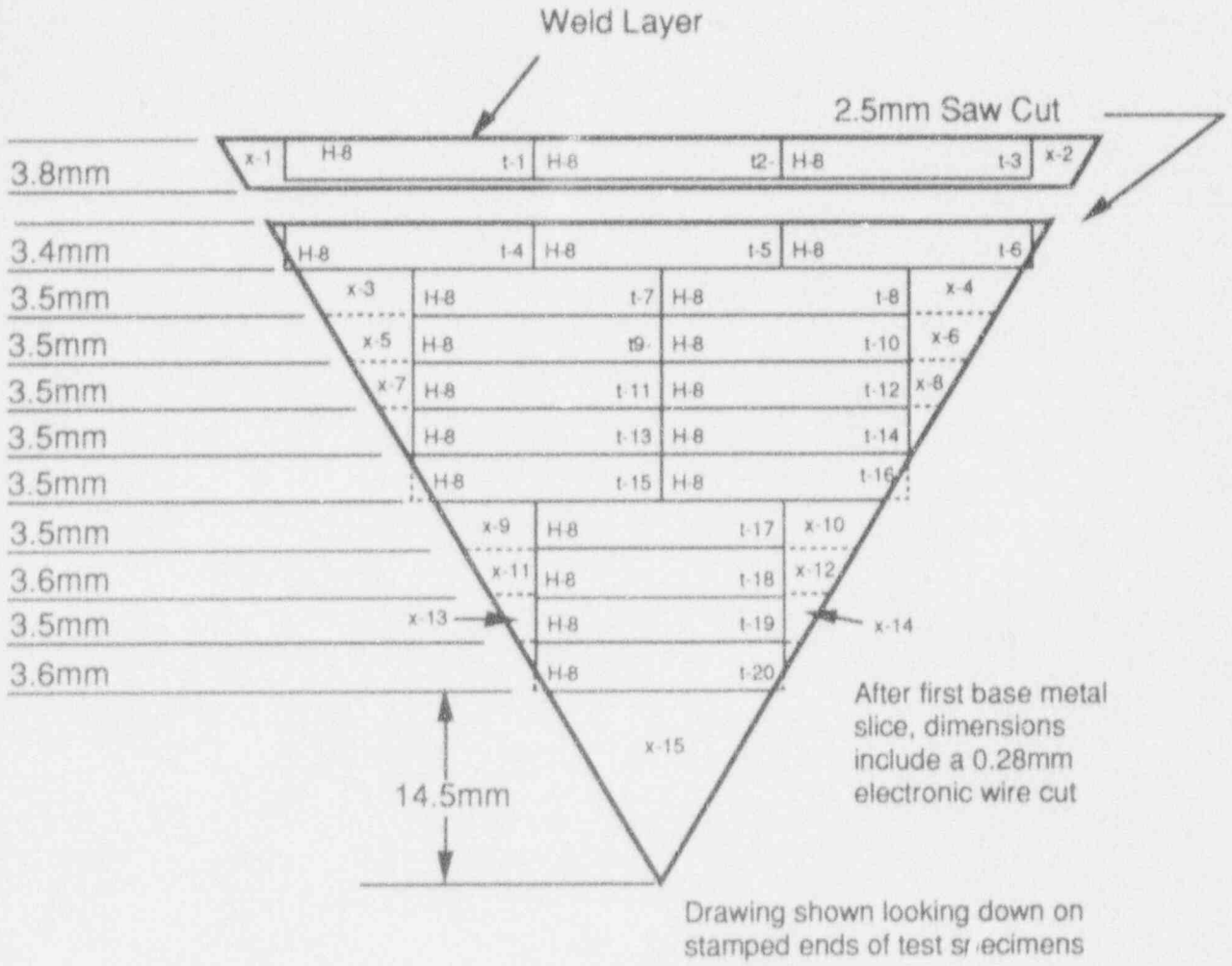

Fig. A21. Locations of mechanical test specimens cut from Sample H-8.

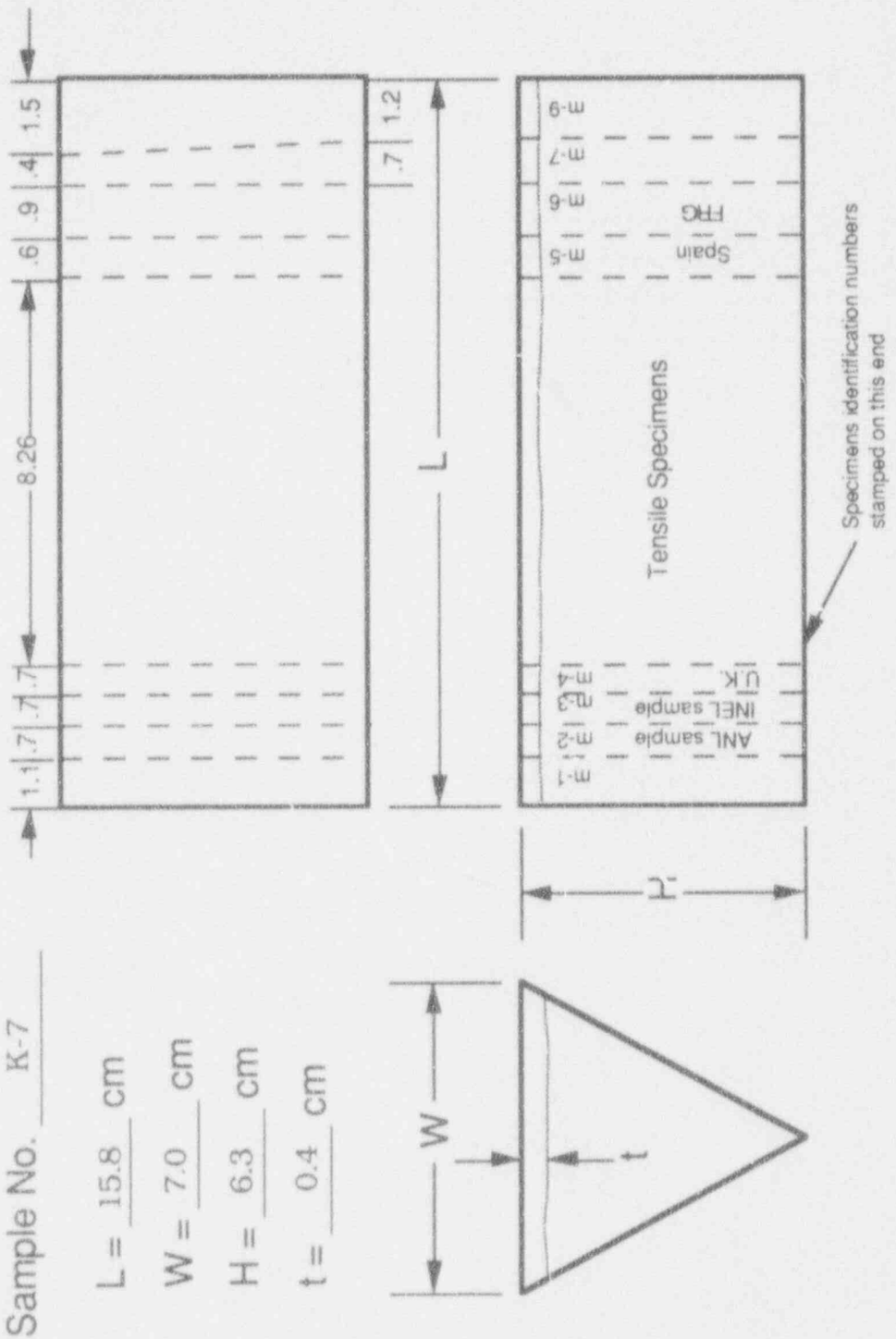

Fig. A22. Dimensions and initial sections from TMI-2 lower head Sample K-7.

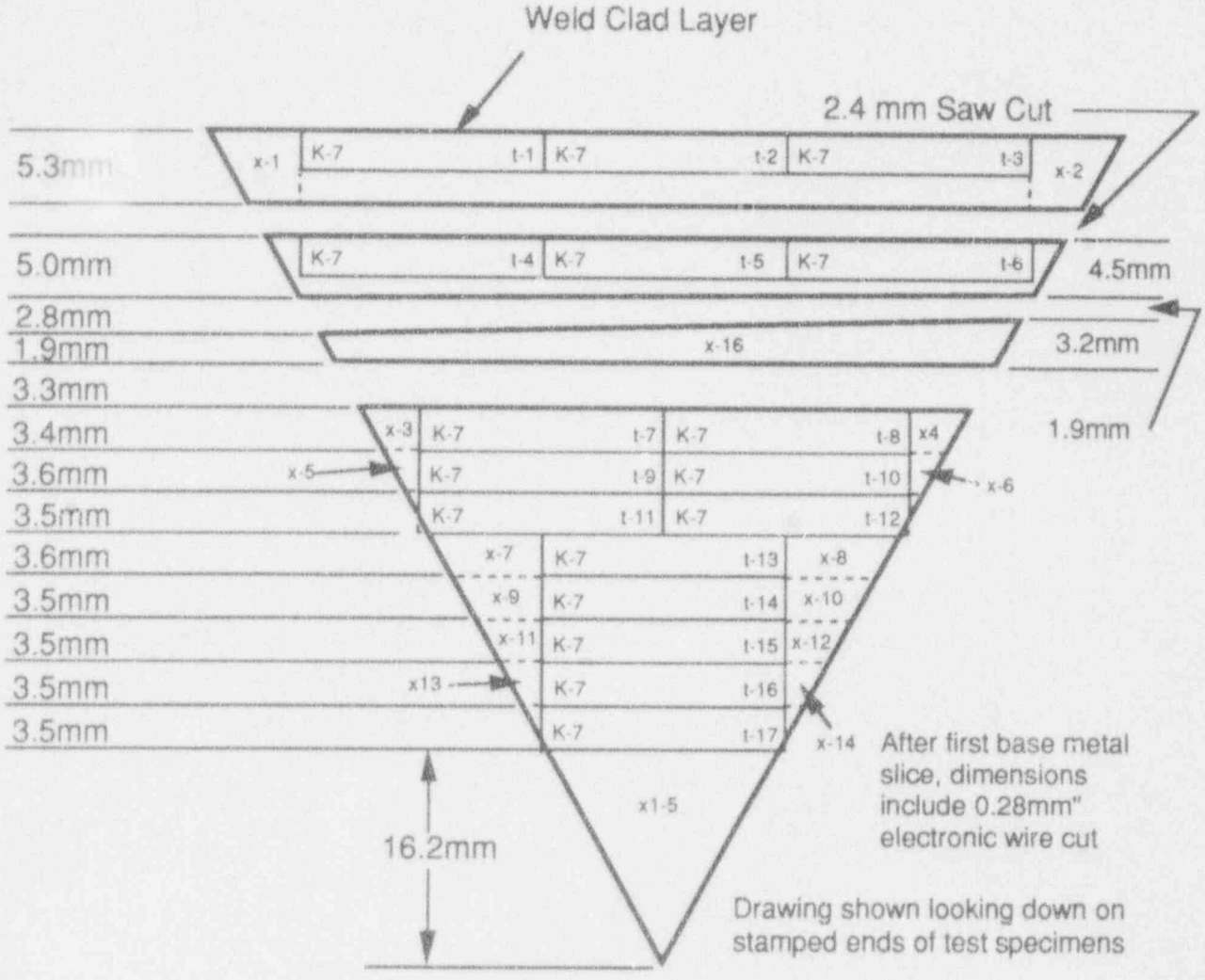

Fig. A23. Locations of mechanical test specimens cut from Sample K-7.

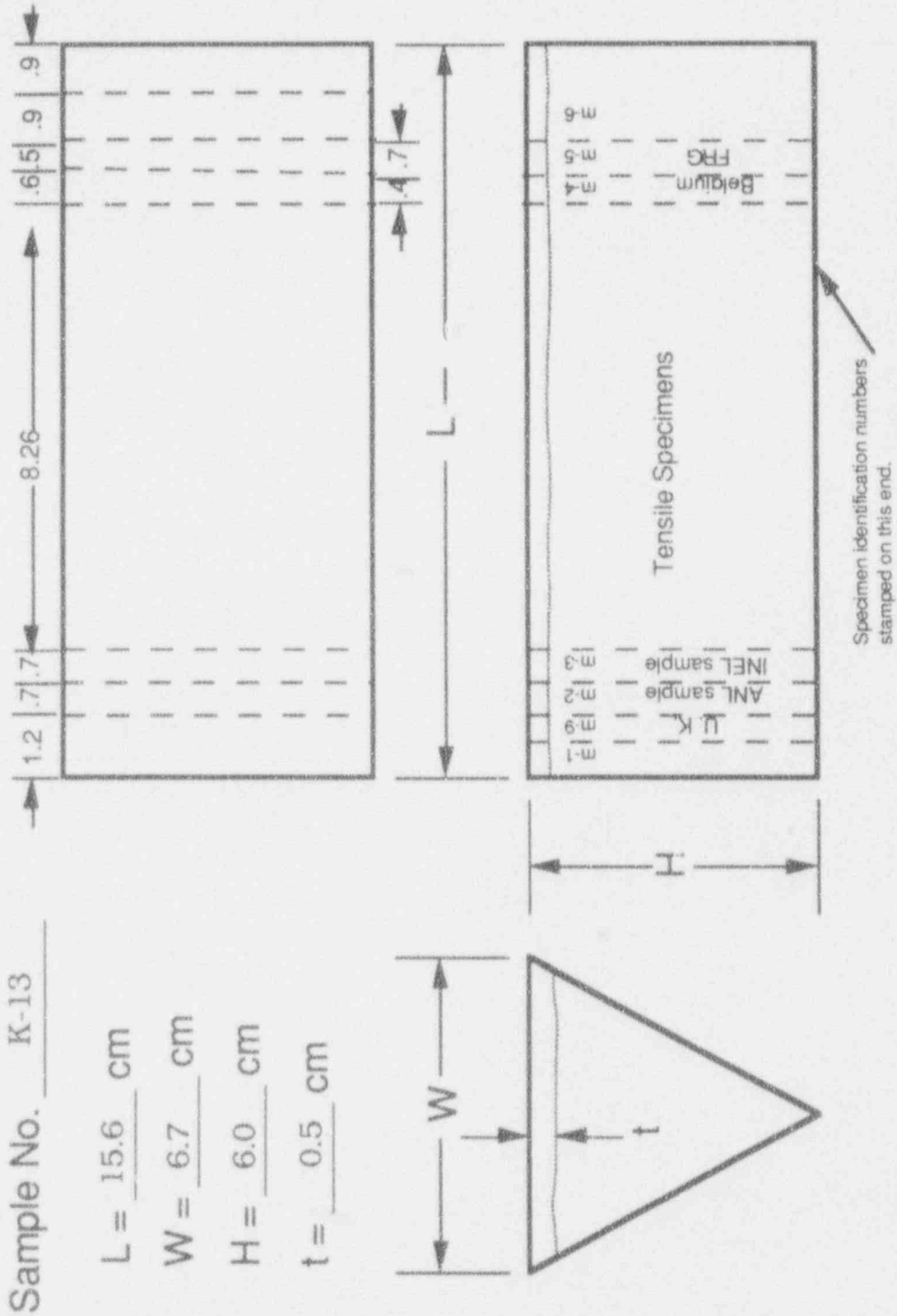

Fig. A24. Dimensions and initial sections from TMI-2 lower head Sample K-13.

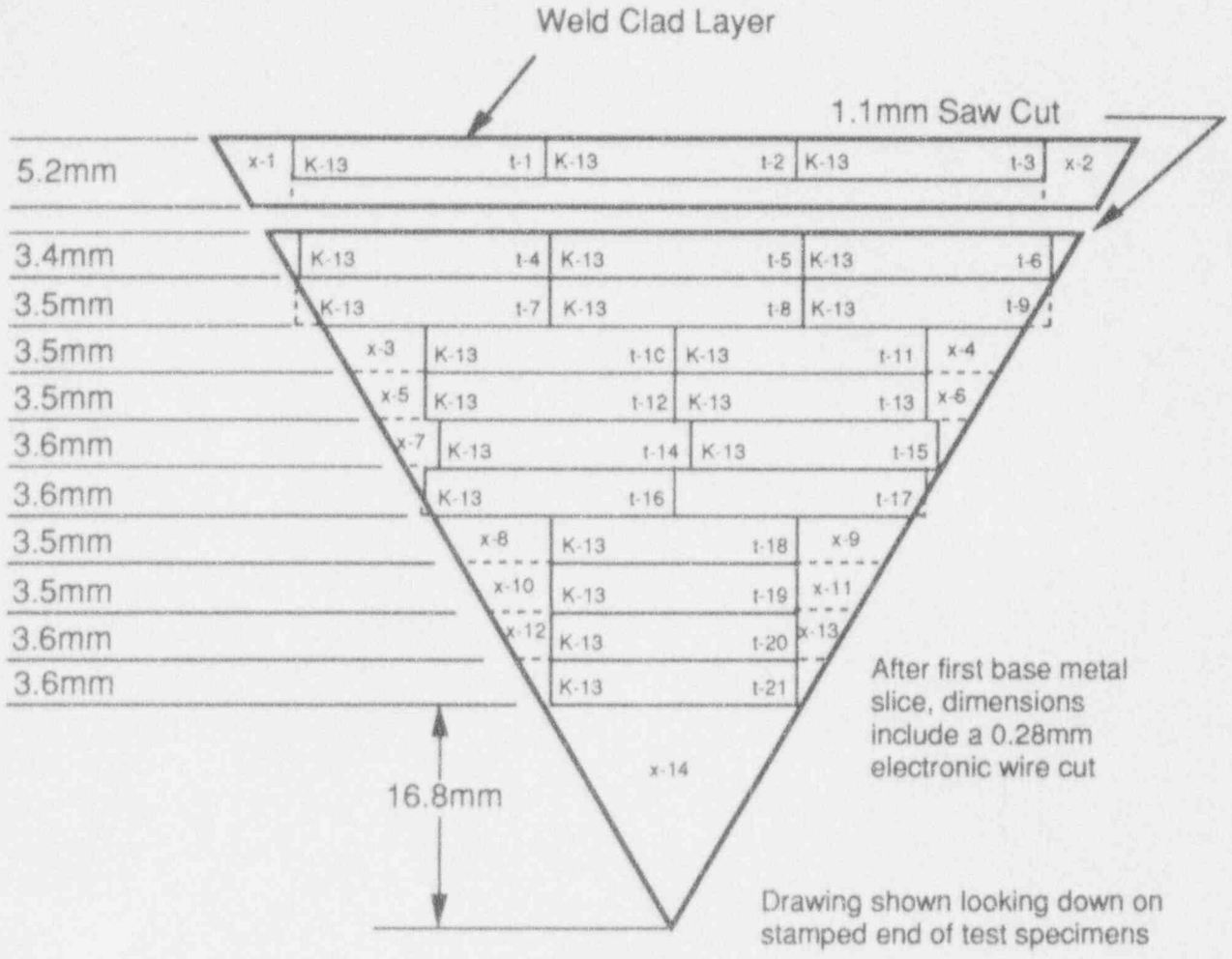

Fig. A25. Locations of mechanical test specimens cut from Sample K-13.

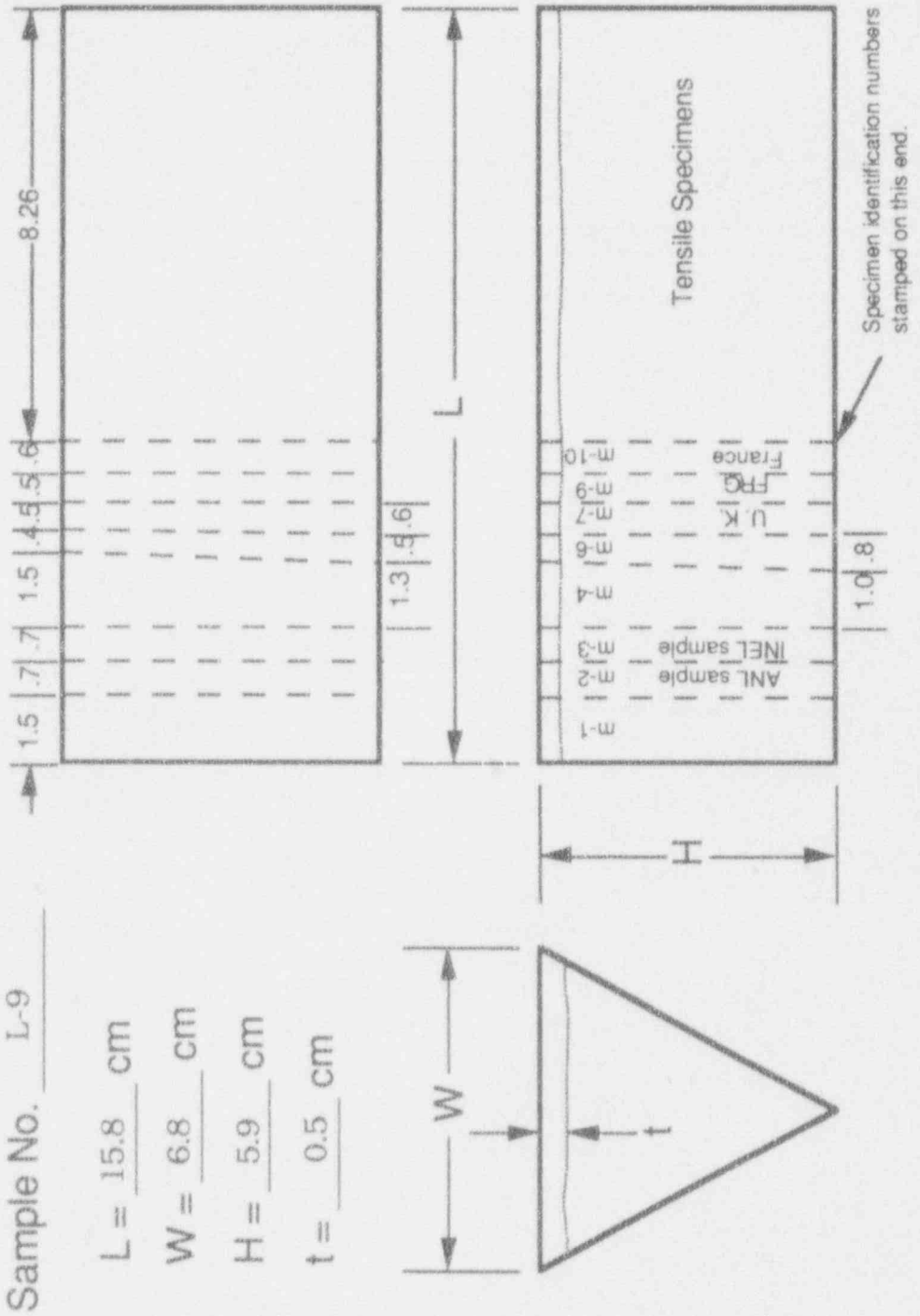

Fig. A26. Dimensions and initial sections from TMI-2 lower head Sample L-9.

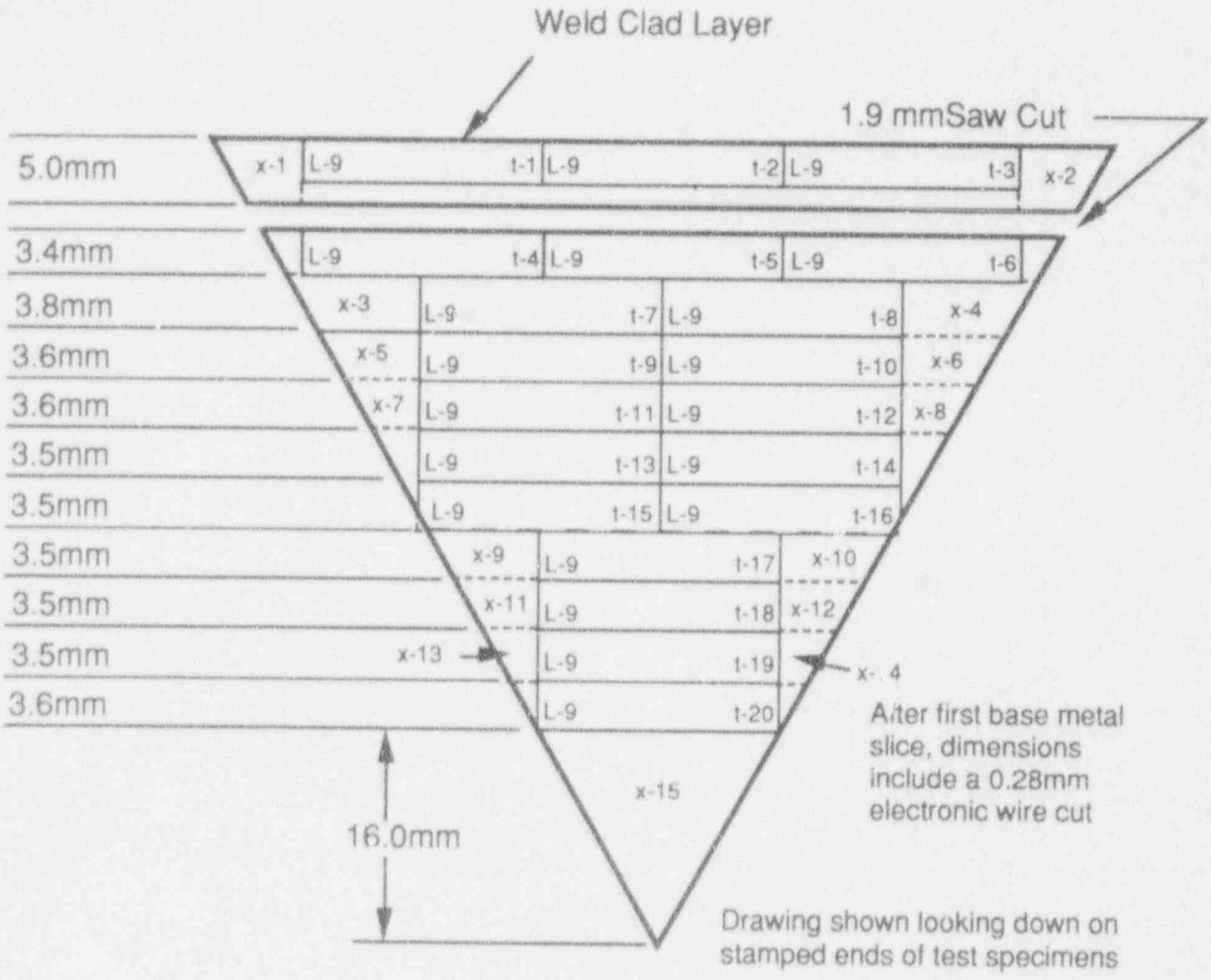

Fig. A27. Locations of mechanical test specimens cut from Sample L-9.

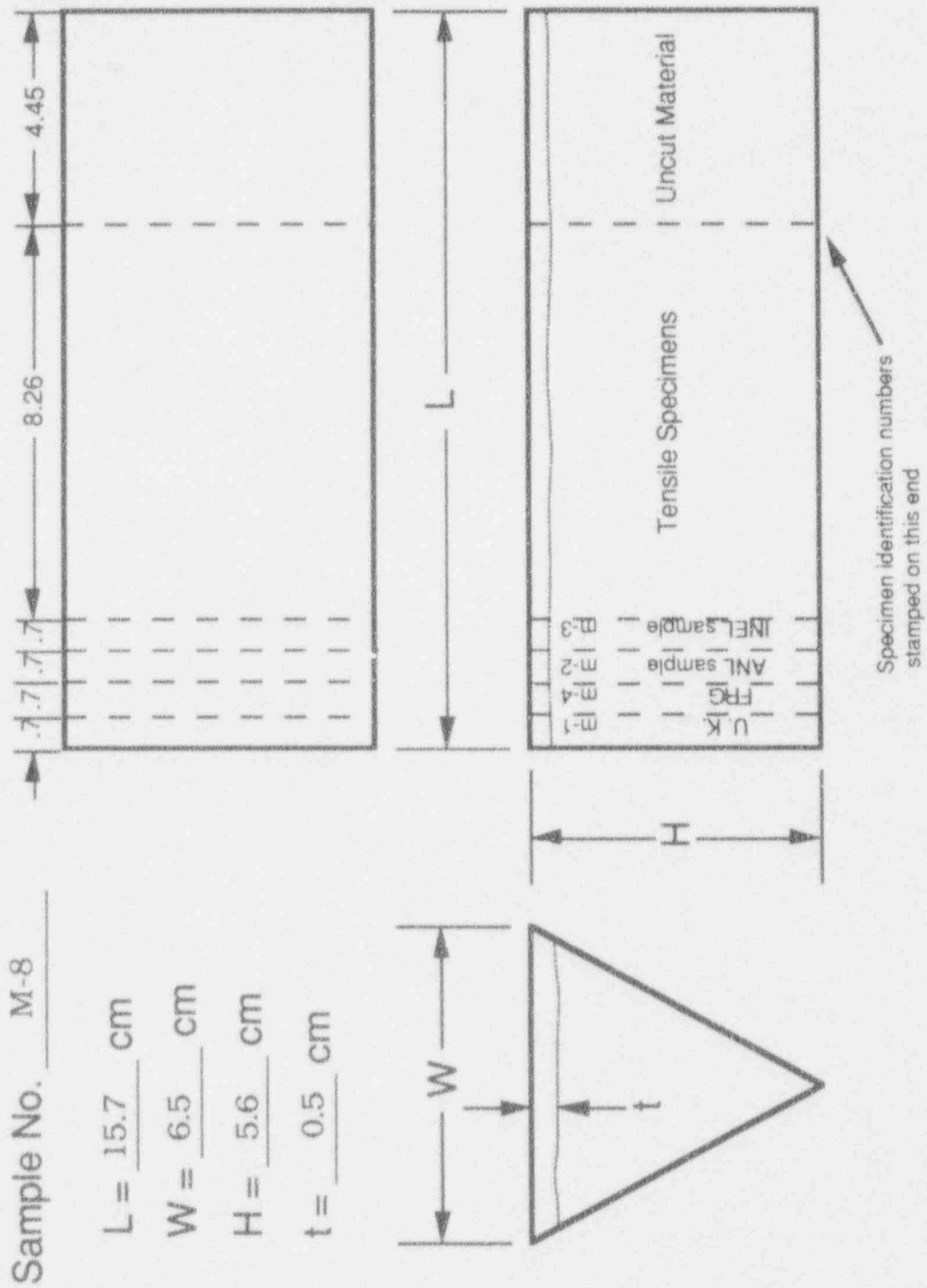

Fig. A28. Dimensions and initial sections from TMI-2 lower head Sample M-8.

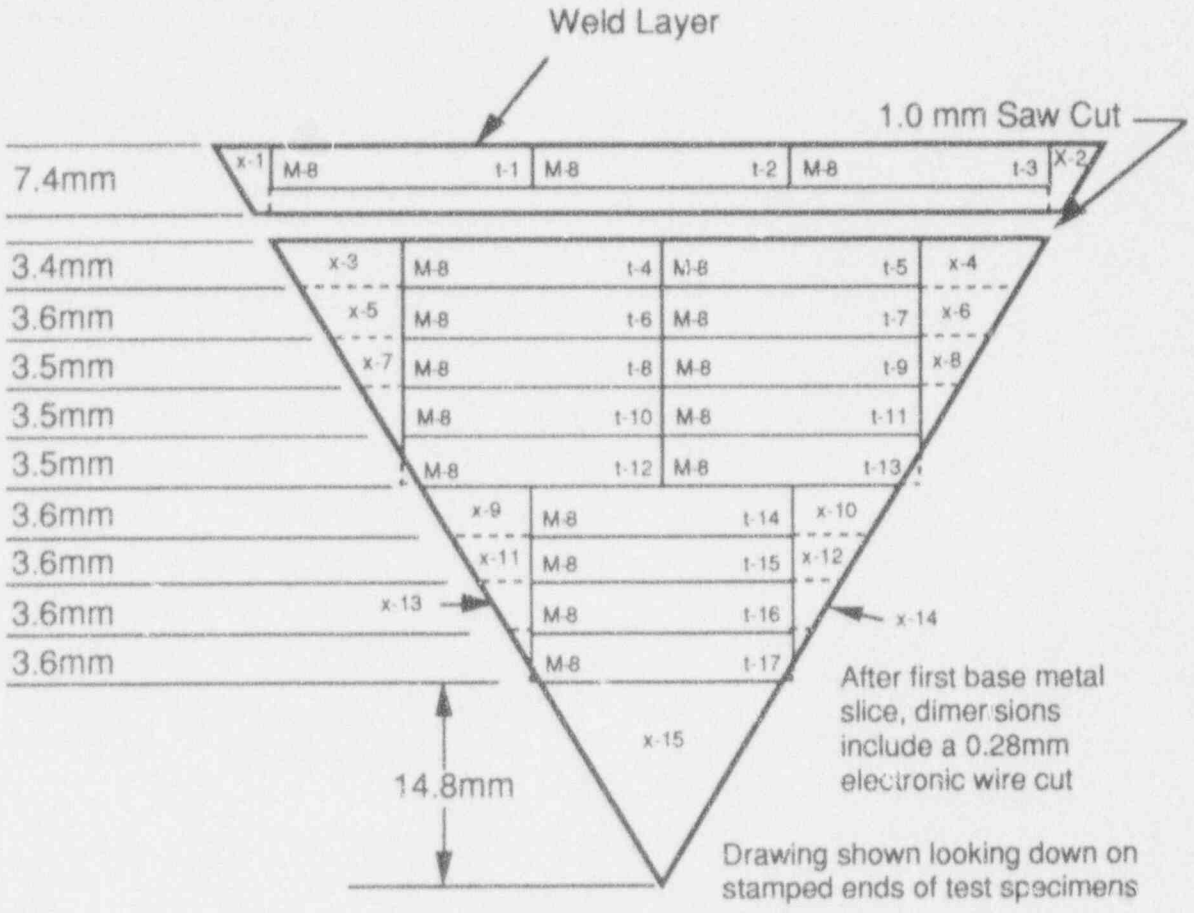

Fig. A29. Locations of mechanical test specimens cut from Sample M-8.

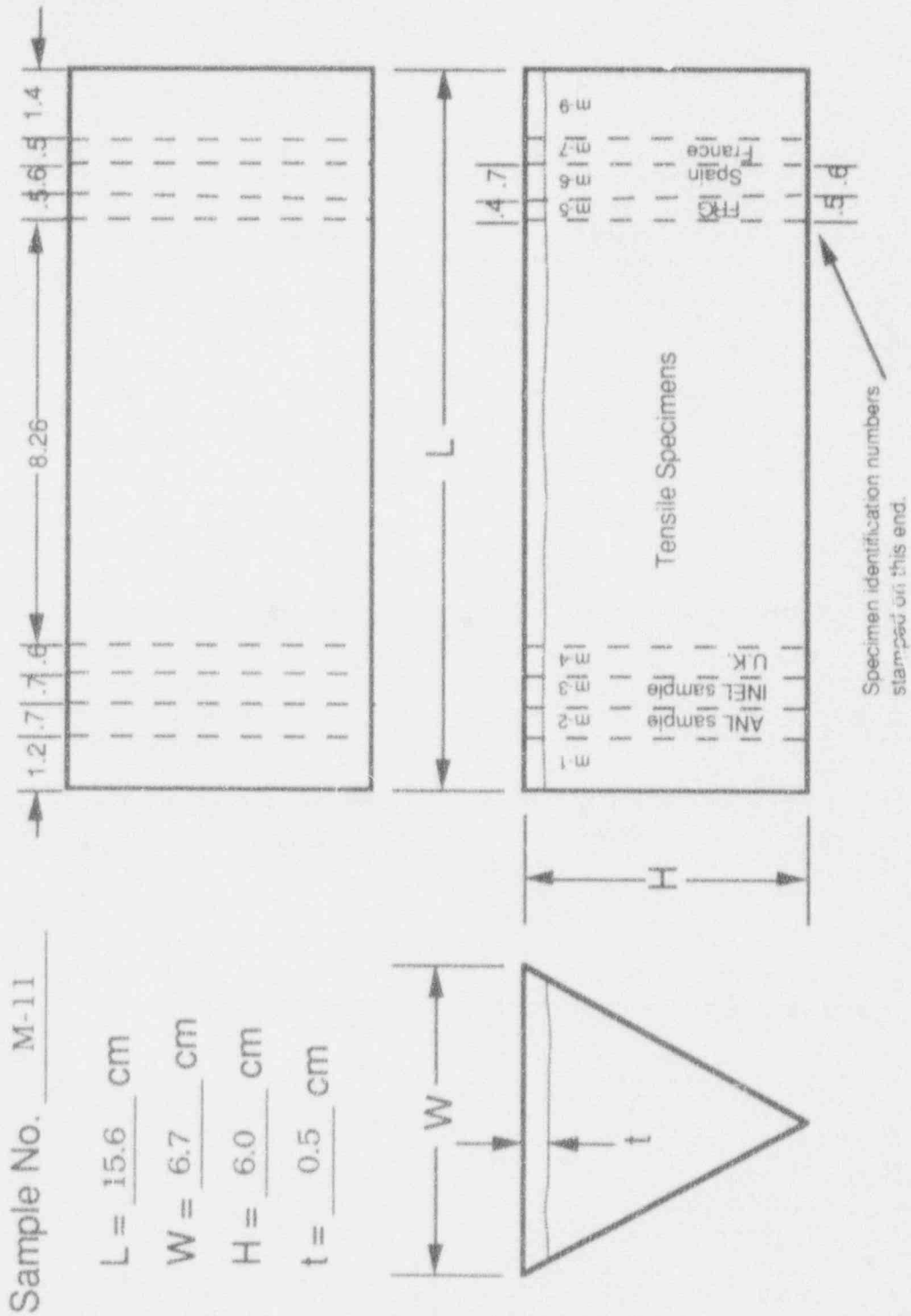

Fig. A30. Dimensions and initial sections from TMI-2 lower head Sample M-11.

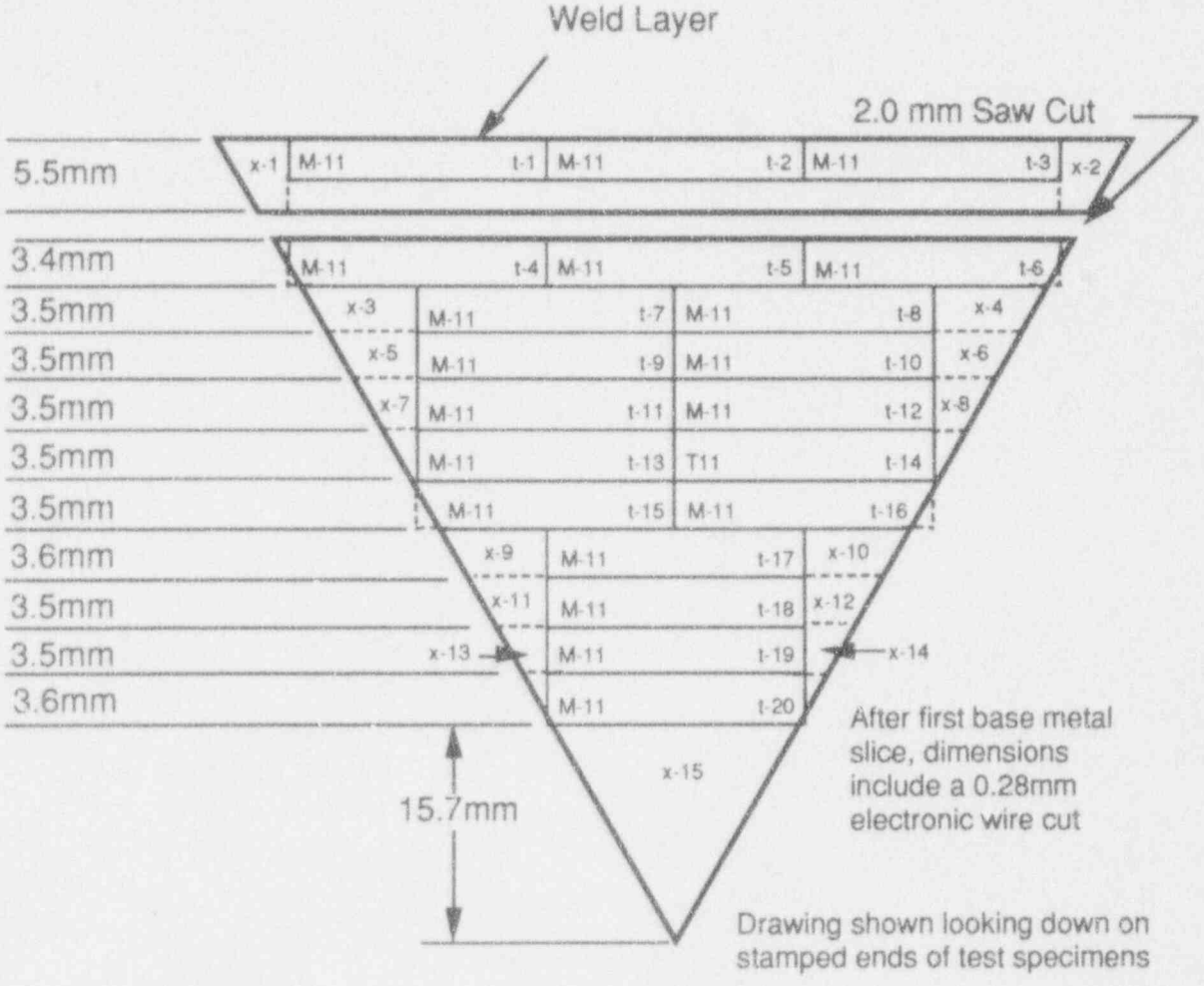

Fig. A31. Locations of mechanical test specimens cut from Sample M-11.

Appendix B:

Strain-vs.-Time Curves for Creep Tests Conducted on TMI-2 Lower Head Material

Test Temperature: 600°C
Applied Stress: 240 MPa
Time to Failure: 0.2 h

Specimen No.: K-13, t8
Laboratory: V.I.T.O.
Belgium

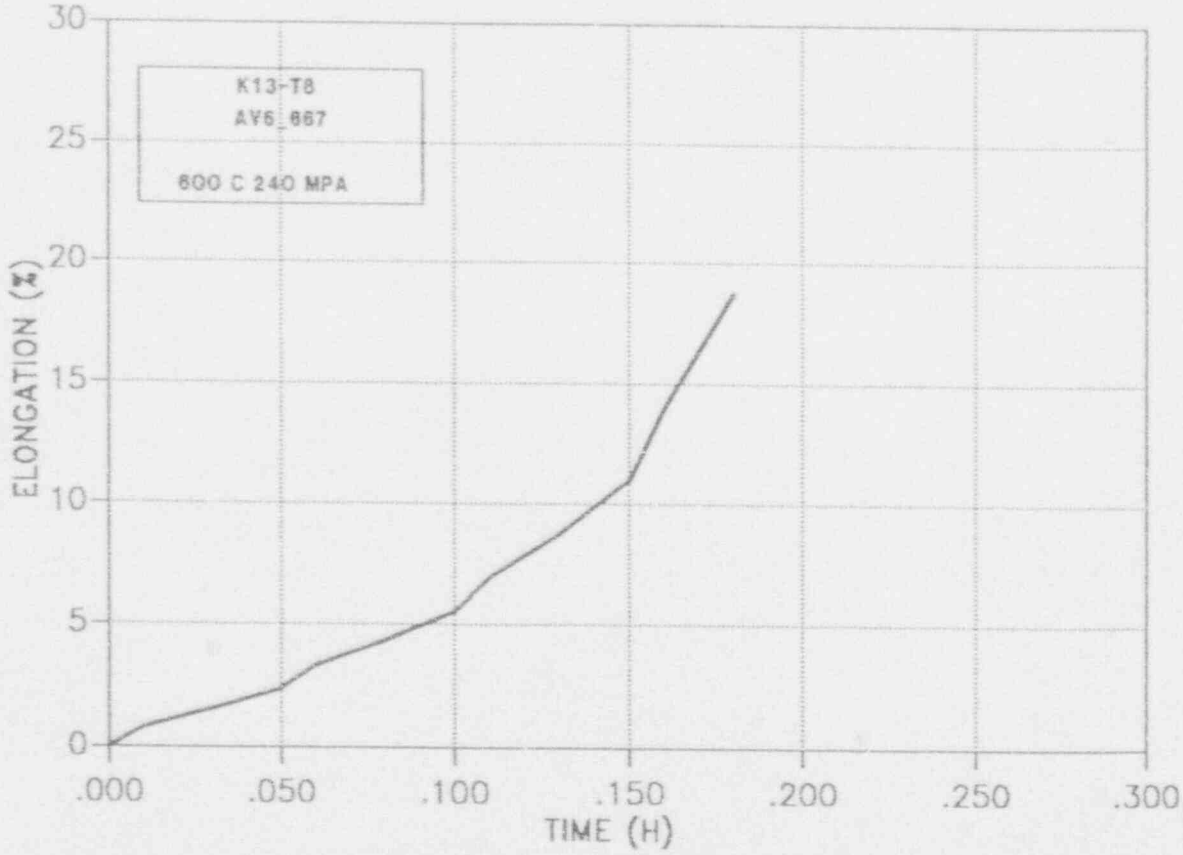

Test Temperature: 600°C
Applied Stress: 225 MPa
Time to Failure: 1.0 h

Specimen No.: K-13, t13
Laboratory: V.I.T.O.
Belgium

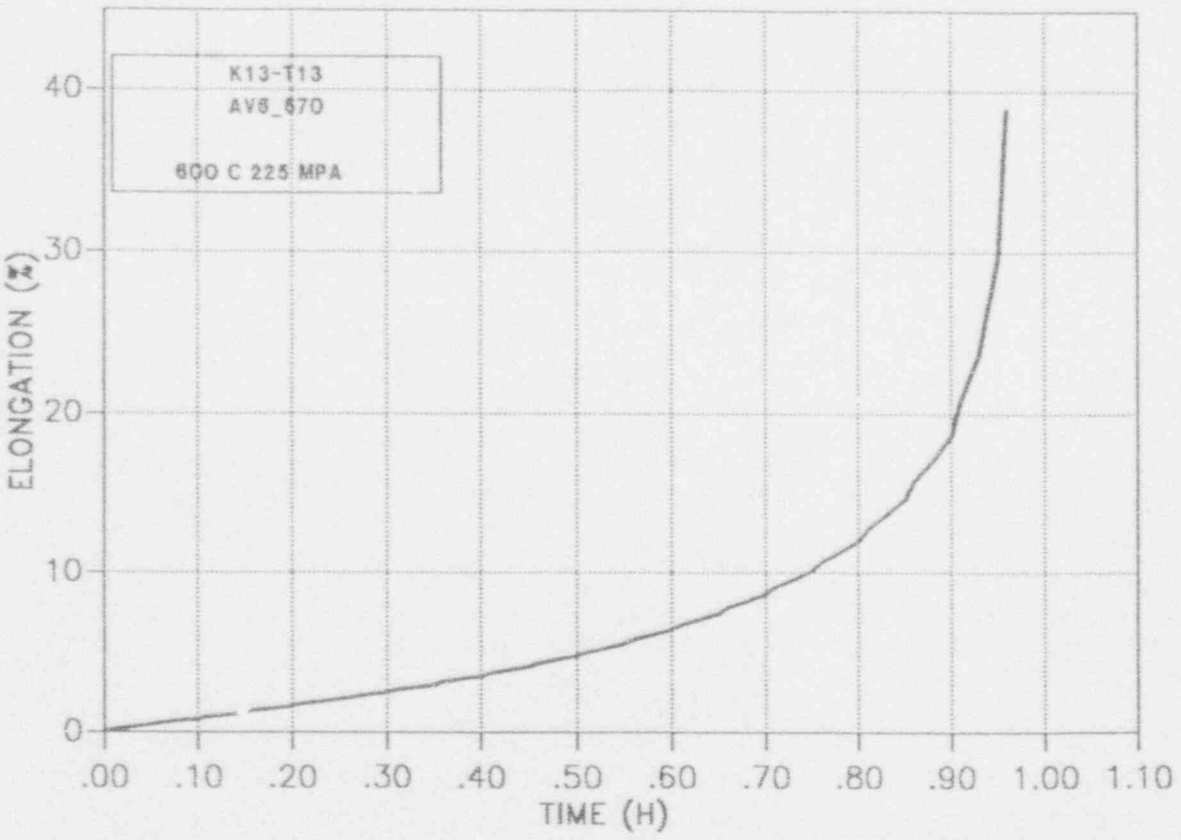

Test Temperature: 600°C
Applied Stress: 155 MPa
Time to Failure: 23.1 h

Specimen No.: K-13, t10
Laboratory: V.I.T.O.
Belgium

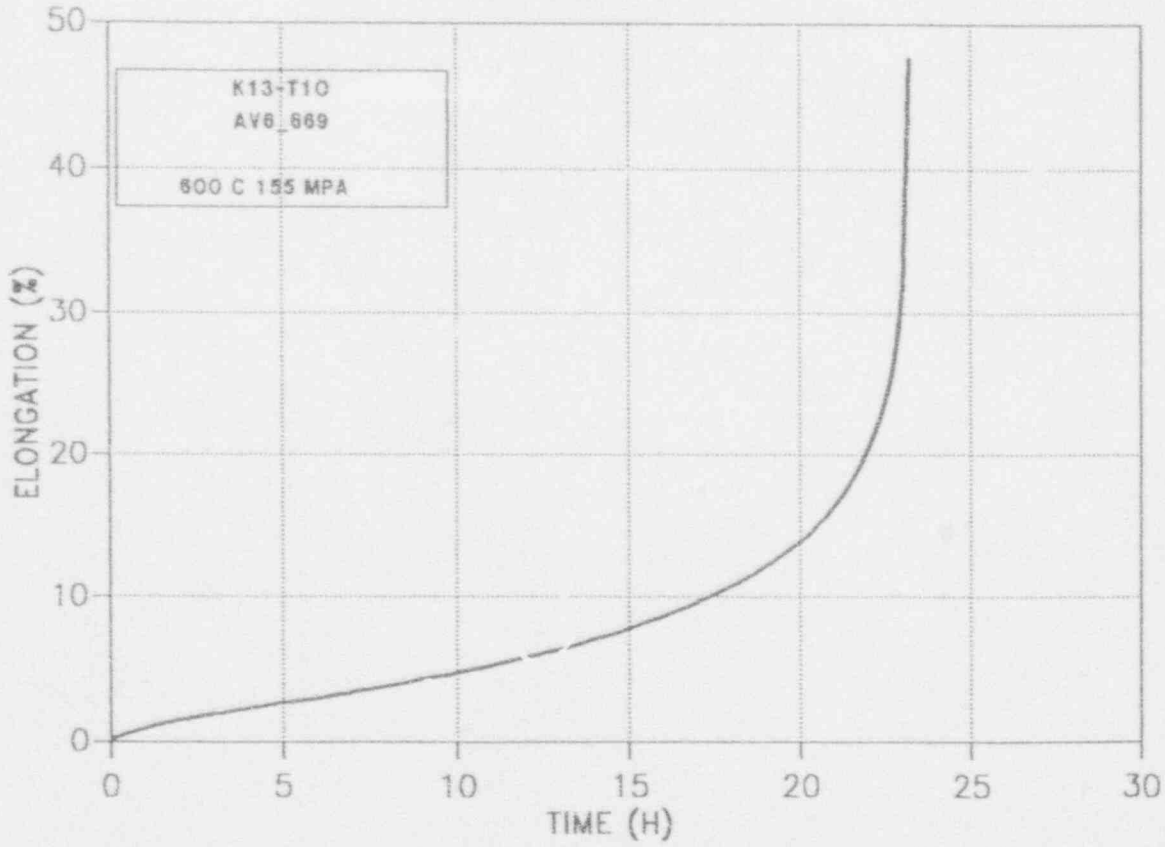

Test Temperature: 600°C
Applied Stress: 115 MPa
Time to Failure: 39 h

Specimen No.: K-13, t9
Laboratory: V.I.T.O.
Belgium

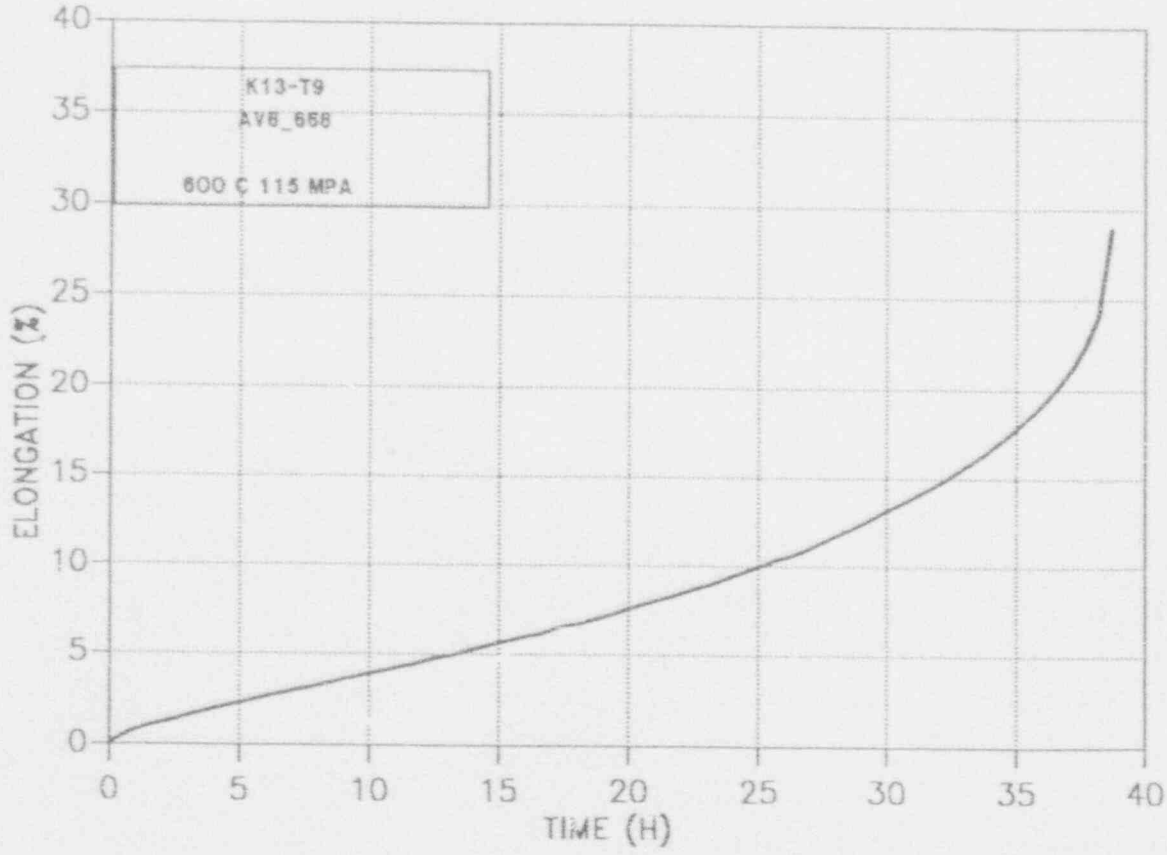

Test Temperature: 600°C
Applied Stress: 115 MPa
Time to Failure: 128 h

Specimen No.: K-13, t14
Laboratory: V.I.T.O.
Belgium

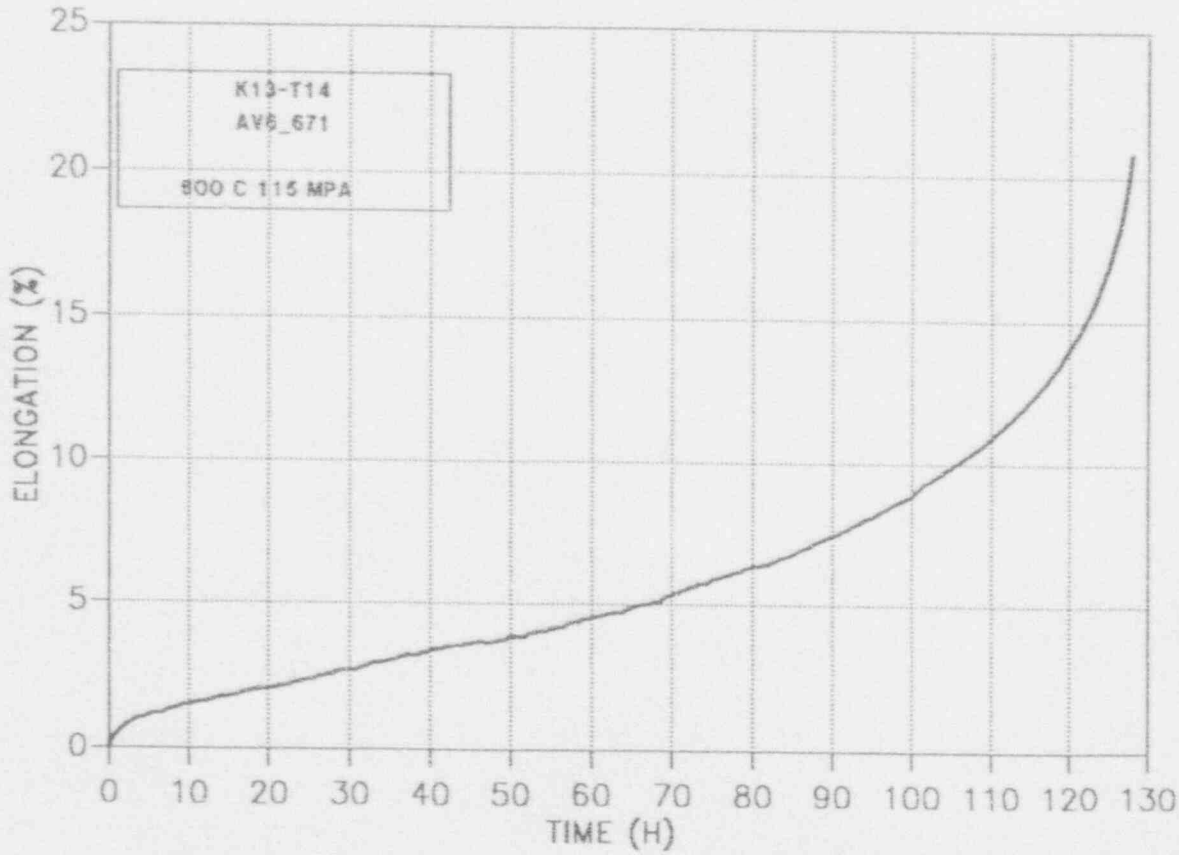

Test Temperature: 600°C
Applied Stress: 232 MPa
Time to Failure: 2.47 h

Specimen No.: F-5, t14
Laboratory: tecnatom, s.a.
Spain

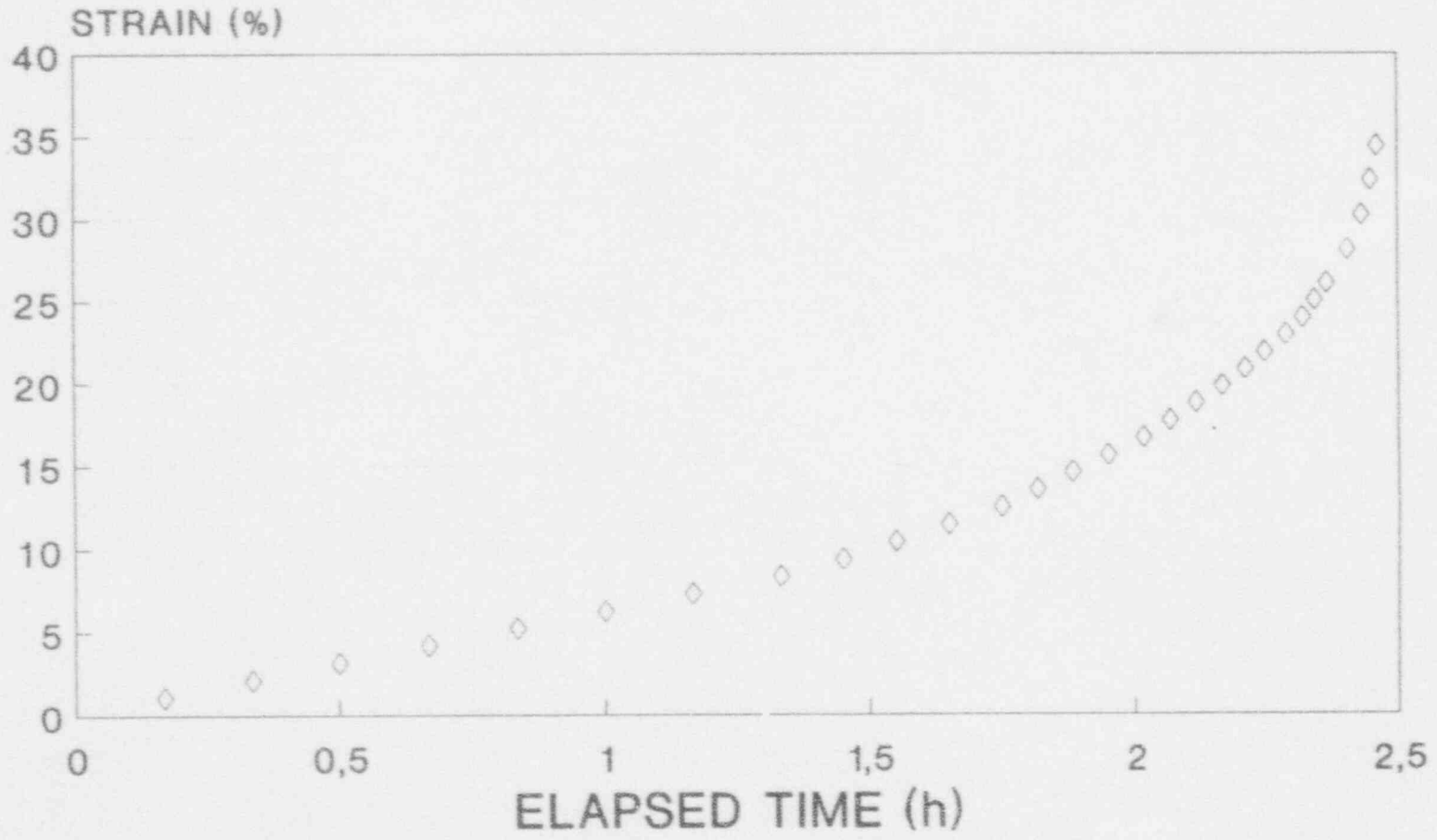

Test Temperature: 600°C
Applied Stress: 221 MPa
Time to Failure: 4.14 h

Specimen No.: F-5, t18
Laboratory: tecnatom, s.a.
Spain

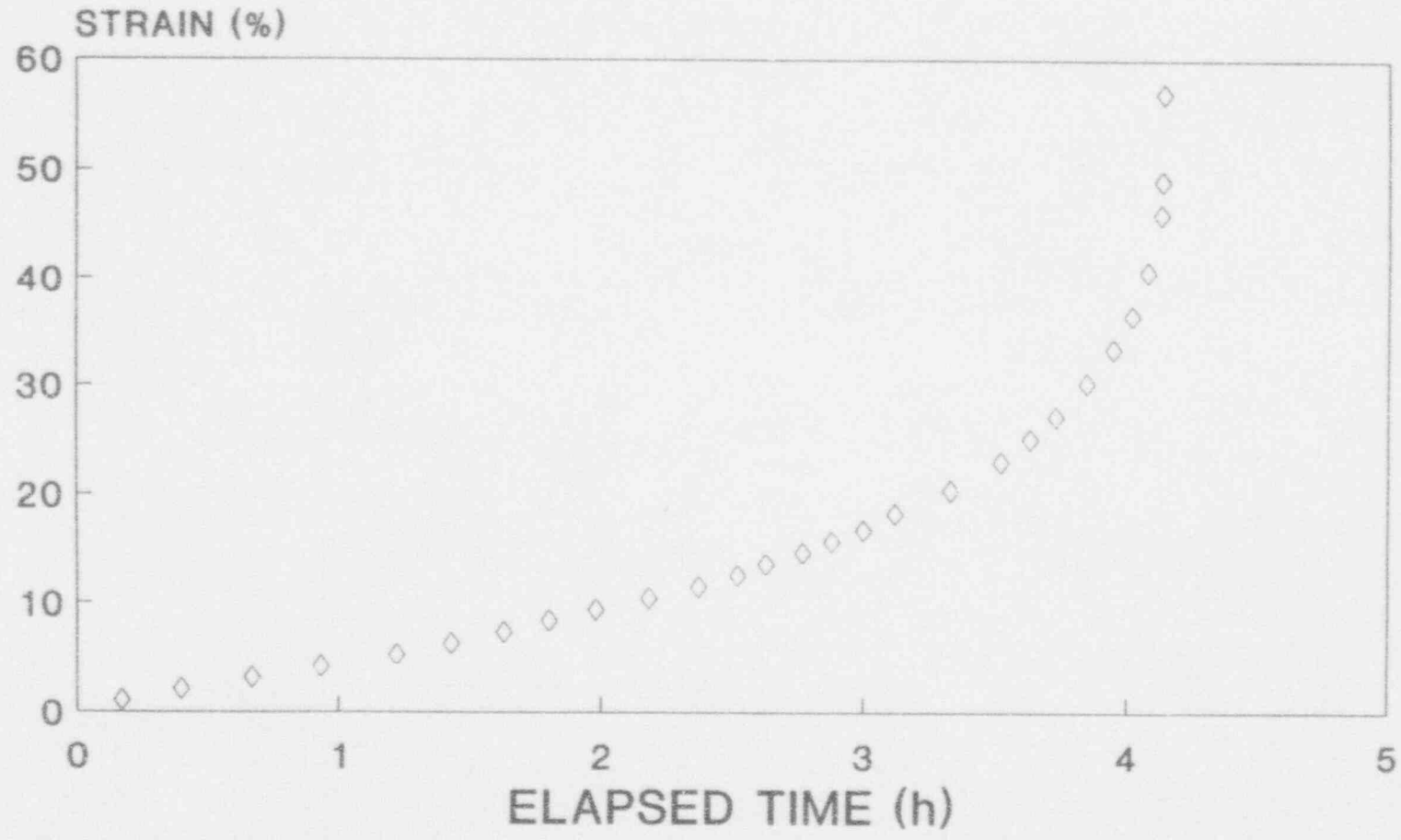

Test Temperature: 600°C
Applied Stress: 194 MPa
Time to Failure: 9.47 h

Specimen No.: F-5, t15
Laboratory: tecnatom, s.a.
Spain

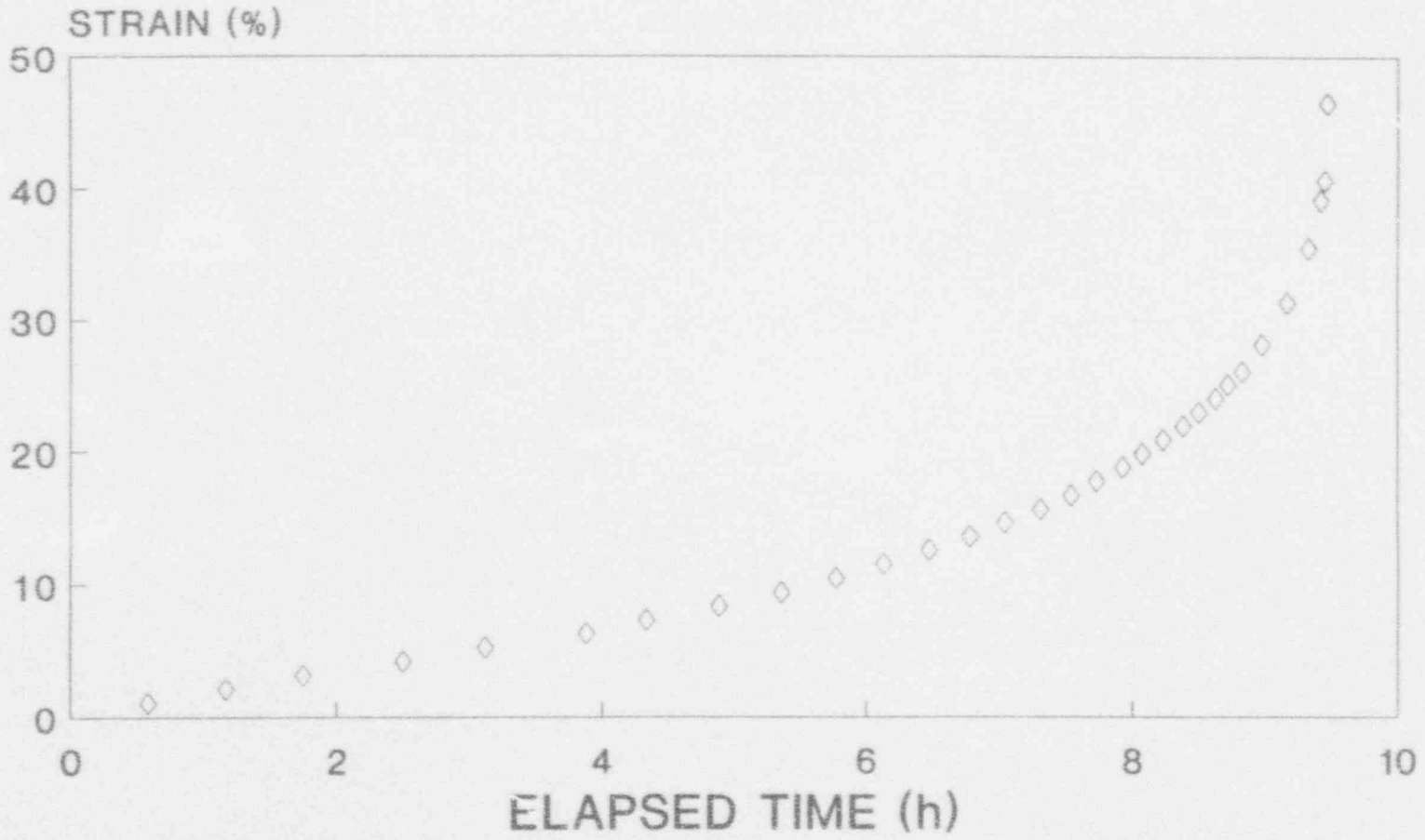

Test Temperature: 600°C
Applied Stress: 157 MPa
Time to Failure: 17.75 h

Specimen No.: F-5, t16
Laboratory: tecnatom, s.a.
Spain

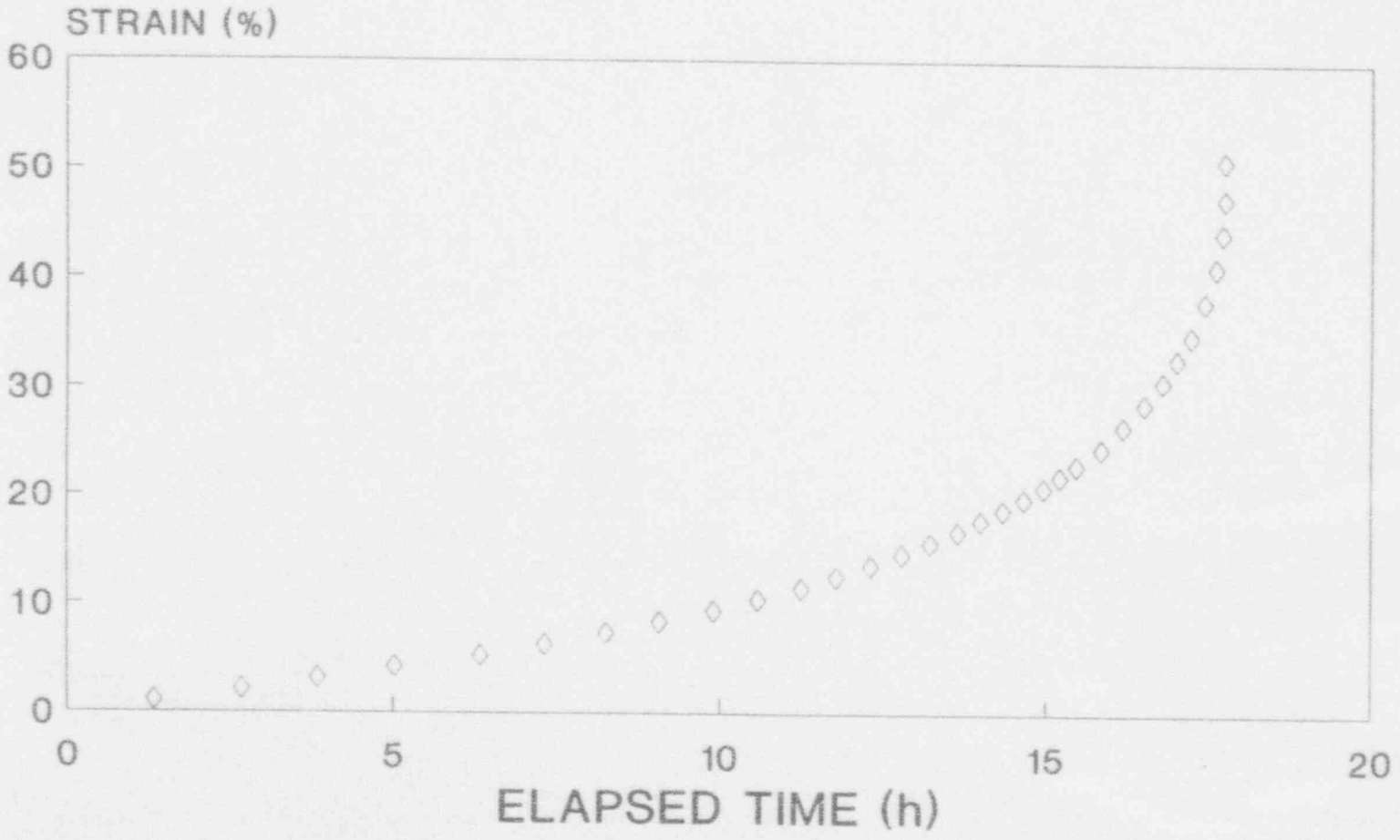

Test Temperature: 600°C
Applied Stress: 114 MPa
Time to Failure: 92.8 h

Specimen No.: F-5, t17
Laboratory: tecnatom, s.a.
Spain

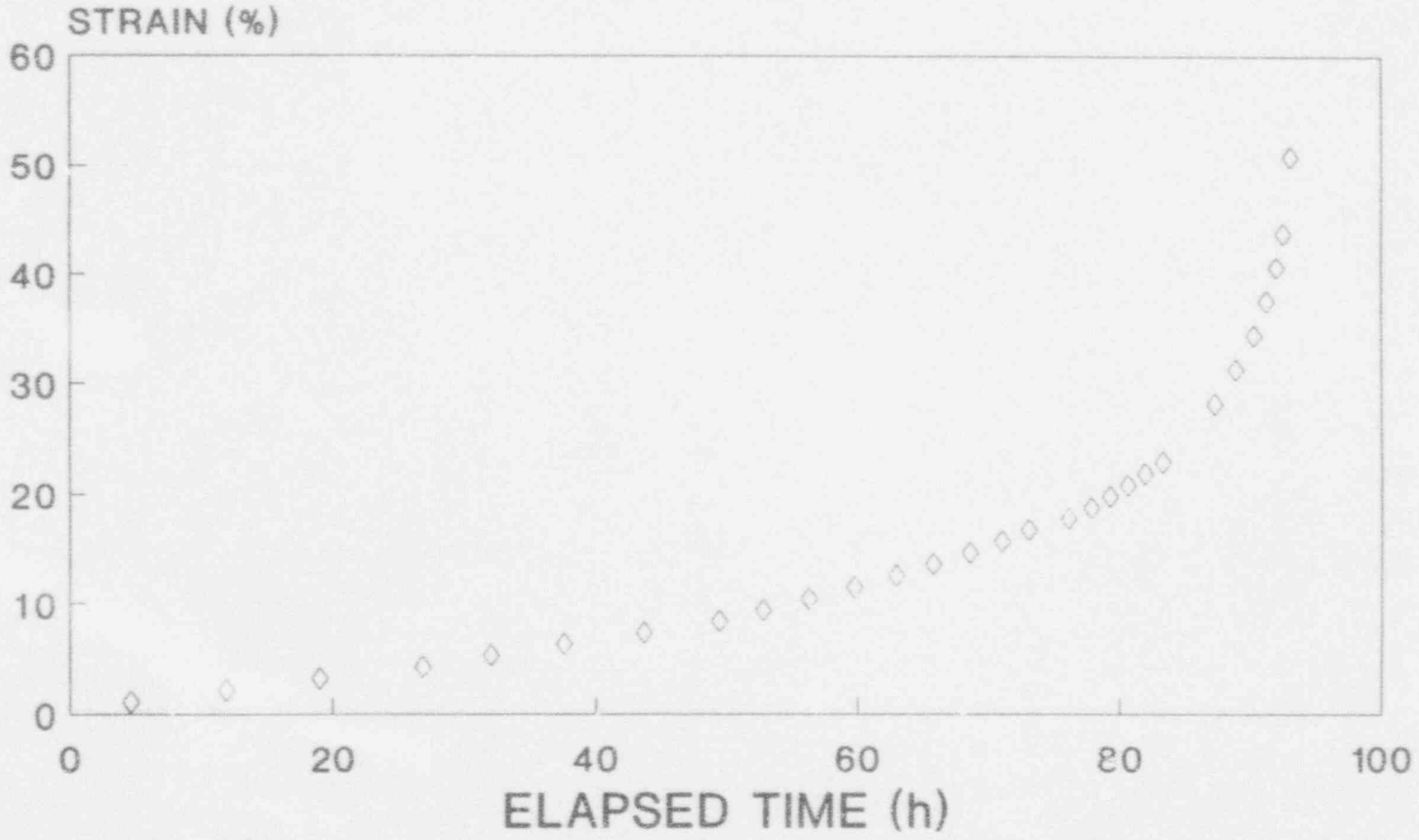

Test Temperature: 700°C
Applied Stress: 60 MPa
Time to Failure: 13.5 h

Specimen No.: M-11, t10
Laboratory: CEA
France

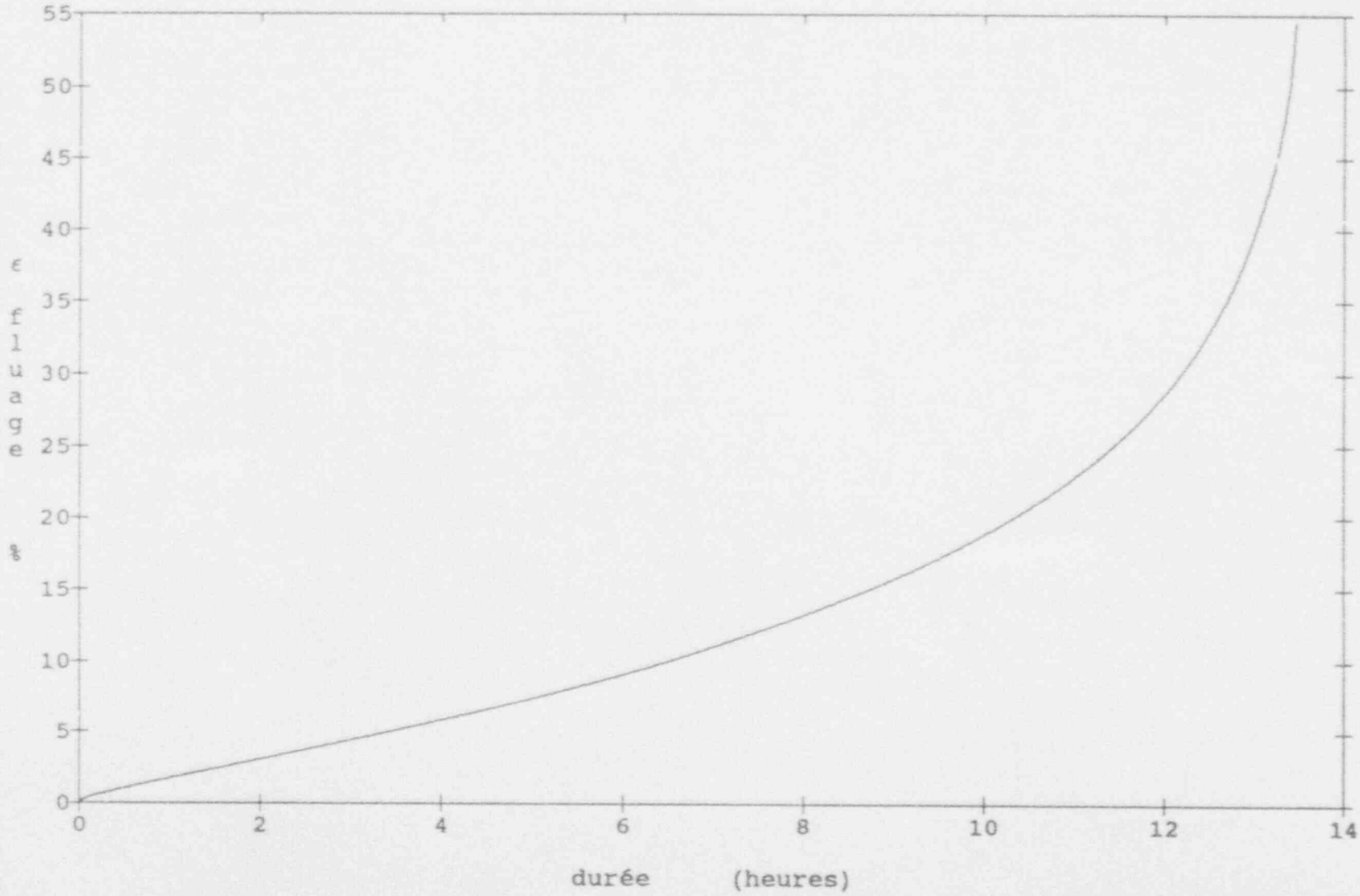

Test Temperature: 700°C
Applied Stress: 55 MPa
Time to Failure: 20 h

Specimen No.: M-11, t9
Laboratory: CEA
France

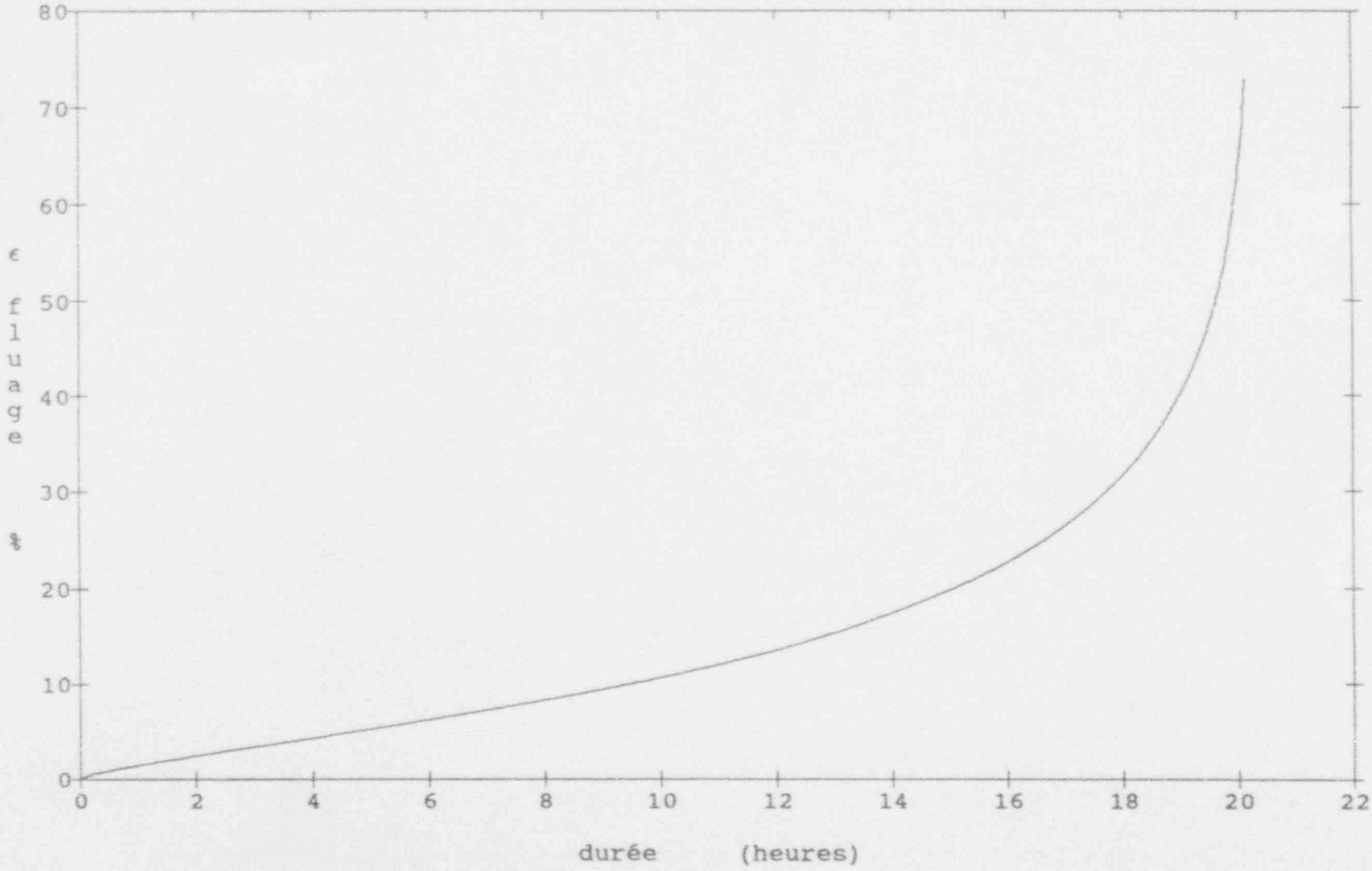

Test Temperature: 700°C
Applied Stress: 40 MPa
Time to Failure: 43 h

Specimen No.: M-11, t11
Laboratory: CEA
France

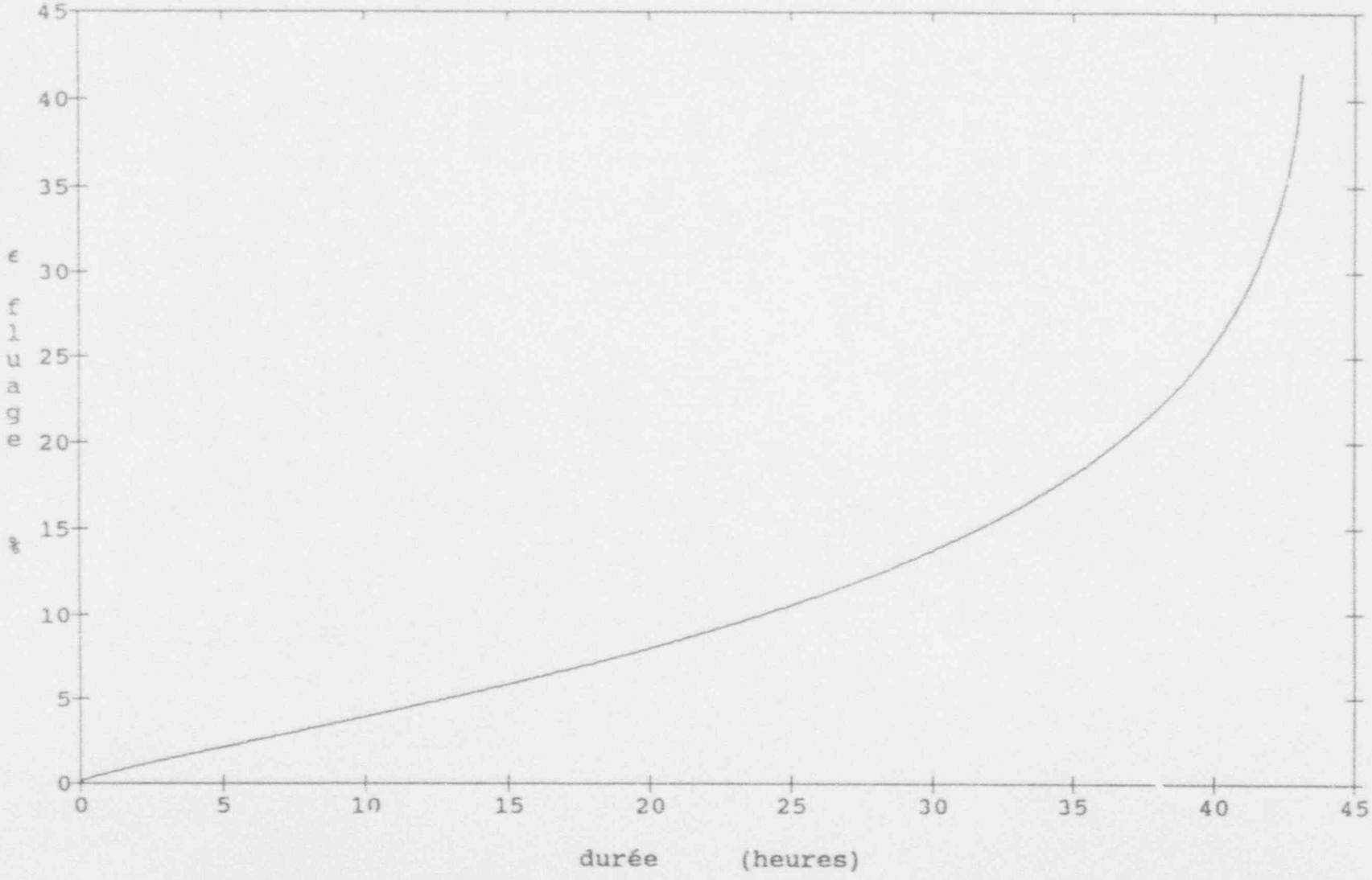

Test Temperature: 700°C
Applied Stress: 95.1 MPa
Time to Failure: 1.34 h

Specimen No.: H-8, t17
Laboratory: ANL
United States

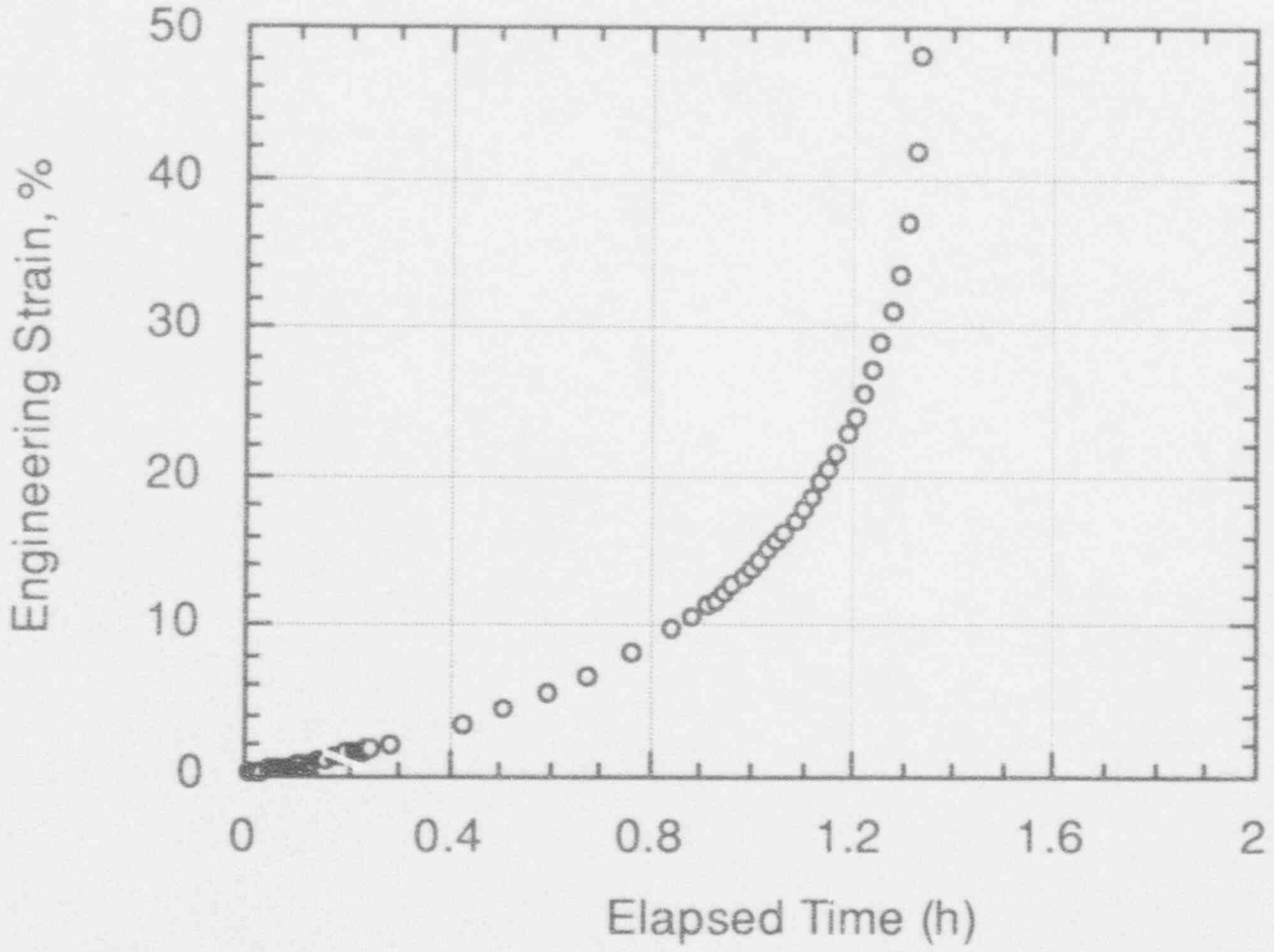

Test Temperature: 700°C
Applied Stress: 80.0 MPa
Time to Failure: 3.27 h

Specimen No.: H-8, t16
Laboratory: ANL
United States

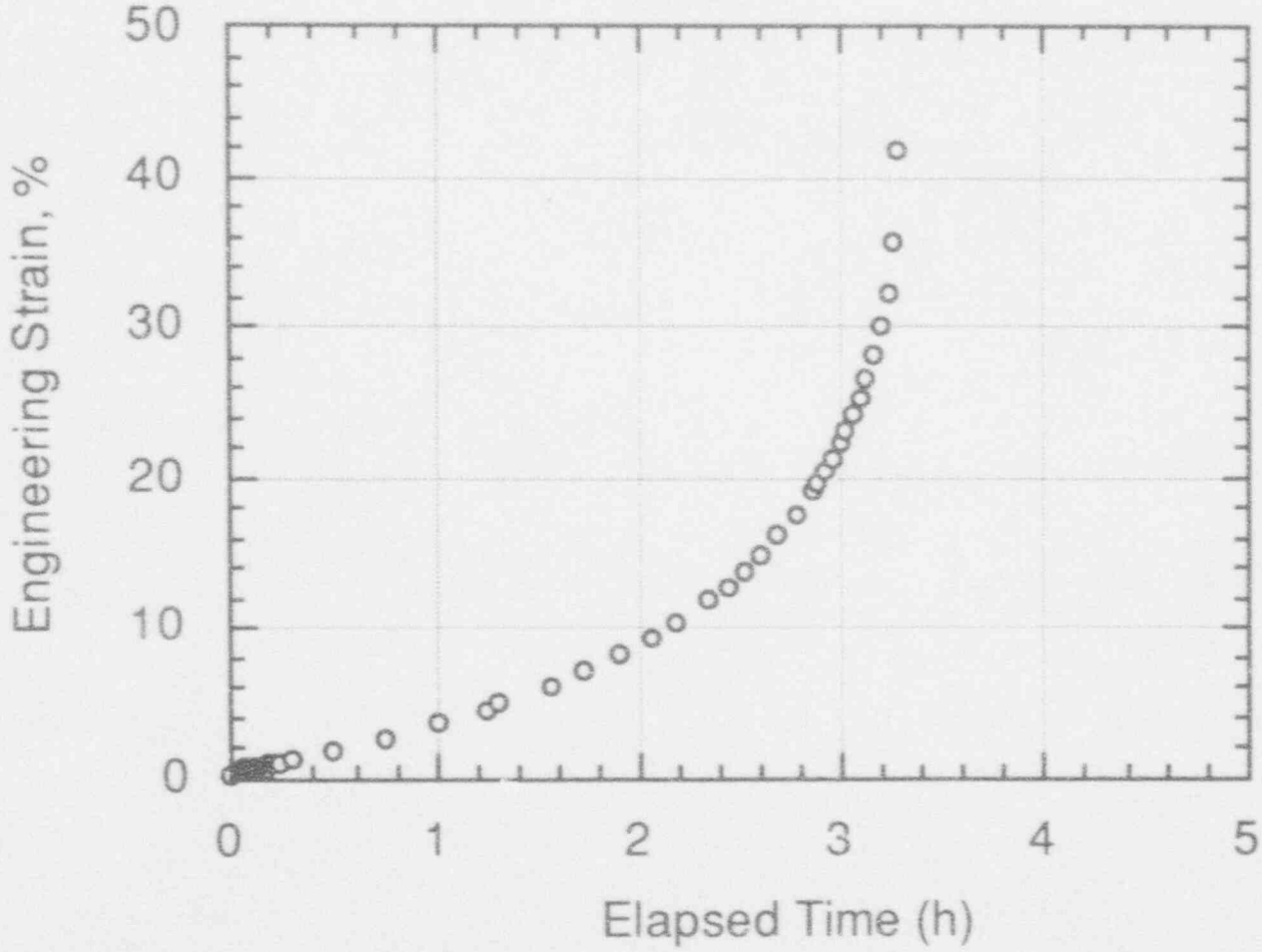

Test Temperature: 700°C
Applied Stress: 52.1 MPa
Time to Failure: 27.6 h

Specimen No.: H-8, t13
Laboratory: ANL
United States

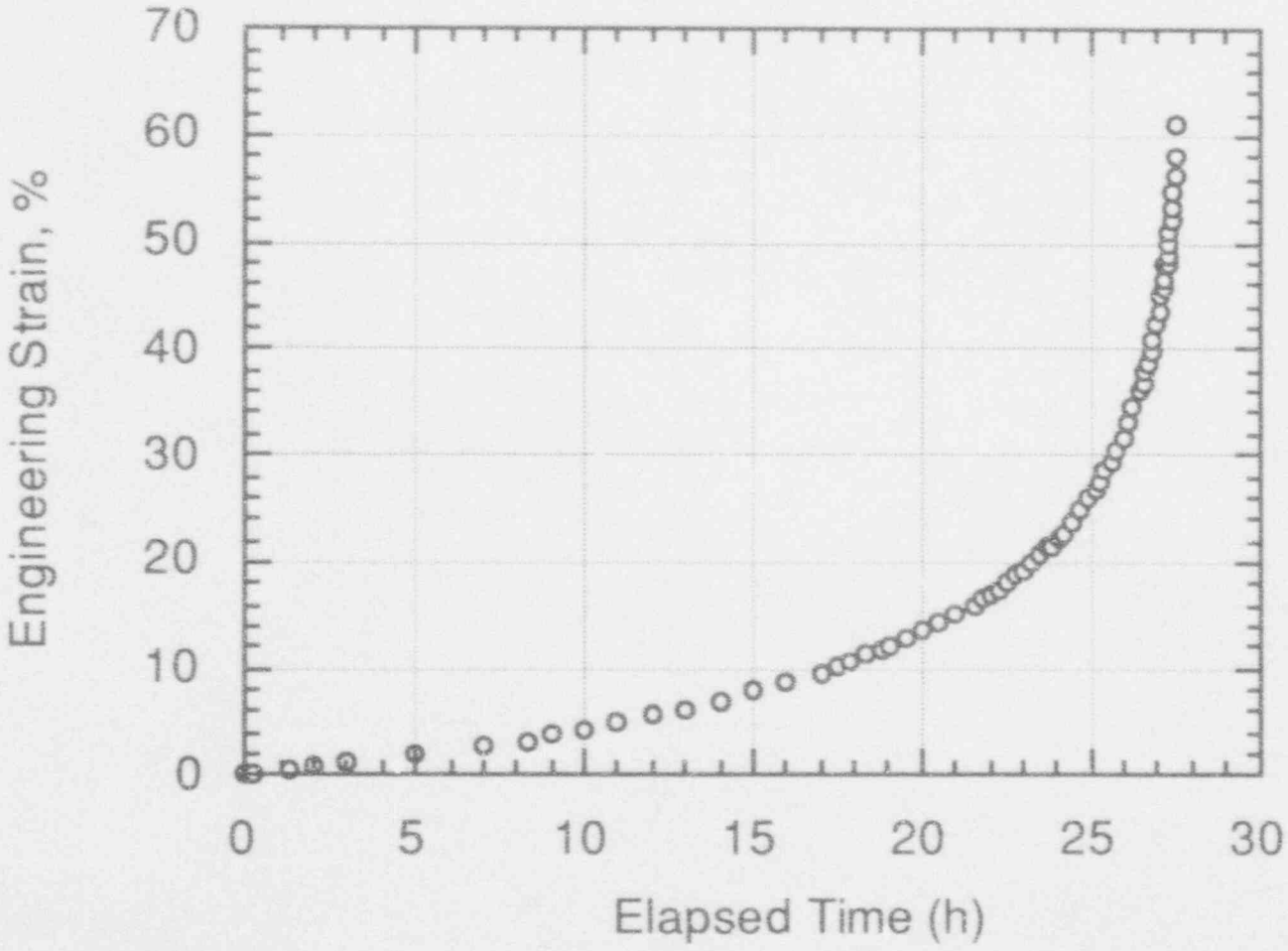

Test Temperature: 700°C
Applied Stress: 41.6 MPa
Time to Failure: 46.0 h

Specimen No.: H-8, t14
Laboratory: ANL
United States

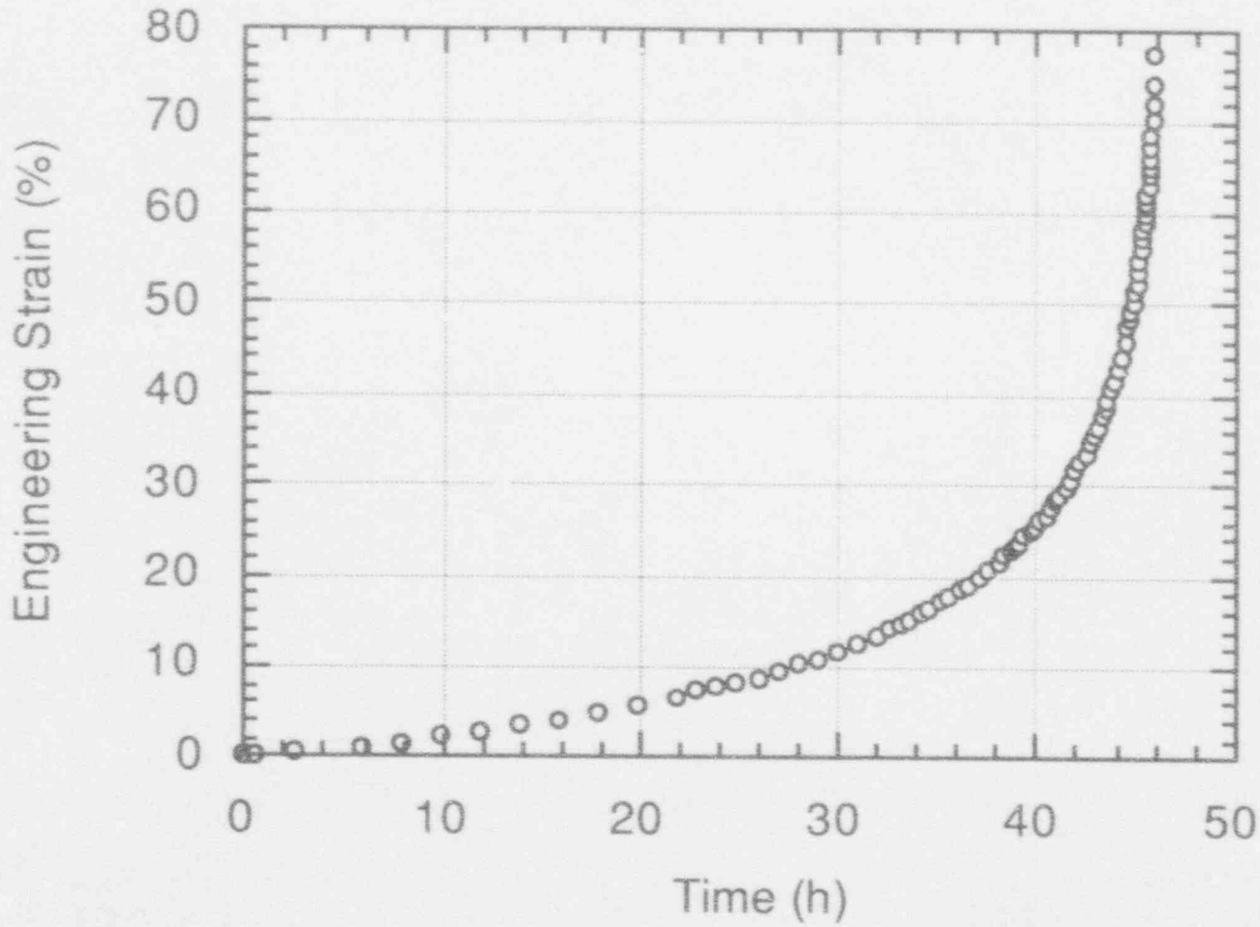

Test Temperature: 700°C
Applied Stress: 34.5 MPa
Time to Failure: 81.6 h

Specimen No.: H-8, t15
Laboratory: ANL
United States

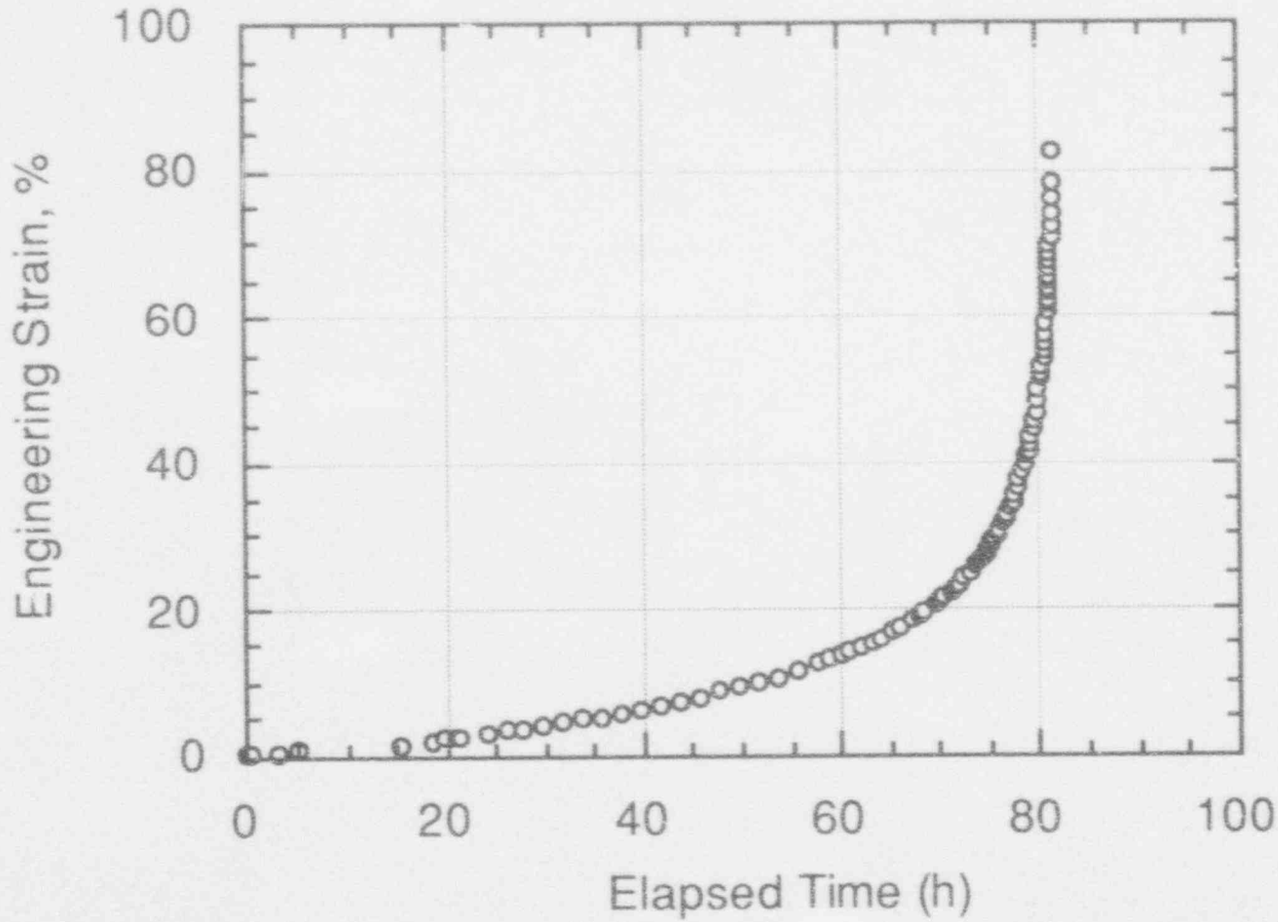

Test Temperature: 800°C
Applied Stress: 70 MPa
Time to Failure: 0.95 h

Specimen No.: F-5, t13
Laboratory: V.I.T.O.
Belgium

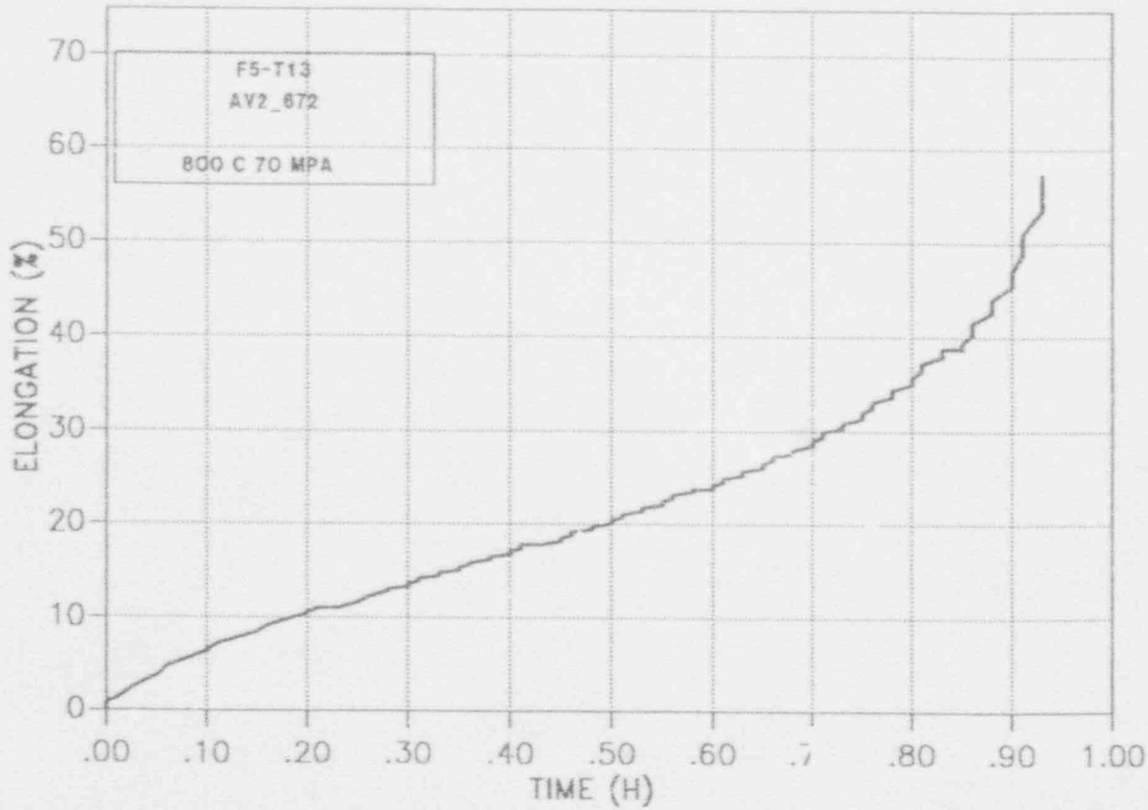

Test Temperature: 800°C
Applied Stress: 50 MPa
Time to Failure: 5.4 h

Specimen No.: F-5, t11
Laboratory: V.I.T.O.
Belgium

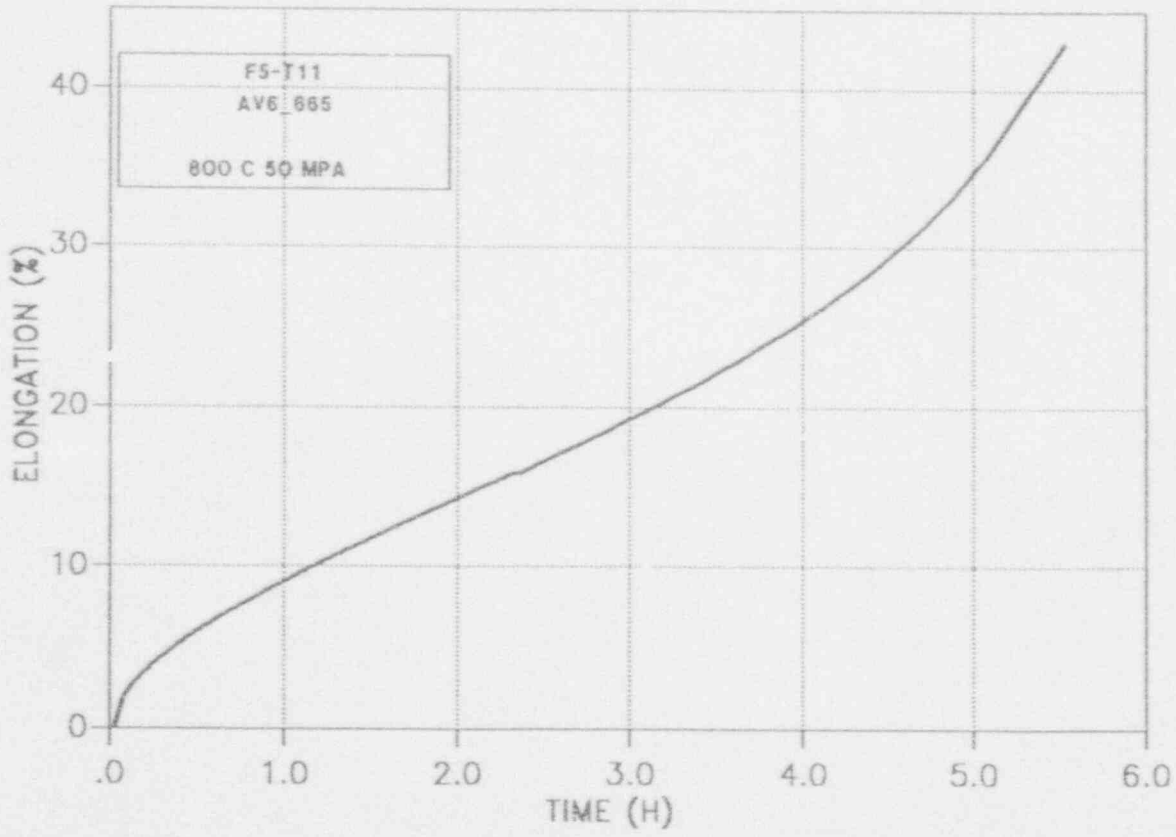

Test Temperature: 800°C
Applied Stress: 40 MPa
Time to Failure: 15.5 h

Specimen No.: F-5, t9
Laboratory: V.I.T.O.
Belgium

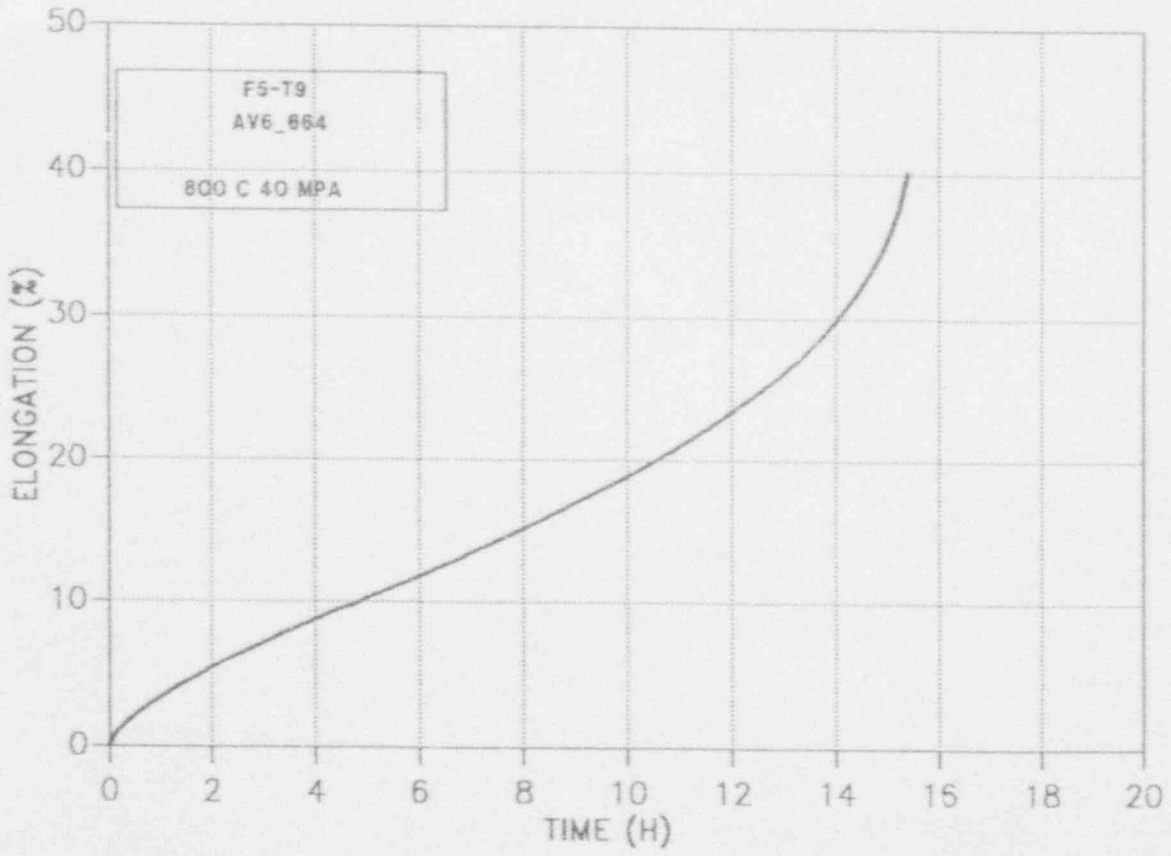

Test Temperature: 800°C
Applied Stress: 30 MPa
Time to Failure: 27 h

Specimen No.: F-5, t8
Laboratory: V.I.T.O.
Belgium

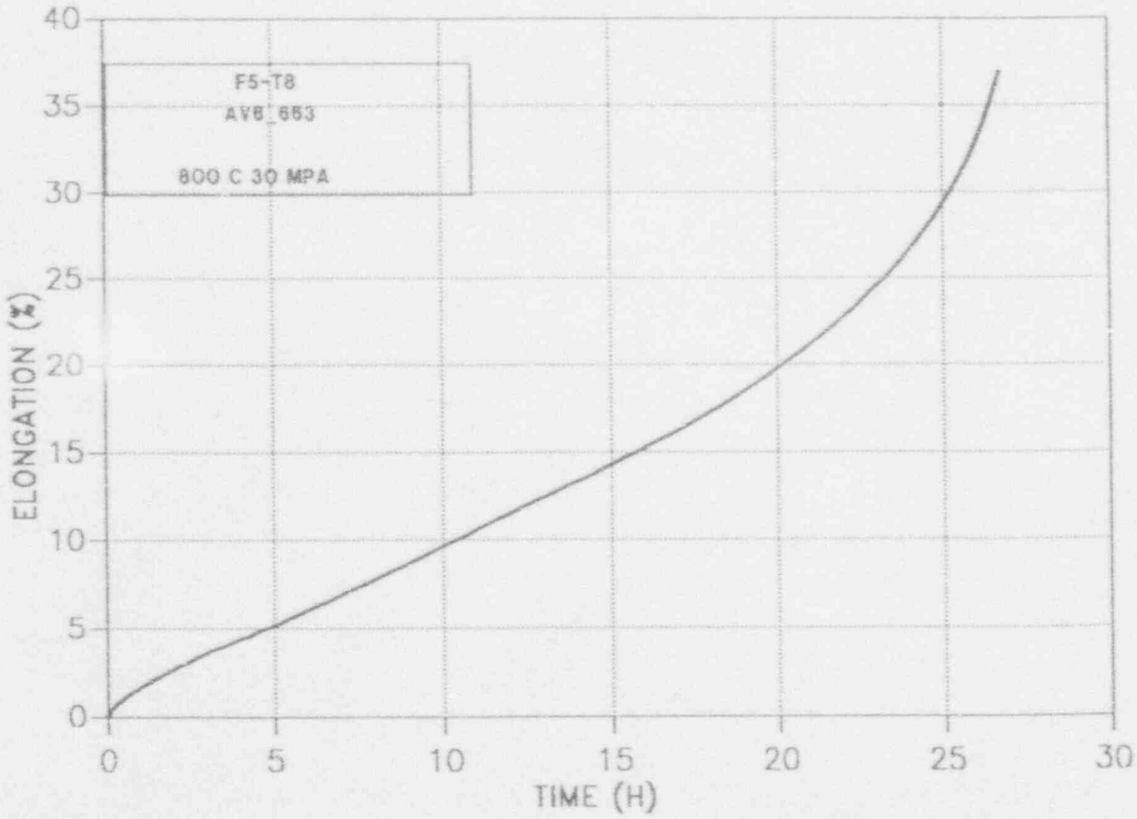

Test Temperature: 800°C
Applied Stress: 23.7 MPa
Time to Failure: 111 h

Specimen No.: F-5, t12
Laboratory: V.I.T.O.
Belgium

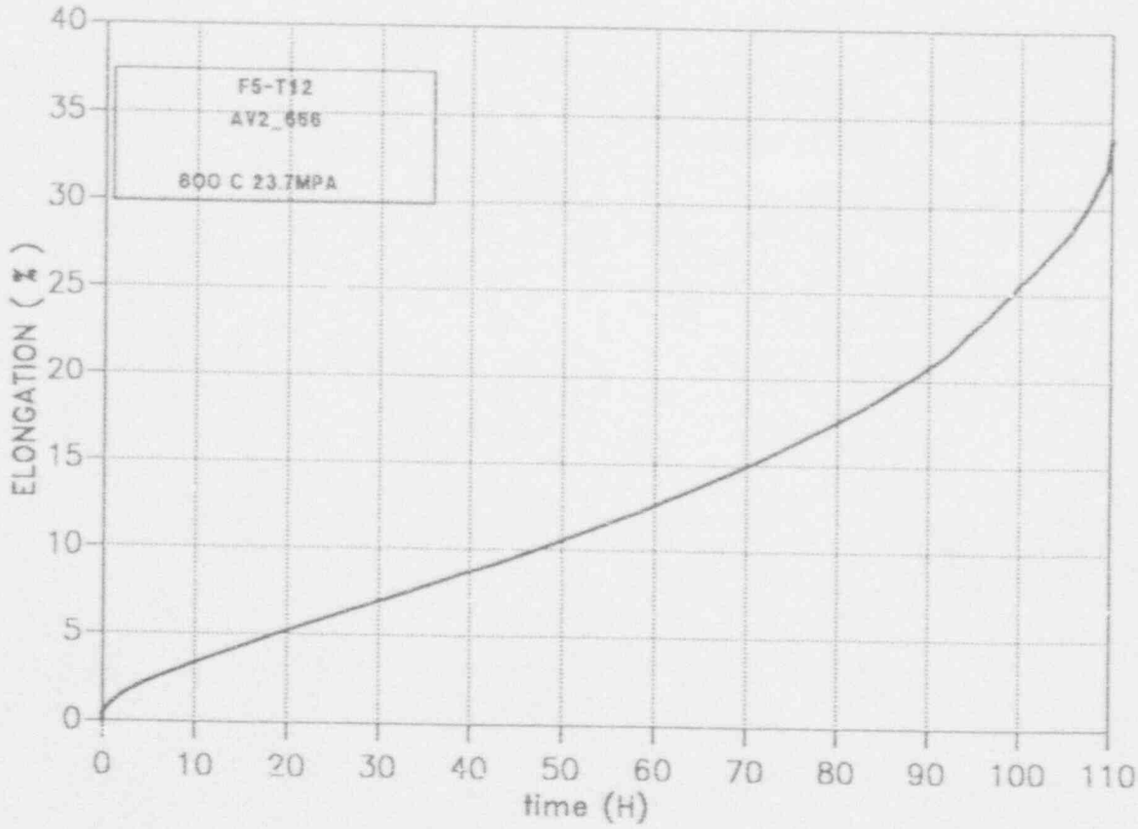

Test Temperature: 900°C
Applied Stress: 35.0 MPa
Time to Failure: 1.09 h

Specimen No.: H-5, t16
Laboratory: ANL
United States

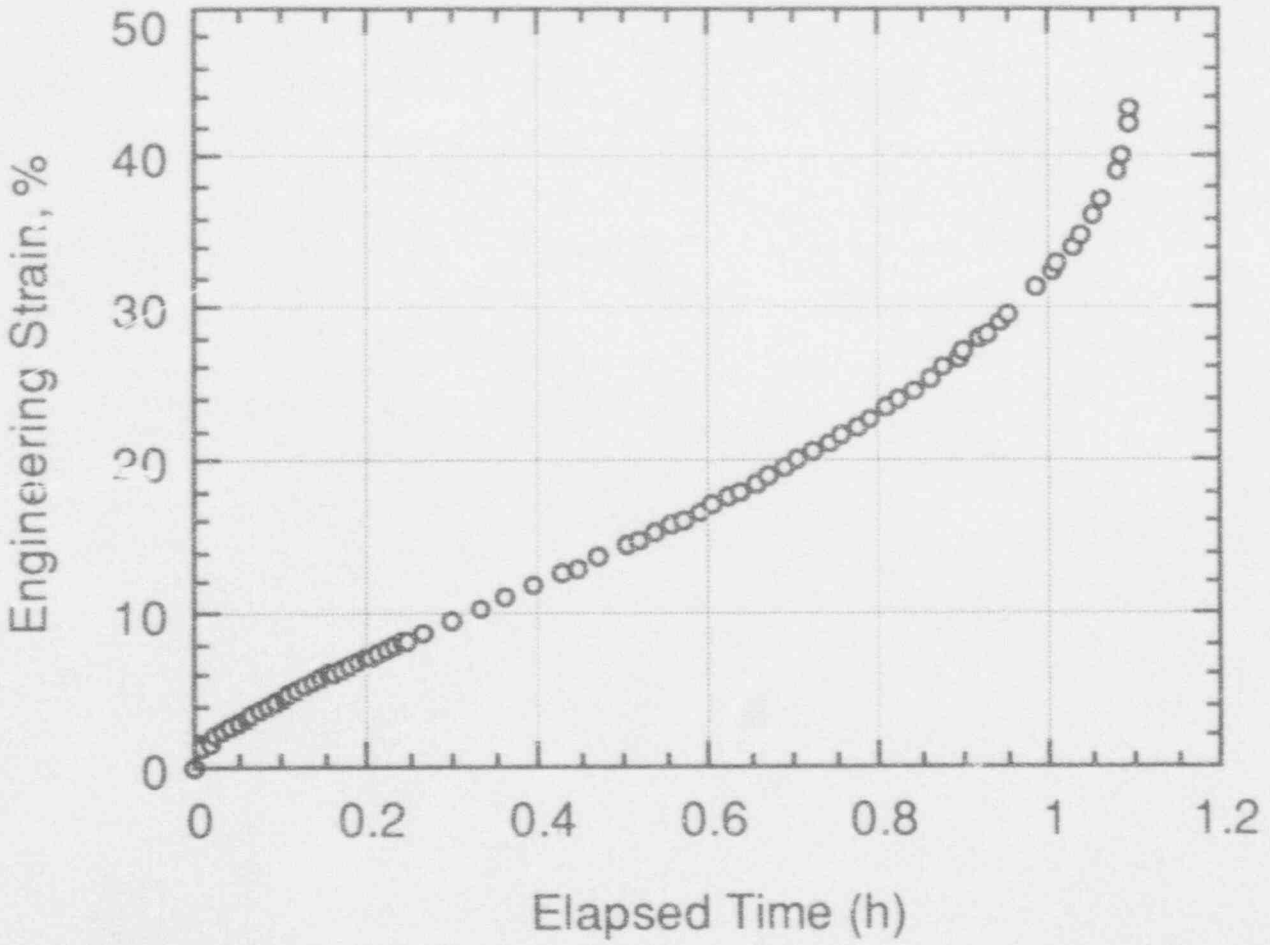

Test Temperature: 900°C
Applied Stress: 26.0 MPa
Time to Failure: 4.55 h

Specimen No.: H-5, t15
Laboratory: ANL
United States

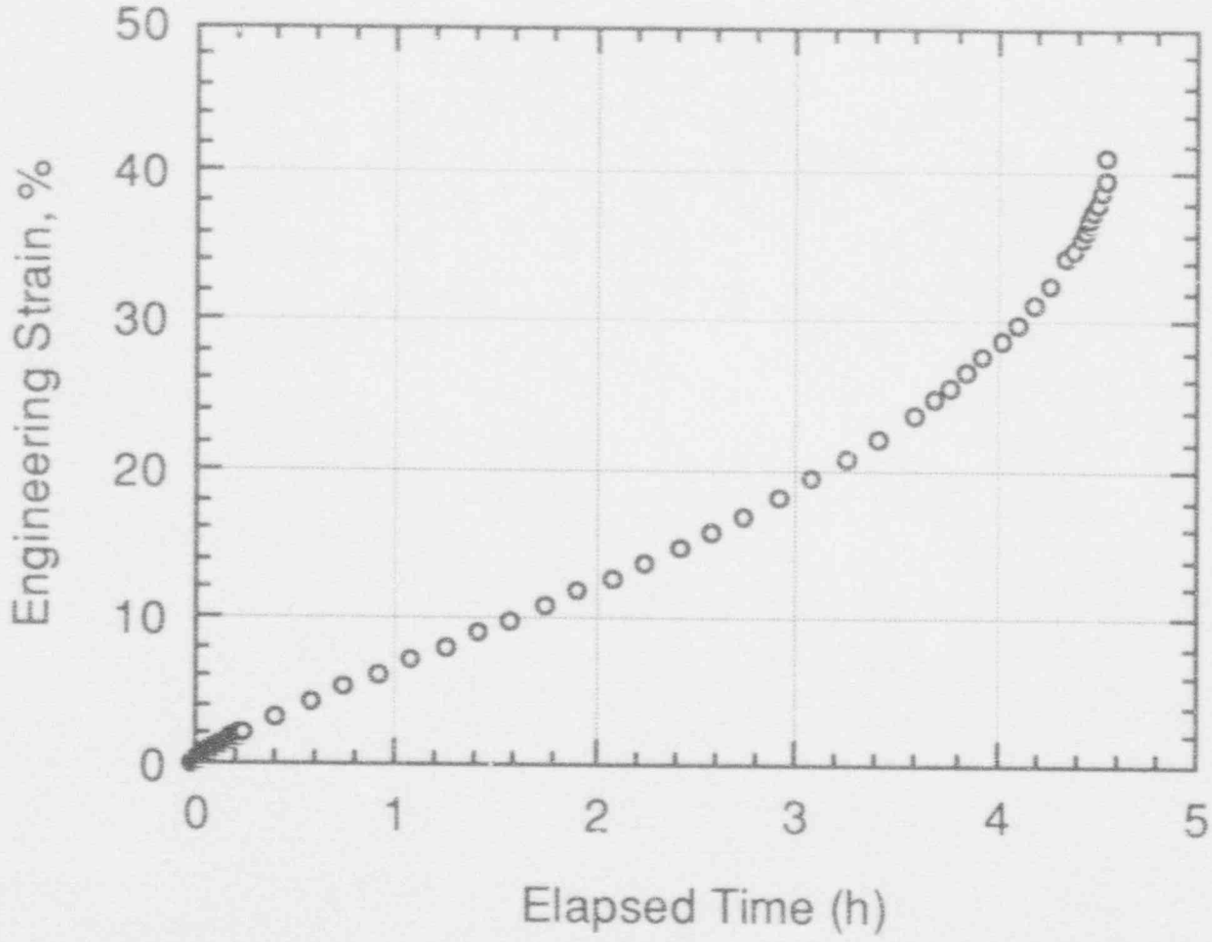

Test Temperature: 900°C
Applied Stress: 19.0 MPa
Time to Failure: 18.1 h

Specimen No.: H-5, t14
Laboratory: ANL
United States

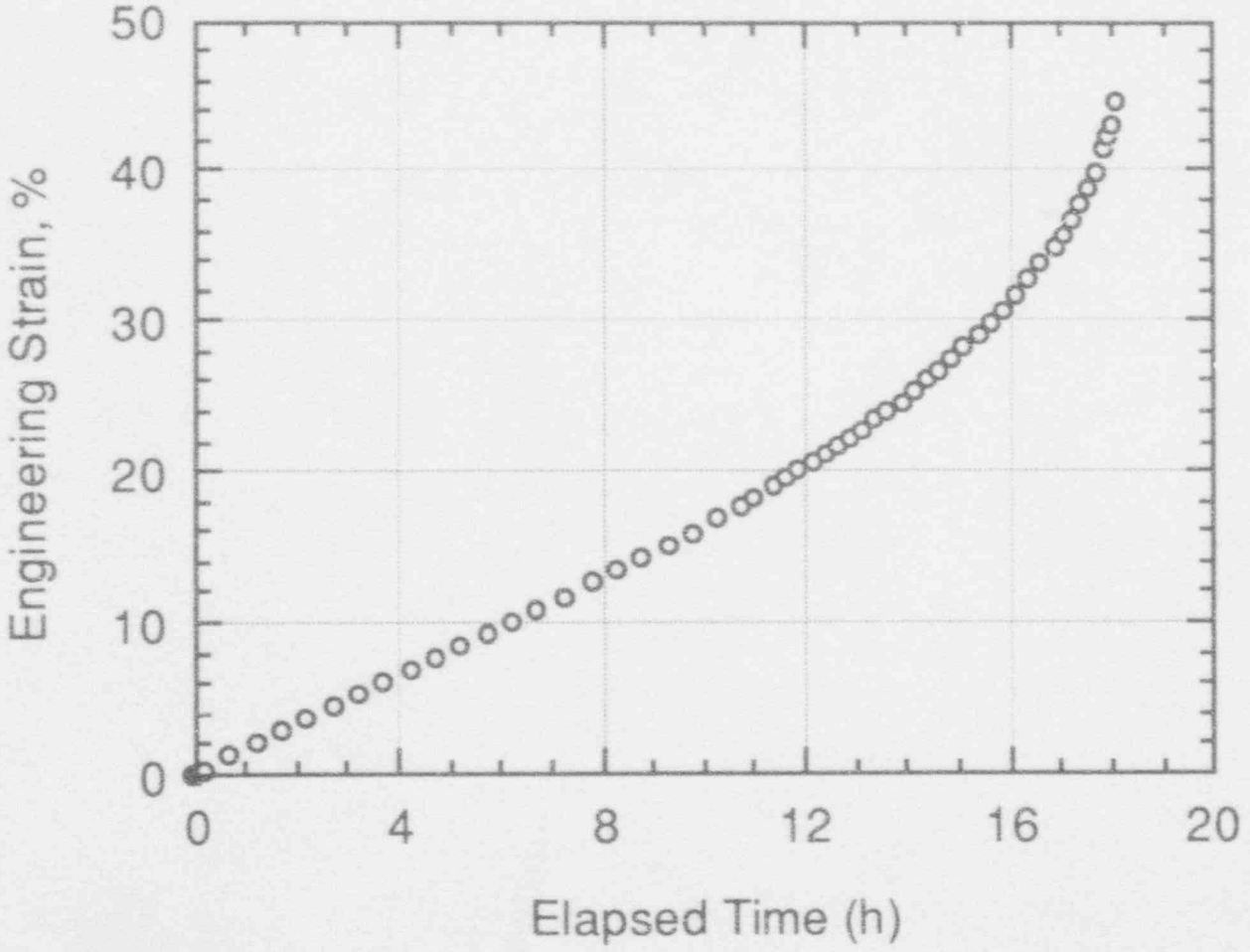

Test Temperature: 900°C
Applied Stress: 14.8 MPa
Time to Failure: 42.3 h

Specimen No.: H-5, t11
Laboratory: ANL
United States

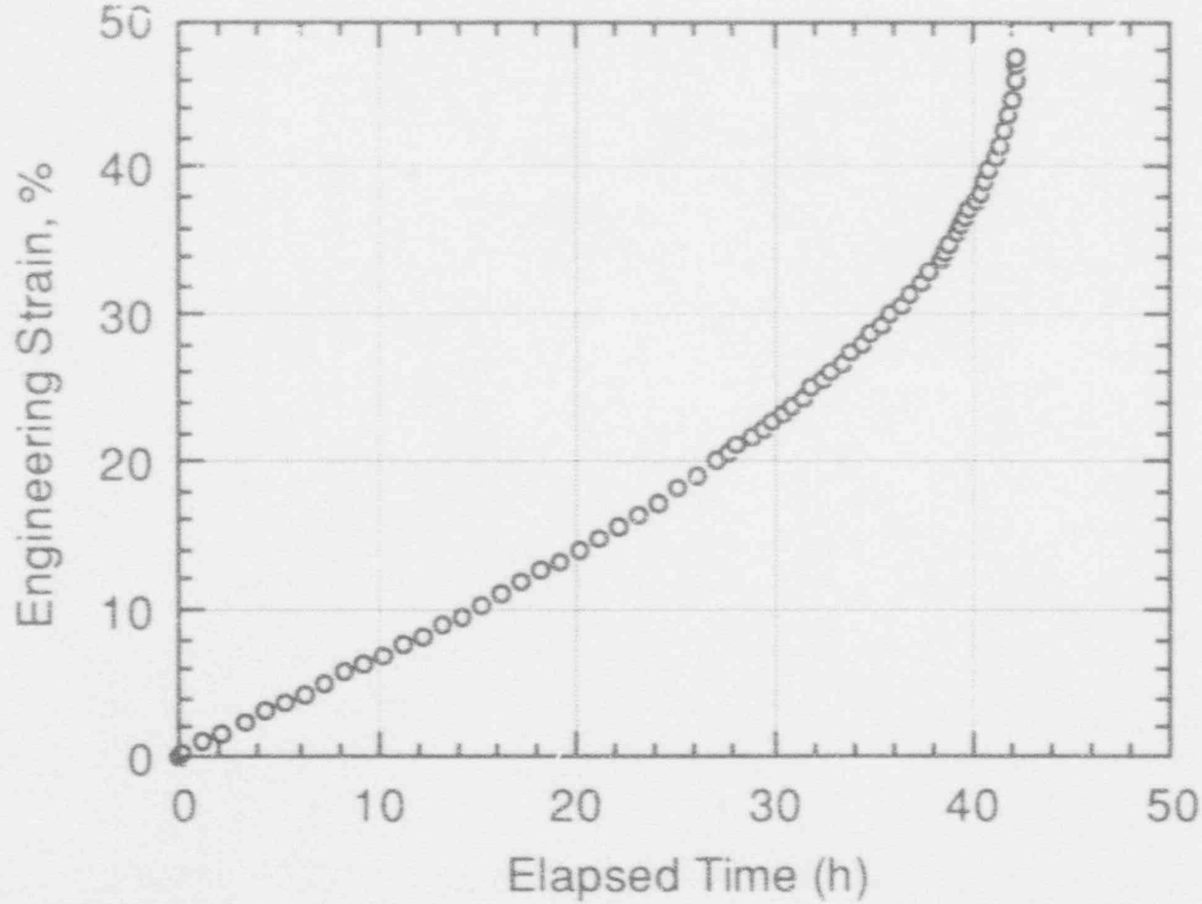

Test Temperature: 900°C
Applied Stress: 9.51 MPa
Time to Failure: 159.5 h

Specimen No.: H-5, t12
Laboratory: ANL
United States

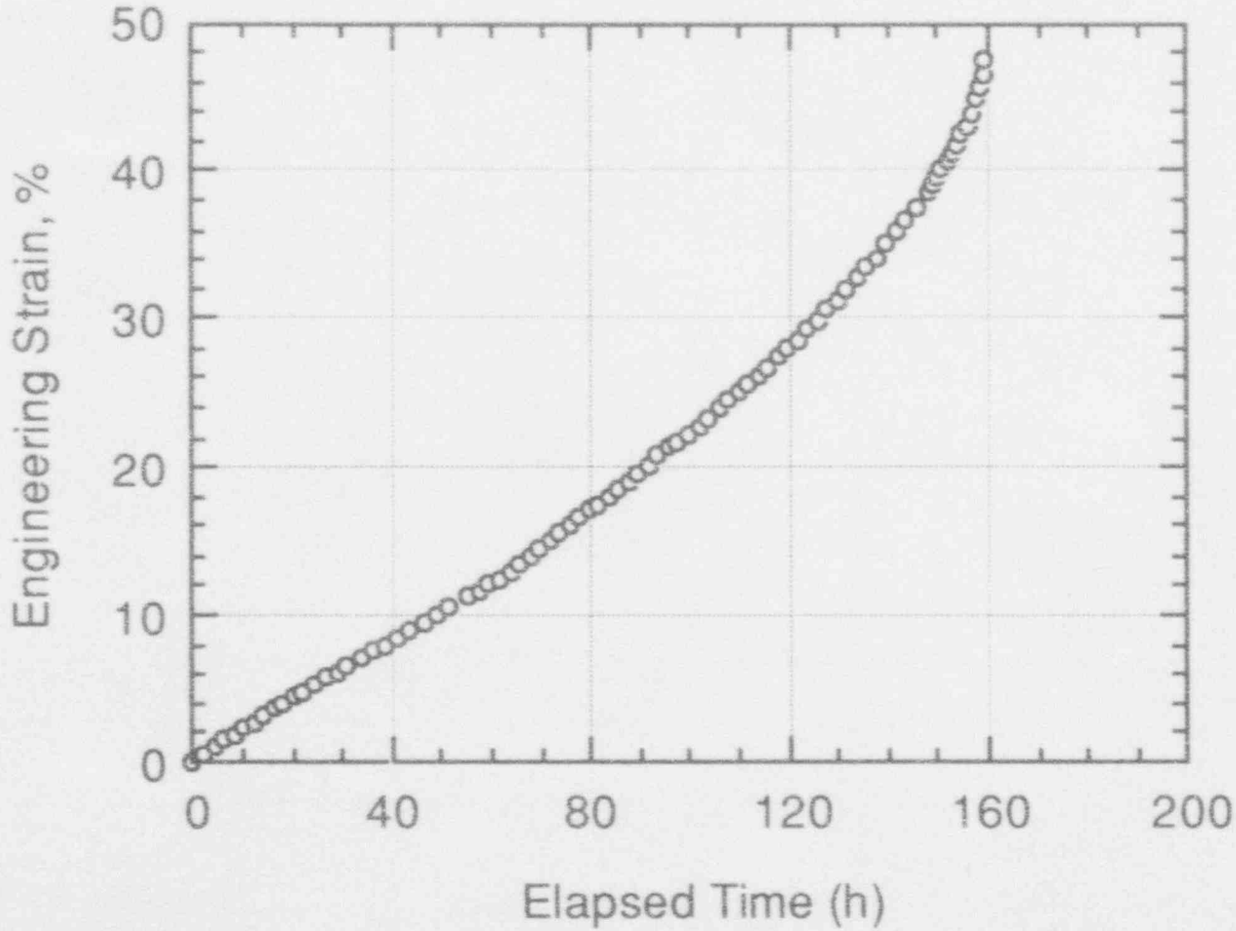

Test Temperature: 1000°C
Applied Stress: 16.9 MPa
Time to Failure: 1.90 h

Specimen No.: K-7, t11
Laboratory: tecnatom, s.a.
Spain

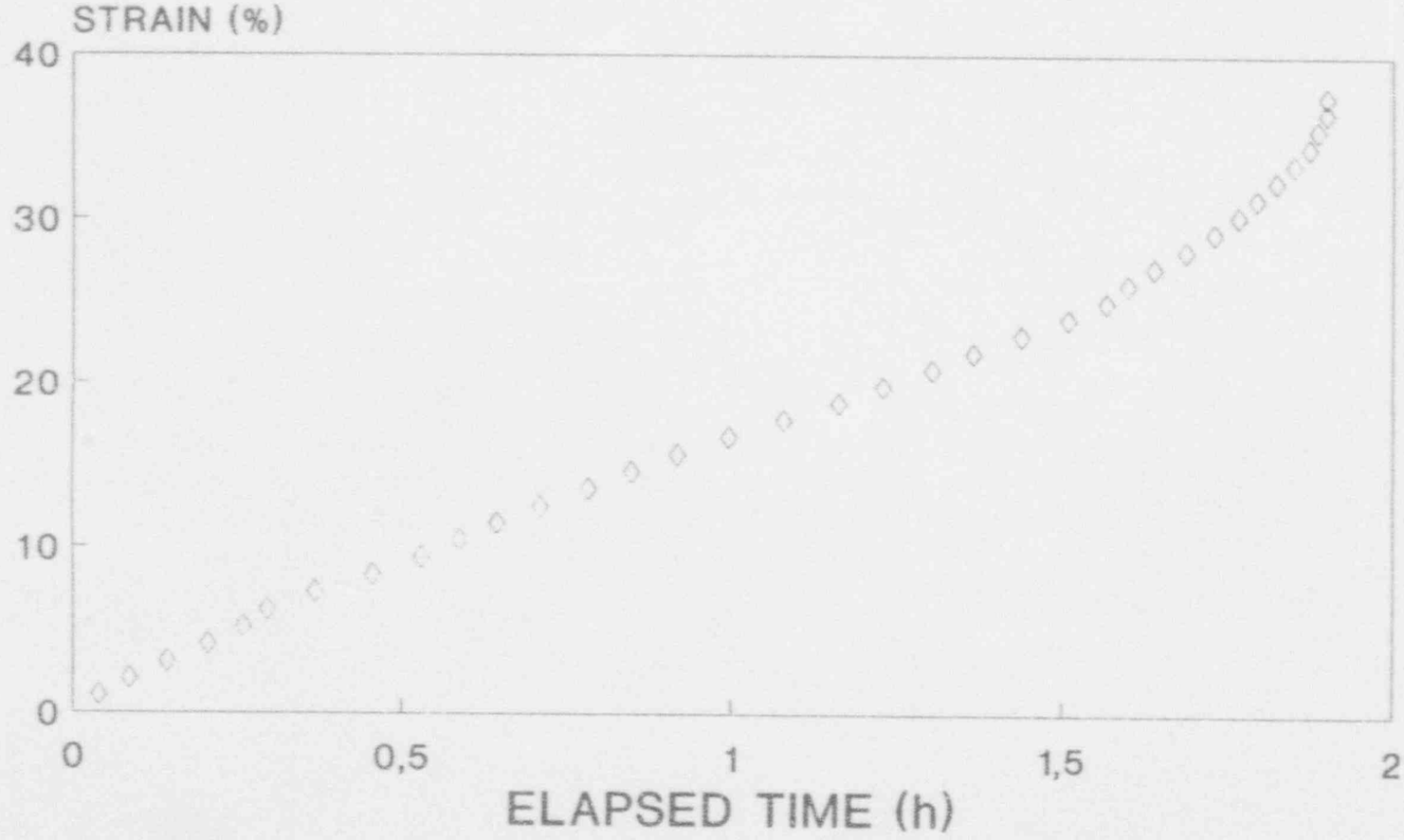

Test Temperature: 1000°C
Applied Stress: 11.5 MPa
Time to Failure: 7.54 h

Specimen No.: K-7, t10
Laboratory: tecnatom, s.a.
Spain

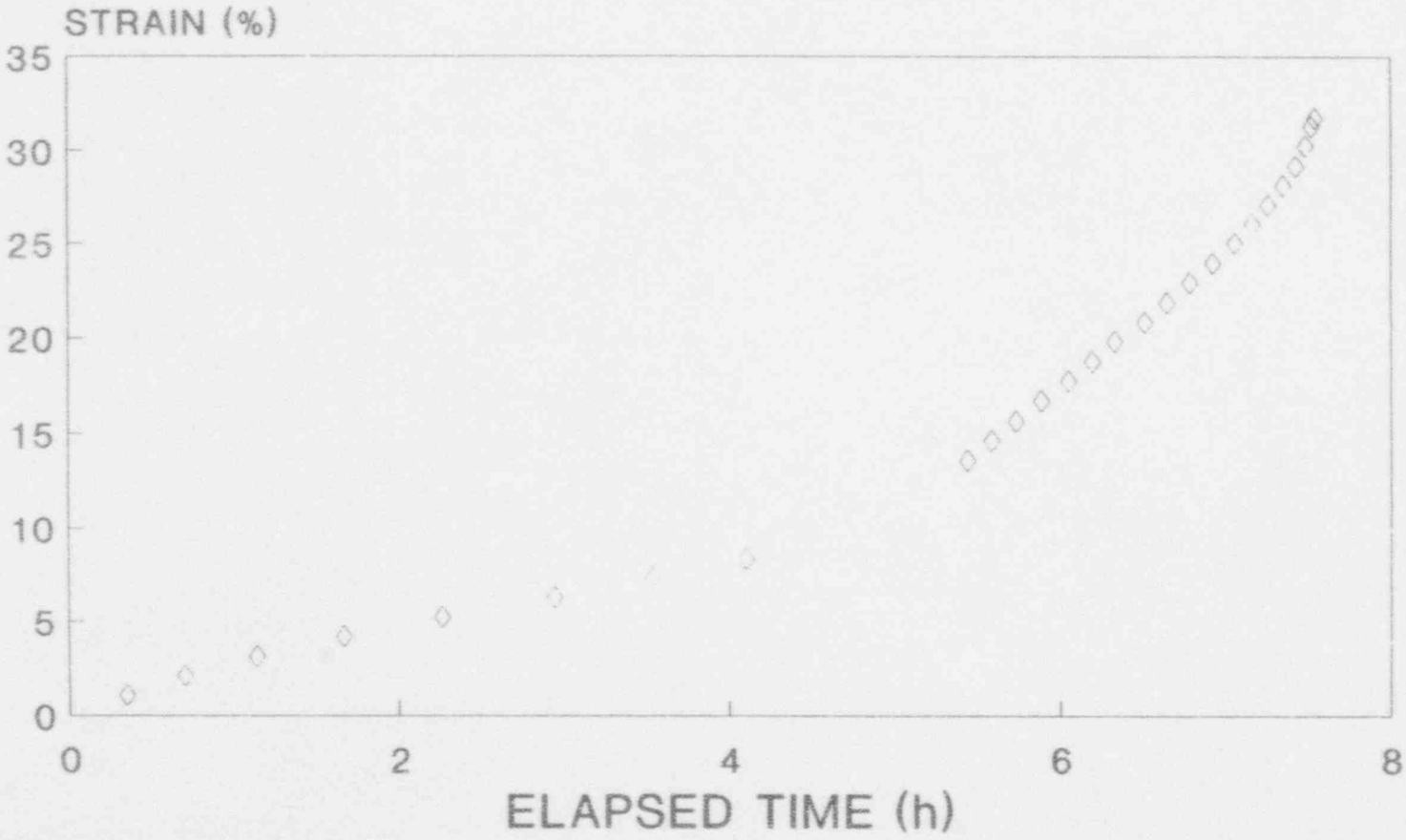

Test Temperature: 1000°C
Applied Stress: 8.7 MPa
Time to Failure: 29.64 h

Specimen No.: K-7, t12
Laboratory: tecnatom, s.a.
Spain

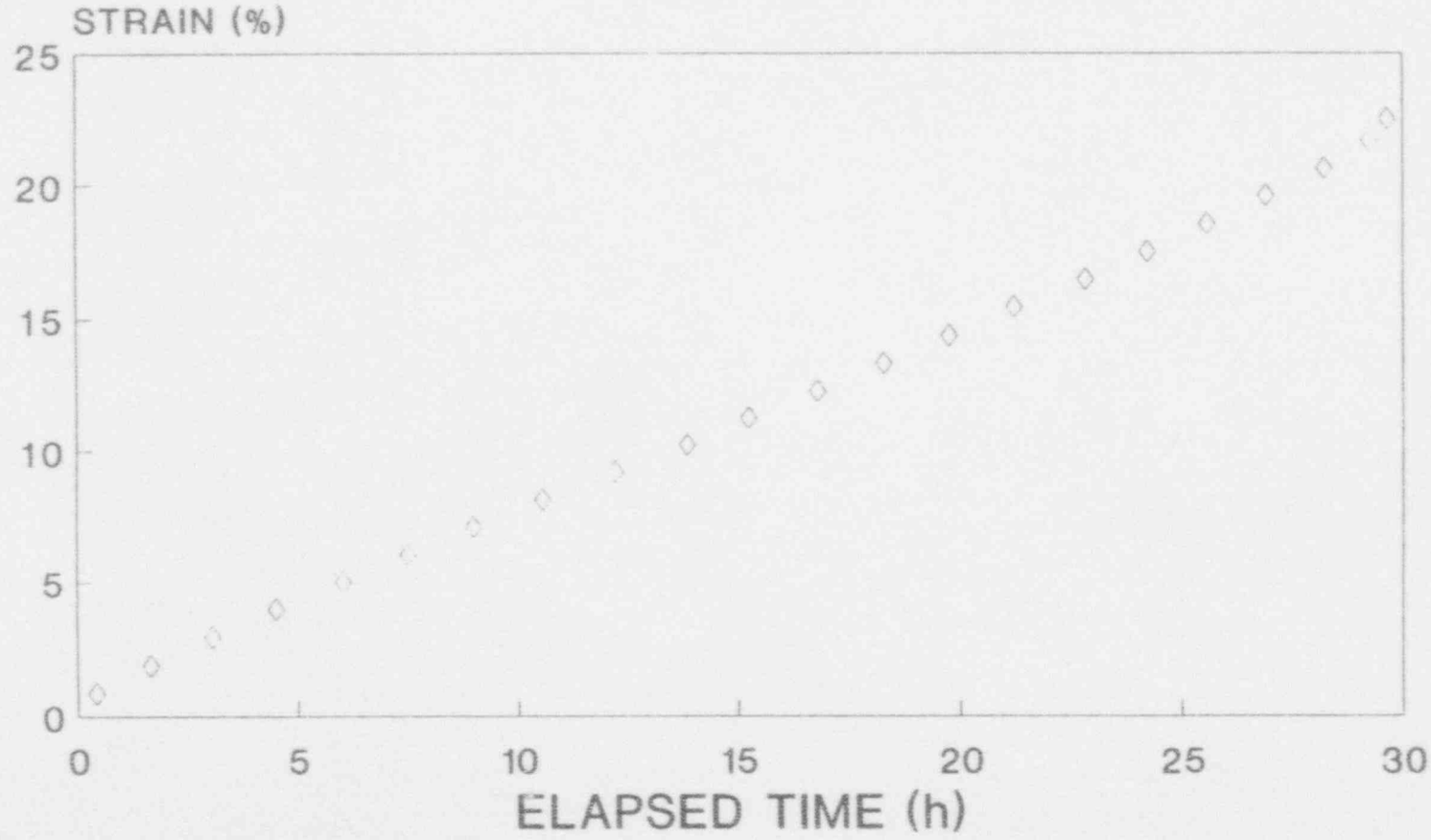

Test Temperature: 1000°C
Applied Stress: 6.3 MPa
Time to Failure: 152.8 h

Specimen No.: K-7, t13
Laboratory: tecnatom, s.a.
Spain

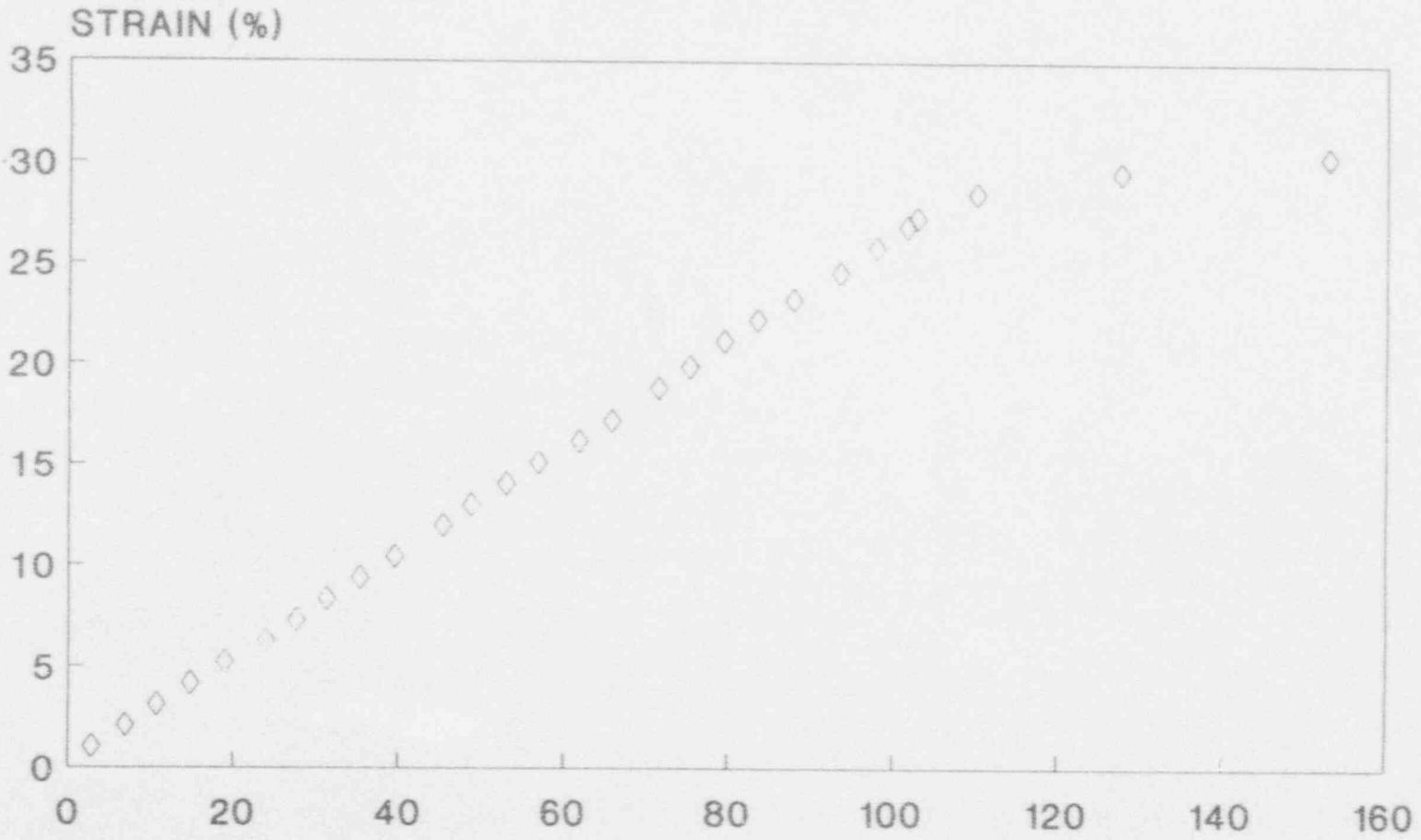

Test Temperature: 1100°C
Applied Stress: 8 MPa
Time to Failure: 4.33 h

Specimen No.: L-9, t10
Laboratory: CEA
France

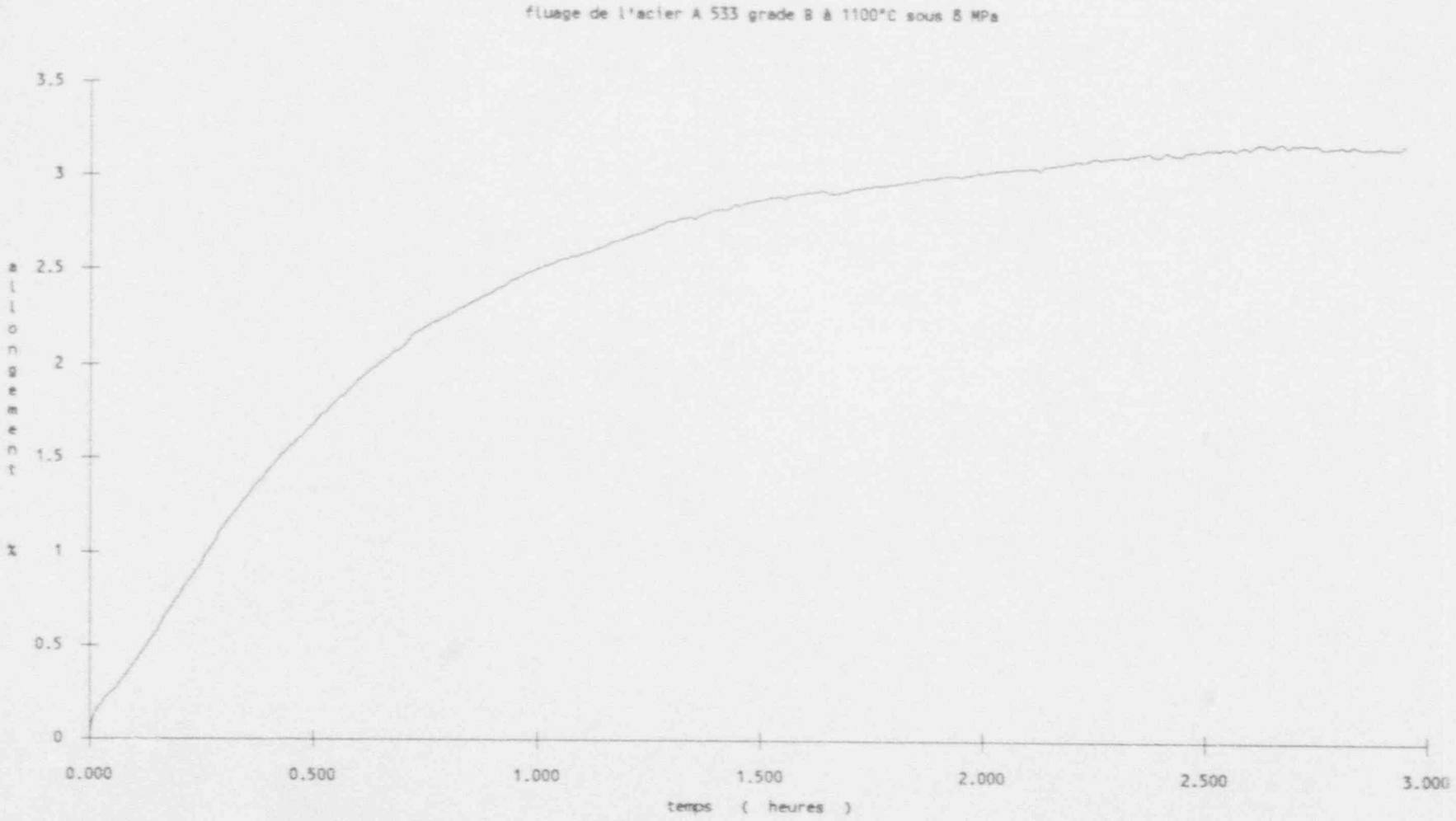

Test Temperature: 1200°C
Applied Stress: 9.0 MPa
Time to Failure: 0.98 h

Specimen No.: M-8, t6
Laboratory: ANL
United States

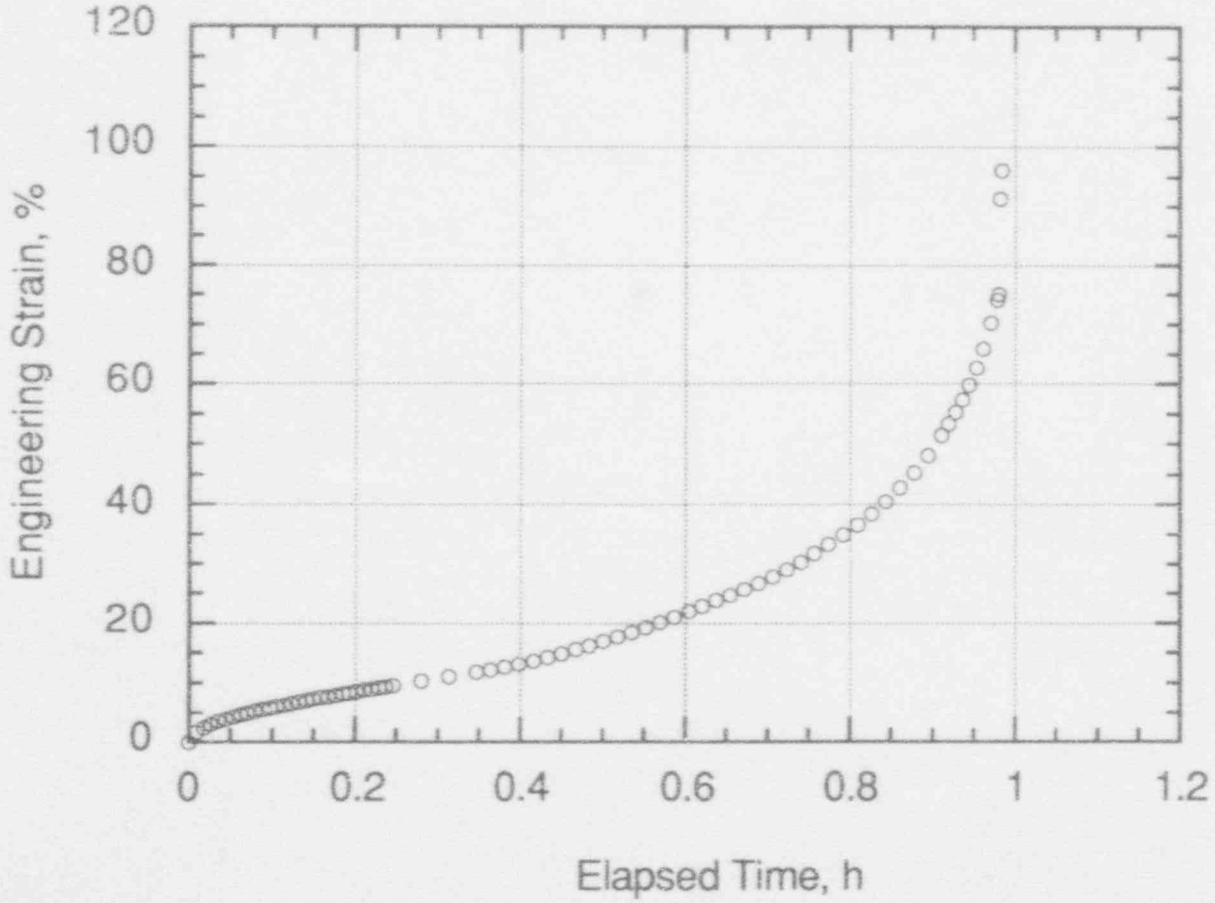

Test Temperature: 1200°C
Applied Stress: 6.0 MPa
Time to Failure: 7.26 h

Specimen No.: M-8, t5
Laboratory: ANL
United States

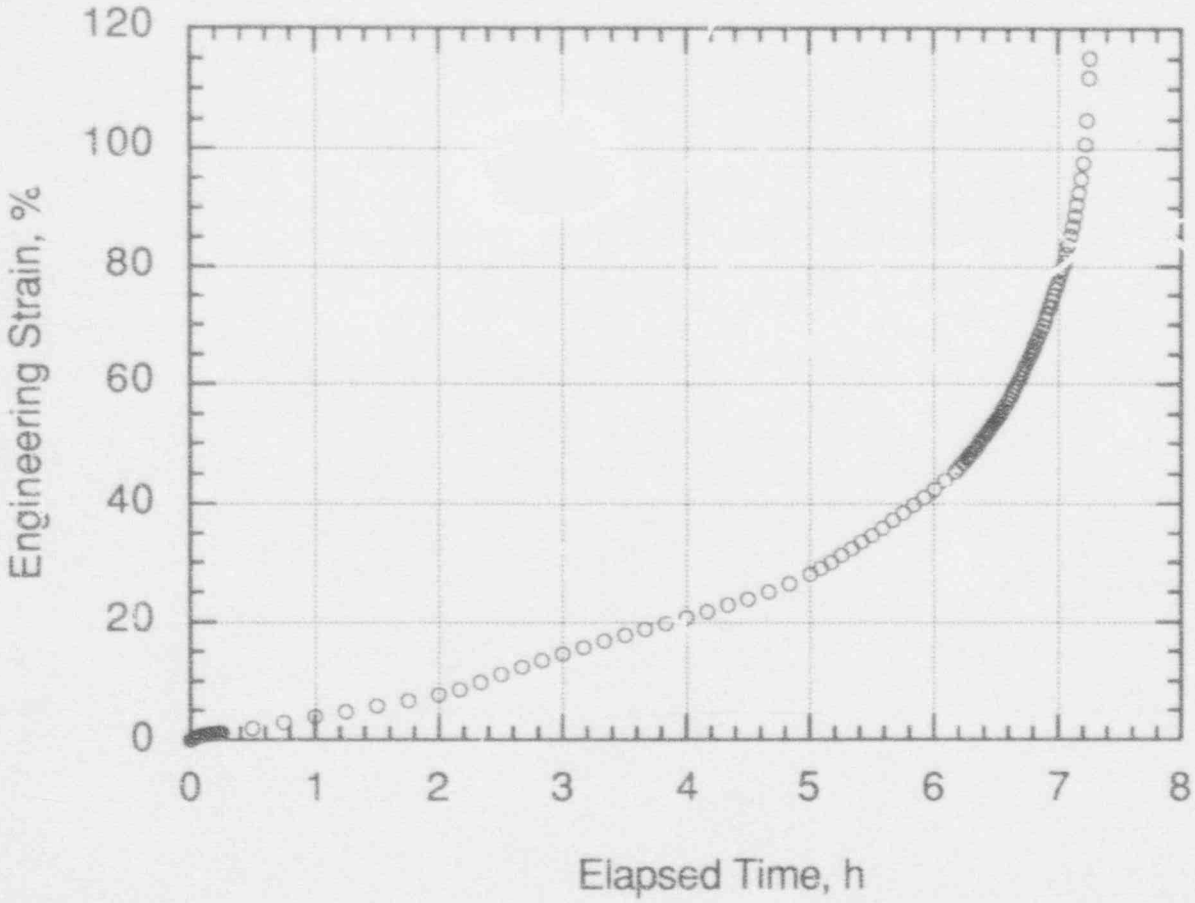

Test Temperature: 1200°C
Applied Stress: 4.0 MPa
Time to Failure: 48.2 h

Specimen No.: M-8, t4
Laboratory: ANL
United States

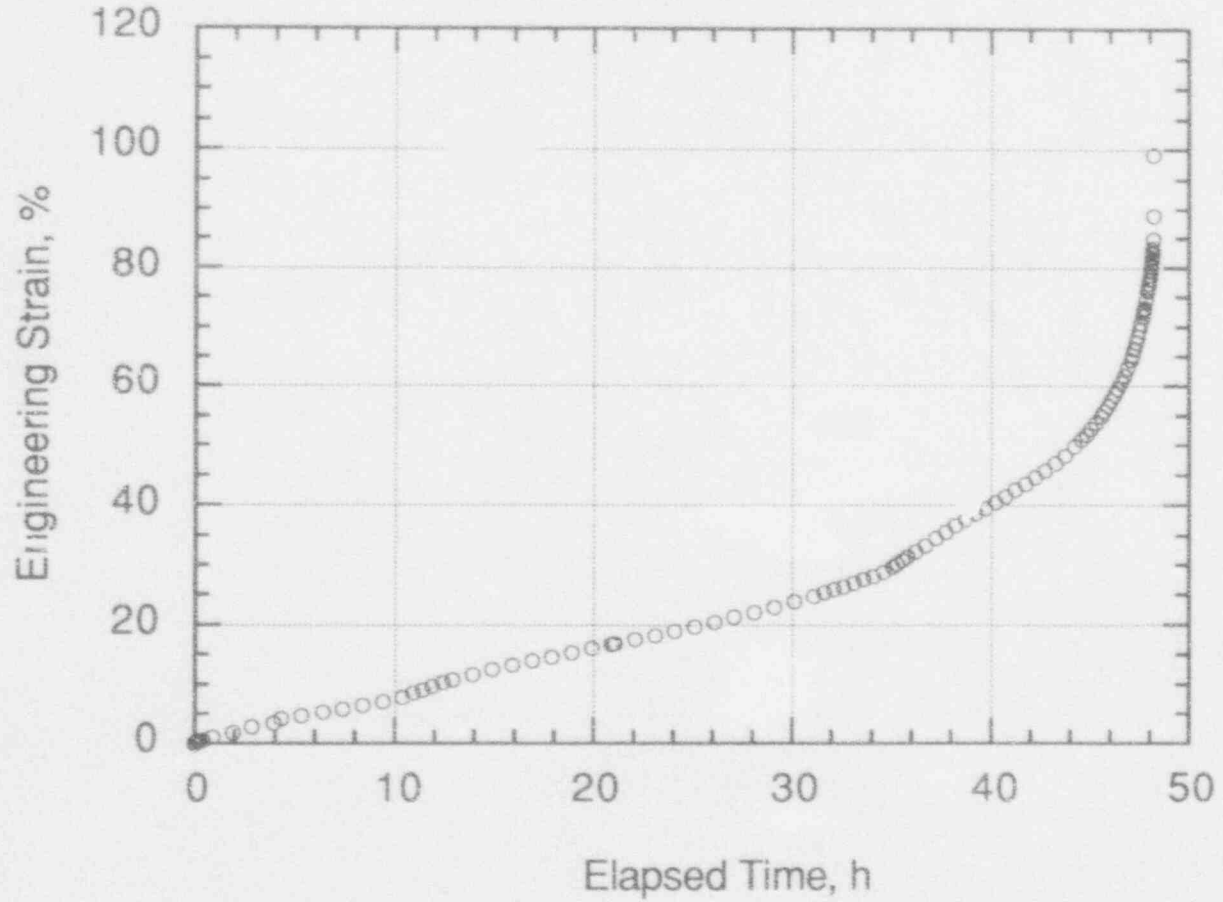

Test Temperature: 1200°C
Applied Stress: 3.4 MPa
Time to Failure: 55.1 h

Specimen No.: M-8, t7
Laboratory: ANL

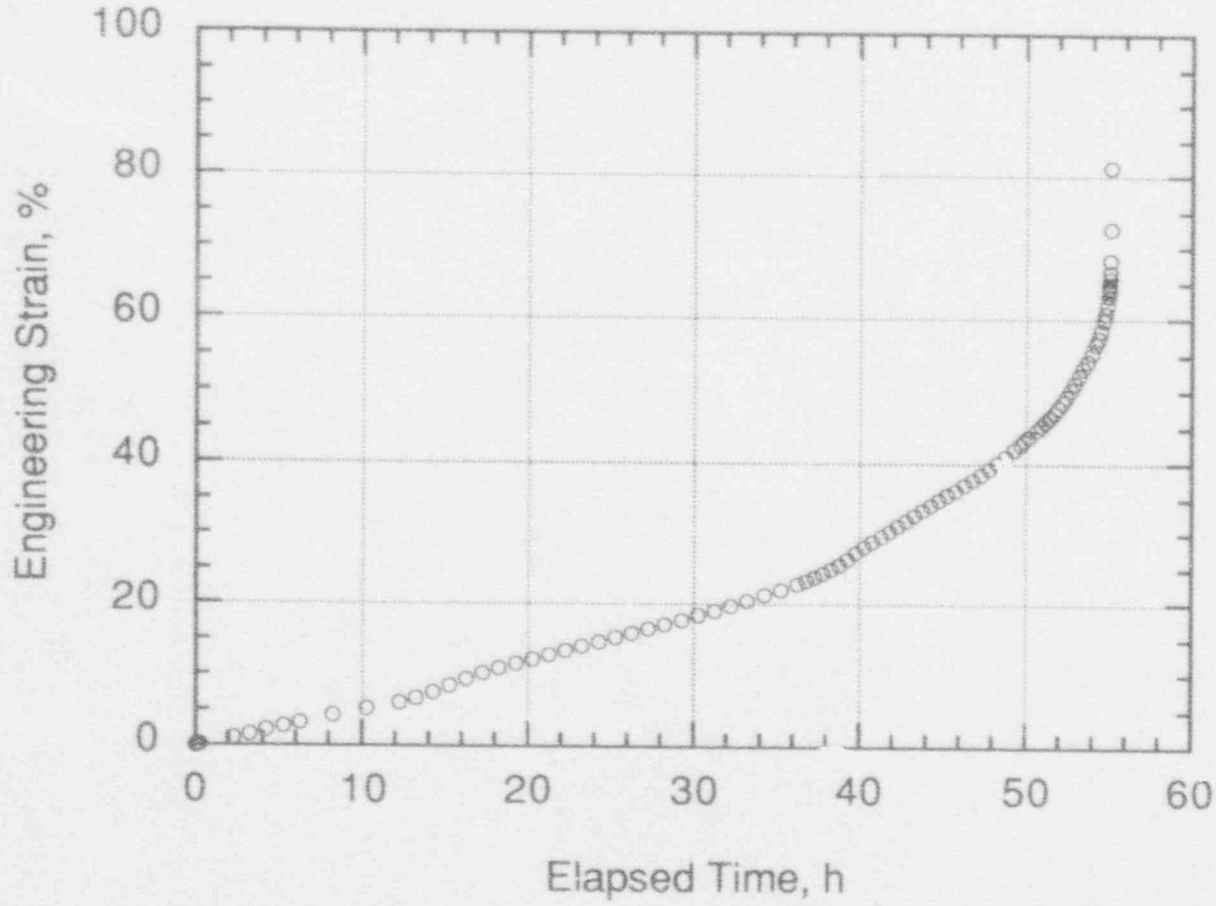

Distribution for NUREG/CR- 6187 (ANL-94/8)

Internal:

D. R. Diercks (25)
H. Drucker
L. A. Neimark
R. B. Poeppel
W. J. Shack
C. E. Till
R. W. Weeks
TIS File

External:

NRC, for distribution per R5
ANL Libraries
ANL-E (2)
ANL-W
Manager, Chicago Field Office, DOE
Energy Technology Division Review Committee:
H. K. Birnbaum, University of Illinois, Urbana
R. C. Buchanan, University of Cincinnati, Cincinnati
M. S. Dresselhaus, Massachusetts Institute of Technology, Cambridge, MA
B. G. Jones, University of Illinois, Urbana
C.-Y. Li, Cornell University, Ithaca, NY
S. N. Liu, Fremont, CA
R. E. Smith, SciTech Inc., Morrisville, NC

D. W. Akers, Idaho National Engineering Laboratory
S. F. Armour, USDOE, Idaho Field Office, Idaho Falls, ID
M. Banaschik, Gesellschaft für Reaktorsicherheit, Zentralstelle Forschungsbetreuung, Köln 1, Federal Republic of Germany
E. Beckjord, Office of Nuclear Regulatory Research, U.S. Nuclear Regulatory Commission, Washington, DC
J. Bros, TECNATOM S.A., Components Integrity Group, Madrid, Spain
S. Chavez, Idaho National Engineering Laboratory, EG&G Idaho, Inc., Idaho Falls, ID
S. Chakraborty, Swiss Federal Nuclear Safety Inspectorate, Würenlingen, Switzerland
N. Cole, MPR Associates, Washington, DC
F. Corsi, ENEA/VEL-MEP, Rome, Italy
J. Cortez, U.S. Nuclear Regulatory Commission, Washington, DC
P. DeJonghe, Study Centre for Nuclear Energy, SCK/CEN, Bruxelles, Belgium
J. Duco, Department d'Analyse de Sûreté, CEN/FAR, Cedex, France
F. Eltawilla, U.S. Nuclear Regulatory Commission, Washington, DC
J. M. Figueras, Consejo de Seguridad Nuclear, Subdireccion de Analysis y Evaluacion, Madrid, Spain
D. W. Golden, Idaho National Engineering Laboratory
W. Gomolinski, IPSN/OSSN, CEN/FAR, Cedex, France
E. M. Hackett, U.S. Nuclear Regulatory Commission, Washington, DC
J. A. Hudson, B388 Harwell Laboratory, UKAEA, Oxfordshire, United Kingdom
K.-H. Katerbau, Staatliche Materialprüfungsanstalt, Universität Stuttgart, Stuttgart, Federal Republic of Germany
S. Kawasaki, Department of Fuel Safety Research, Japan Atomic Energy Research Institute, Ibaraki-ken, Japan
S. Kinnersly, Technical Area, Severe Accident Analysis, UKAEA, Dorset, United Kingdom

G. Korth, Idaho National Engineering Laboratory
S. Levin, TMI-2, GPU Nuclear, Middletown, PA
C. Maricchiolo, ENEA/DISP, Division of Mechanical Analysis & Technology, Rome, Italy
M. Mayfield, Office of Nuclear Regulatory Research, Materials Engineering Branch, U.S. Nuclear Regulatory Commission, Washington, DC
R. K. McCardell, Idaho National Engineering Laboratory
D. McGoff, USDOE, Washington, DC
M. Merilo, EPRI, Palo Alto, CA
P. Milella, ENEA/DISP, Division of Mechanical Analysis & Technology Rome, Italy
A. G. Miller, Nuclear Safety Division. OECD, Agence pour l'Énergie Nucleaire, Paris, France
R. C. Monroy, Planning Department, Nuclear R&D Projects, UNIDAD Electrica, S.A., Madrid, Spain
H. Njo, Swiss Federal Nuclear Safety Inspectorate, Würenlingen, Switzerland
C. Ottoson, Finnish Centre for Radiation and Nuclear Safety, Helsinki, Finland
D. E. Owen, EPRI-TMI-2 Site Office, Middletown, PA
W. F. Pasedag, USDOE, Office of LWR Safety and Technology, Washington, DC
R. Pelli, Technical Research Centre of Finland, Espoo, Finland
G. Petrangeli, ENEA/DISP, Sector for Development and Research, Rome, Italy
K. Pettersson, Department of Structural Integrity, Swedish Nuclear Power Inspectorate, Stockholm, Sweden
J. R. Rashid, Anatech Research Corp., San Diego, CA
J. Rempe, Idaho National Engineering Laboratory
A. M. Rubin, U.S. Nuclear Regulatory Commission, Washington, DC
G. Saponaro, ENEA-DISP, Regulatory Research Commitment, Rome, Italy
H. Schulz, Gesellschaft für Reaktorsicherheit, Zentralstelle Forschungsbetreuung, Köln 1, Federal Republic of Germany
C. Z. Serpan, Office of Nuclear Regulatory Research, Materials Engineering Branch, U.S. Nuclear Regulatory Commission, Washington, DC
L. C. Shao, Division of Engineering, RES, U.S. Nuclear Regulatory Commission, Washington, DC
B. Sheron, U.S. Nuclear Regulatory Commission, Washington, DC
P. Soulat, Service de Recherches Metallurgiques Appliquees, CEN Saclay, Cedex, France
T. Speis, U.S. Nuclear Regulatory Commission, Washington, DC
K. B. Stadie, OECD, Agence pour l'Énergie Nucleaire, Paris, France
J. Strosnider, U.S. Nuclear Regulatory Commission, Washington, DC
D. Sturm, Staatliche Materialprüfungsanstalt, Universität Stuttgart, Stuttgart, Federal Republic of Germany
G. Thinnes, Idaho National Engineering Laboratory
M. Trotabas, DMT/SETIC, CEN Saclay, Cedex, France
W. Vandermeulen, Study Centre for Nuclear Energy, SCK/CEN, Bruxelles, Belgium
P. Veron, Equipos Nucleares S.A., Maliano, Cantabria, Spain
F. Weehuizen, Swiss Federal Nuclear Safety Inspectorate, Würenlingen, Switzerland
R. J. Witt, Dept. of Nuclear Engineering, U. of Wisconsin, Madison, WI
J. R. Wolf, Idaho National Engineering Laboratory

NRC FORM 335 (2-89) NRCM 1102, 3201, 3202

U. S. NUCLEAR REGULATORY COMMISSION

BIBLIOGRAPHIC DATA SHEET

(See instructions on the reverse)

1. REPORT NUMBER *(Assigned by NRC. Add Vol., Supp., Rev., and Addendum Numbers, if any.)*
NUREG/CR-6187
ANL-94/8
TMIV(93)AL02

2. TITLE AND SUBTITLE
Results of Mechanical Tests and Supplementary Microstructural Examinations of the TMI-2 Lower Head Samples

3. DATE REPORT PUBLISHED
MONTH: March
YEAR: 1994

4. FIN OR GRANT NUMBER
L1005

5. AUTHOR(S)
D. R. Diercks and L. A. Neimark

6. TYPE OF REPORT
Technical

7. PERIOD COVERED *(Inclusive Dates)*

8. PERFORMING ORGANIZATION – NAME AND ADDRESS *(If NRC, provide Division, Office or Region, U.S. Nuclear Regulatory Commission, and mailing address; if contractor, provide name and mailing address.)*
Argonne National Laboratory
9700 South Cass Avenue
Argonne, IL 60439

9. SPONSORING ORGANIZATION – NAME AND ADDRESS *(If NRC, type "Same as above"; if contractor, provide NRC Division, Office or Region, U.S. Nuclear Regulatory Commission, and mailing address.)*
Division of Systems Research
Office of Nuclear Regulatory Research
U.S. Nuclear Regulatory Commission
Washington, DC 20555–0001

10. SUPPLEMENTARY NOTES

11. ABSTRACT (200 words or less)

Metallographic examinations of 15 samples from the lower head of the TMI-2 pressure vessel confirmed that four samples attained temperatures as high as 1100°C during the accident and cooled at ≈10-100°C/min. Portions of two adjacent samples, and possibly a third sample away from the hot spot, also exceeded 727°C. Results from tensile tests conducted on this material at 600-1200°C generally agreed well with literature data on A533, Grade B steel. The material from the hot spot exhibited higher strengths than the remaining material, reflecting the heat treatment received during the accident. Charpy V-notch impact tests similarly found significantly lower upper shelf energies and higher transition temperatures for the material from the hot spot. However, creep tests conducted at ≈600-1200°C revealed little difference between material at and away from the hot spot. Cracks were found in the stainless steel cladding of boat samples from the hot spot. The cracks appeared to be the result of hot-tearing, probably assisted by intergranular penetration of liquid Ag-Cd. Crack propagation into the A533 vessel steel was a maximum of ≈6 mm. Materials in the cracks suggest the presence of control-assembly debris on the lower head before the massive fuel flow arrived.

12. KEY WORDS/DESCRIPTORS *(List words or phrases that will assist researchers in locating this report.)*
Three Mile Island Reactor
Mechanical Properties
Tensile Properties
Creep Properties
Impact Properties
Metallography

13. AVAILABILITY STATEMENT
Unlimited

14. SECURITY CLASSIFICATION
(This Page)
Unclassified
(This Report)
Unclassified

15. NUMBER OF PAGES

16. PRICE

Federal Recycling Program

UNITED STATES
NUCLEAR REGULATORY COMMISSION
WASHINGTON, D.C. 20555-0001